LIDAR Remote Sensing for Estimation of Biophysical Vegetation Parameters

Dissertation

zur

Erlangung der naturwissenschaftlichen Doktorwürde
(Dr. sc. nat.)

vorgelegt der

Mathematisch-naturwissenschaftlichen Fakultät

der

Universität Zürich

von

Felix Morsdorf

aus

Deutschland

Promitionskomitee

Prof. Dr. Klaus I. Itten (Vorsitz)
Dr. Britta Allgöwer (Leitung)
Dr. Erich Meier
Prof. Dr. Robert Weibel
Dr. Emmanuel Baltsavias

Zürich 2006

Almost everything - all external expectations, all pride, all fear of embarrassment or failure - these things just fall away in the face of death, leaving only what is truly important. Remembering that you are going to die is the best way I know to avoid the trap of thinking you have something to lose. You are already naked. There is no reason not to follow your heart.

Steve Jobs (1955 -)

Abstract

Wildland fires pose an immensive threat to social and economic values in many countries around the world. These fires are ecological phenomena subject to boundary conditions which vary spatially and temporally. Airborne laser scanning (ALS) is an active remote sensing methodology capable of directly measuring the location of reflecting points on the earth's surface. ALS systems scan the earth surface with a laser beam, resulting in a three-dimensional point cloud containing structural aspects of the vegetation canopy. Thus, it was hypothesized that ALS could provide structural information relating to the spatial arrangement of fuels to assess either the risk or the potential impact of wildland fires. The presented dissertation focuses on the derivation of such structural parameters from ALS data in its raw form and attempts to develop, implement and validate robust methods for biophysical vegetation parameter estimation.

An approach for the estimation of the canopy geometry at the scale of single trees from ALS data was implemented and validated using field data. It was shown that the tree geometry, including position, tree height and crown diameter, of single trees could be derived from the laser point cloud with an accuracy that matches the one of traditional field work. A methodology for the derivation of canopy density measures such as leaf area index (LAI) and fractional cover (fCover) was implemented using a physically based ALS estimator related to different echo types inside the canopy as a predictor variable. The validation was done using field data being geolocated with centimeter precision. This allowed for matching field data and ALS estimates for very small areas, opposed to more commonly used stand wise approaches.

The methods developed provide a high degree of automation, once they were calibrated with field measurements and were found to be robust in respect to changes of ALS scanning angles used in this study, while changing the flying altitude significantly affects the methods for derivation of vegetation density. In such cases, a recalibration of the methodologies for different flying altitudes is needed, as long as the dependence of flying altitude is not well enough understood to allow for a direct correction. The methodologies developed for deriving structural and density related information of the fuel bed sustain the large potential that ALS data has for the derivation of biophysical vegetation properties. One key finding of this thesis is that if one wants to exploit this potential even further, one will need to consider the interaction of the laser beam and the canopy more thoroughly.

Zusammenfassung

Waldbrände stellen eine enorme Bedrohung für Menschenleben und ökonomische Werte in vielen Ländern dar. Diese Feuer sind ökologische Prozesse, welche räumlich und zeitlich variierenden Randbedingungen unterworfen sind. Airborne (flugzeugbasiert) laser scanning (ALS) ist eine aktive Fernerkundungsmethode, welche die direkte Messung der Position von zurückstreuenden Elementen auf der Erdoberfläche ermöglicht. Durch die Abtastung der Erdoberfläche mit einem Laserstrahl erzeugen ALS Systeme eine dreidimensionale Punktwolke, welche die strukturellen Eigenschaften der Vegetation enthalten sollte. Deswegen wurde vermutet, dass man aus dieser Punktwolke Information über die räumliche Verteilung von Brandgut extrahieren kann, welche hilfreich zum Einschätzen des Risikos oder der Auswirkungen von Waldbränden sein könnte.

Die vorgelegte Dissertation beschäftigt sich mit der Ableitung von struktureller Information aus ALS Daten in ihrer rohen, unverarbeiteten Form (3D-Punktwolke) und versucht robuste Methoden zur Bestimmung von biophysikalischen Vegetationparametern zu entwickeln, zu implementieren und zu validieren. Eine Methode zur Erfassung der Geometrie von Einzelbäumen wurde entwickelt und mit Hilfe von Feldmessungen validiert. Es wurde gezeigt, dass Eigenschaften wie Baumposition, Baumhöhe und Kronendurchmesser in einem automatischen Verfahren aus der Punktwolke abgeleitet werden können, und dieses mit einer Genauigkeit, welche der von Feldmessungen entspricht. Ebenfalls wurde eine Methodik entwickelt, die es erlaubt Grössen, die die Dichte der Vegetation beschreiben, aus ALS Daten abzuleiten. Hierzu wurde der Blattflächenindex (leaf area index, LAI) und der Bedeckungsgrad (fractional cover, fCover) mit Hilfe von physikalisch basierten Statistiken der einzelnen ALS Echotypen (erstes und letztes Echo, first/last echo) und Regressionsmodellen bestimmt. Die Validierung dieser Methode erfolgte mittels Feldmessungen, welche mit differentiellen GPS auf einige Zentimeter genau lokalisiert waren. Dadurch war es möglich Feldmessungen und die aus den ALS Daten abgeleiteten Parameter auf kleinen Skalen von wenigen Metern zu korrelieren, im Gegensatz zu bisherigen Methoden, welche meist auf der Fläche eines Bestandes implementiert wurden.

Die entwickelten Methoden verfügen über einen hohen Grad der Automation, sobald sie mit Feldmessungen kalibriert werden und sind unempfindlich gegenüber Änderungen des Abtastwinkels, zumindest für den kleinen Bereich in dem der Winkel des in dieser Arbeit verwendeten Systems variiert. Hingegen beeinflusst eine grössere Änderung der Flughöhe die Methoden zur Ableitung der Vegetationsdichte erheblich, während die Methode zur Einzelbaumextraktion weniger beeinflusst wird. In beiden Fällen ist allerdings eine Rekalibrierung der Algorithmen mit Felddaten für un-

terschiedliche Flughöhen erforderlich, es sei denn man kann die Auswirkungen der veränderten Flughöhe für jeden Parameter direkt quantifizieren.

Die im Rahmen dieser Arbeit entwickelten Methoden und Algorithmen zur Ableitung von Struktur und Dichte der Vegetation unterstreichen das grosse Potential von ALS Daten für die Extraktion von biophysikalischen Parametern der Vegetation. Aus den gewonnenen Erkenntnissen lässt sich weiterhin die Schlussfolgerung ziehen, dass man die Interaktion des Laserpulses mit den streuenden Objekten besser verstehen muss, um dieses Potential weitergehend ausnützen zu können.

Contents

List of Figures

List of Tables

List of Abbreviations

AGL	Above Ground Level
ALS	Airborne Laser Scanning
ASCII	American Standard Code for Information Interchange
CHM	Canopy Height Model
CHRIS	Compact High-Resolution Imaging Spectroscopy sensor
DLR	Deutsches Zentrum für Luft- und Raumfahrt
DSM	Digital Surface Model
DTM	Digital Terrain Model
ENVI	Environment for Visualizing Images
ESA	European Space Agency
fCover	Fractional Cover
FMS	Flight Management System
FOV	Field of View
FPAR	Fraction of PAR (Photosynthetically Active Radiation)
FWHM	Full Width at Half Maximum
GLAS	Geoscience Laser Altimeter System
GORT	Geometric Optical Radiative Transfer
GPS	Global Positioning System
ICESat	Ice, Cloud and land Elevation Satellite
IDL	Interactive Data Language
IEEE	Institute of Electrical and Electronics Engineers
IFOV	Instantaneous Field of View
INS	Inertial Navigation System
IMU	Inertial Measurement Unit
LAI	Leaf Area Index
LASER	Light Amplification by Stimulated Emission of Radiation
LIDAR	Light Detection and Ranging; or Laser Imaging Detection and Ranging
LVIS	Laser Vegetation Imaging Sensor

MERIS	Medium Resolution Imaging Spectrometer
MATLAB	Matrix Laboratory
MODIS	Moderate Resolution Imaging Spectrometer
MODTRAN	Moderate Resolution Transmittance Code
NASA	National Aeronautics and Space Administration
NDVI	Normalized Difference Vegetation Index
NIR	Near-infrared range of the electromagnetic spectrum
PAR	Photosynthetically Available Radiation
PRODEX	PROgramme de Developpement d'Experiences
RMS	Root Mean Square
RT	Radiative Transfer
RTM	Radiative Transfer Model
RSL	Remote Sensing Laboratories
SI	Système International (d'Unités)
SNR	Signal-to-Noise Ratio
SWIR	Short-wave infrared range of the electromagnetic spectrum
UTC	Coordinated Universal Time

Chapter 1

Introduction

1.1 Wildland fire - a multidimensional problem

Wildland fire is a common threat in many countries in Europe, especially to those in the Mediterranean. Every summer, in countries such as Portugal, Spain and France thousands of hectares of forests and shrub-land are burned and people are endangered and even killed (Forestry Department and FAO of the United Nations, 2001). Even in Switzerland, especially in Ticino, Grison and Valais, tens to hundreds of fires occur per year, but due to good monitoring and well equipped fire fighters, the burned areas remain small. Since wildland fires manifest a risk to social and economic values in society, the interest in understanding these wildland fires to have better means to either suppress them or to weaken their impact has been high. Nowadays, it is well acknowledged that wildland fires are a part of the natural ecological system (Habeck and Mutch, 1973; Bernard et al., 2000; Guyette and Spetich, 2003). Since wildland fires spread in two spatial dimension (horizontal), ignite trees by torching (vertical) and progress with time one can call wildland fires a four-dimensional process. This process relies on an ignition source (e.g. lightning, negligence), a fuel bed that is in the condition to burn (e.g. dry needles) and environmental conditions that allow for fire spread (e.g. wind or terrain slope) (Finney, 2005).

One key component in understanding wildland fire is characterizing the fuel bed, even more so since it is the only of the above mentioned variables that can be controlled by human interaction, at least to a certain extent. A lot of research has been focused on predicting fire occurrence and fire behavior. While the first is done on the basis of statistical models incorporating databases of past occurrences and weather indices, the latter is simulated using models of fire behavior. These fire behavior models were originally based on empirical relations derived from observations and laboratory experiments (Rothermel, 1972). The most commonly used model of this kind is probably FARSITE (Finney, 1998) (for applications see Stephens (1998) and Russell and McBride (2003)). These models need input parameters related to terrain and fuel structure, that must be provided on two-dimensional grids. Thus, there is a long history of providing this information (Countryman, 1972; Pyne et al., 1996) on spatial scales, mostly by assessing the fuel structure and fuel type on the ground using defined field protocols.

As computing power and the understanding of involved processes advanced, re-

cently developed fire behavior models are capable of simulating fire spread in three-dimensions, including the vertical (Morvan and Dupuy, 2001; Linn et al., 2002; Séro-Guillaume and Margerit, 2002; Margerit and Séro-Guillaume, 2002). These fire behavior or combustion models are based on a closed set of physical equations that are very similar to the Navier-Stokes equations in fluid dynamics (Pedlosky, 1992). They need input related to the fuel structure on all scales that they either explicitly simulate or parametrize based on empirical findings, from micro-structure (e.g. cells) to macro-structure (e.g. stands of trees). Especially important is the spatial arrangement of trees, their geometry and their density (including the height of the crown base for effects like torching). These parameters are strictly geometrical properties of the vegetation canopy and they need to be known with high precision on larger scales, a criteria that is hard to fulfill by using the traditional field protocols. Thus, remote sensing plays an important role in the derivation of fuel bed and fuel type characterization for fire behavior modeling (Mbow et al., 2004). Other studies (Miller and Yool, 2002) already focus on the interface of fire behavior models and externally provided data, especially on the issue of which scales are relevant for an empirical fire behavior model such as FARSITE.

1.2 Remote Sensing - providing multidimensional observations

Remote sensing has a long tradition for observing fires and monitoring the effects of wildland fires on larger scales. Most often, space-borne passive imaging sensors have been used for these approaches (Chuvieco, 2003), since they allow for covering large areas. With the availability of space-borne high resolution systems interest rose on deriving information relating to the fuel bed that could be used to assess the risk of fire occurrence and fire severity. Nowadays, space-borne imaging sensors exist that provide spatial resolutions of up to one meter (e.g. Quickbird, Ikonos). These systems offer a high potential for classification of fuel types. However, these sensors still lack the direct measurement of the vertical structure. There are very recent studies that show how to use stereo pairs of these sensors for the derivation of a surface model (Gruen and Zhang, 2006; St-Onge et al., 2006). Still, a terrain model of high quality is needed to defer vegetation height accurately, but as St-Onge et al. (2006) point out this can be gained from other sources, since the terrain shape does not change that much over time.

During the 1990ies, a new technology was added to the portfolio of remote sensing methods, namely LIght Detection and Ranging (LIDAR). These systems directly provide the coordinate of a back scattering element (scatterer) on the earth's surface and (by using a scanner) sample larger areas providing a detailed insight on the spatial structures on the ground. Their primary use has always been the derivation of elevation models, since the active technology allowed for mapping of the terrain even in forested areas; areas where traditional methods (e.g. orthophotos) would not provide satisfying results. These precise elevation models alone would be a great benefit for predicting fire behavior, since break-lines such as riverbeds and roads are contained in these elevation models and such break-lines could hinder a fire to spread or at least alter the fire spread. These models are computed from a set of raw laser echos (x,y,z-coordinates), that are generally discarded after model interpolation. Since this model interpolation comprises loss of information (a three-dimensional point cloud is con-

verted to 2.5-dimensional elevation models) there was the expectation that LIDAR data could provide more information on the fuel bed than just the surface elevations. The raw laser data provide a three-dimensional description of the earth surface as well as the vegetation layer that needs to be exploited.

Thus, on the one hand we have an ecological process which needs structural information on spatial scales and on the other hand we have a remote sensing technology that is supposed to provide this information. However, to truly exploit the potential of LIDAR data for fuel characterization one has to know more about the nature of this data and what kind of information it could contain. This is the subject of this thesis and it's outcomes are presented in the following chapters.

1.3 Objectives and Context

The objective of this thesis is to exploit the information provided by ALS data to derive biophysical properties of the vegetated earth's surface, relevant to fire researchers and other ecologists. The methods that are to be developed and implemented for this purpose shall provide robust and reproducible results with only a little need for user interaction. Since a more precise formulation of the objectives requires detailed knowlegde of the technical capabilities of ALS and of previous methodologies related to vegetation applications, the detailed research questions will be presented after an introduction into ALS technology and a state of the art of its application for the derivation of vegetation properties.

1.3.1 Practical Context

The guiding framework of this dissertation project has been the European Community project *Forest Fire Spread and Mitigation* **SPREAD**. The main objective of the project **SPREAD** was to understand and characterize wildland fires as a natural hazard. Involved in that project were researchers from many disciplines and users related to all aspects of wildland fire, be it the social-economic component, the behavior modeler or the ecologist. The final aim was to use all the complementary knowledge to set up a decision support system for the policy maker to better prevent fires and better understand their impact on nature and society. As a test site for the methodologies to be developed and implemented, the Eastern Ofenpass valley, being part of the Swiss National Park (SNP), was selected. The Ofenpass represents a dry inner-alpine valley at an average altitude of about 1900 m a.s.l.. The forest stands within the study area can be classified as woodland associations of Erico-Pinetum mugo (Zoller, 1995). The understory is characterized by low and dense vegetation composed mainly of Ericaceae and Sesleria species. Furthermore, the study area has been affected by few but intense (stand-replacing) fires (Allgöwer et al., 1998, 2003).

1.3.2 Structure of the thesis

In the following chapter, Airborne Laser Scanning (ALS) including it's measurement principle and technical aspects that are relevant for this thesis will be introduced. Fur-

thermore, a state of the art regarding vegetation applications, not only from the perspective of the fire community, but generally for foresters and ecologists will be presented. All this information is needed to precisely formulate the objectives of the thesis and research questions, those are elaborated at the end of the chapter providing the state of the art (Section 3.9). The research questions will be handled in four different publications, with each being a separate chapter of this thesis. Following that, a synopsis will discuss the findings from the publications and provide an outlook regarding future research.

Chapter 2

Airborne Laser Scanning

In recent years, airborne laser scanning (ALS) has manifested its role in generating high resolution, high precision 3D information of the earth's surface. ALS is an active remote sensing technology that directly provides 3D coordinates of scatterers on the surface. These coordinates can be converted to surface and terrain models by algorithms with a high degree of automation. Thus, ALS is far less labour intensive to deploy than traditional photogrammetry and its direct 3D measurement offers a high potential for new applications. In the following section, the principle and components of an ALS will be presented, together with some theoretical considerations concerning the measurement process.

2.1 Measurement Principle

The principle of LIDAR is based on combining a range information and a location and attitude information of a measurement platform to yield the location of an object in three-dimensional space. The range information is gained through a return time measurement of a laser pulse, while the location and attitude of the platform are derived by combining differential Global Positioning System (GPS) and Inertial Navigation Systems (INS) measurements. Using a laser as light source is not necessarily needed (Wehr and Lohr, 1999), in some cases strong xenon lamps could be used as well, but due to it's monochromatic character laser offers advantages in filtering out background radiation.

Figure 2.1 illustrates the underlying vectored equation of a LIDAR system. The position vector $\vec{p}$ of a location P is derived by the sum of the vector $\vec{f}$ to measurement platform and the vector $\vec{d}$ from plane to the scattering element on the surface, which is derived by range and orientation measurements.

The components that make up an airborne laser scanner and are needed to deduce these vectors are presented in the next section. LIDAR and ALS are often used synonymously in literature, but in this thesis it will be differentiated between the two in the following manner: A LIDAR system differs from an ALS in the way that it does not have a method of beam deflection (see Section 2.2.4) for across track scanning. Thus, a LIDAR system to which a mechanism of beam deflection is added can be called ALS. The denotation ALS is furthermore important to discriminate airborne laser scanning systems from upward looking atmospheric LIDAR, which are for instance used for

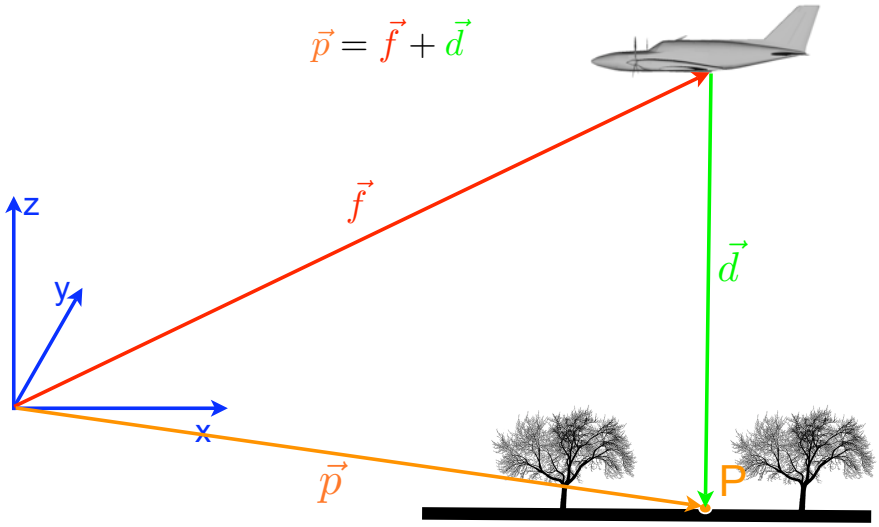

Figure 2.1: LIDAR measurement principle as vectored equation.

aerosol concentration retrieval.

2.2 Components of an ALS

2.2.1 Laser Range Finder

The laser range finder includes the laser, emitter/receiver optics, the signal detector and an amplifier plus the necessary electronic components. The laser pulse is emitted from the laser transmitter and the time that passes until a reflected and modified version of the laser pulse is received. The laser pulse does not travel with the speed of light, but with a *packet velocity* of the coherent light packet, which is a little less than the speed of light (Wagner et al., 2006). Since the packet velocity of the laser pulse can be considered invariant for the distances commonly used in ALS practise, this return time measurement can easily be converted to a distance by multiplying it with the speed of the light packet:

$$D = \frac{t * c_{packet}}{2} \tag{2.1}$$

Note the number two in the denominator, which is due to the fact that the laser pulse travels the distance between scattering element and emitter/receiver twice. c_{packet} is a little less than the speed of light, but can in most computations be exchanged for the real speed of light (Wagner et al., 2006).

2.2.2 Differential GPS

For determining the precise location of the ALS system differential GPS is required at least. Differential GPS uses a fixed ground station inside the study area (baseline should be as small as possible) as a reference in order to correct the GPS signal received at the measurement platform for random and systematic errors. This correction is generally

done by a post-processing step and not real-time during the overflight. With this correction, the error for the position estimation of the measurement platform can be as low as 5-15 cm depending on satellite visibility, atmospheric conditions and baseline length (Baltsavias, 1999a). Since the GPS signal is generally sampled only with 1 to 10 Hz and the measurement platform can travel with several tens of meters per second, only every several meters a positional fixing could be provided by dGPS alone. Since the spatial resolutions of ALS acquisitions can be smaller than a meter, differential GPS alone is not enough to provide precise locations. dGPS positions need to be interpolated by additional locational information and that is best achieved by utilizing Inertial Navigation Systems (INS).

2.2.3 Inertial Navigation System

Inertial navigation systems consist of three sensors measuring the accelerations in all three coordinate system directions of the moving platform over time. An integration of these accelerations leads to a relative flight track, with the dGPS location information providing absolute locations for the INS based location information to start off with. Since the INS is generally much higher sampled (40 to 200 Hz), the relative INS information can be used to *interpolate* the flight track in-between absolute dGPS based fixings of the measurement platform's location. Furthermore, an INS consists of three gyroscopes, which provide the attitude information needed to compute the range vector $\vec{d}$ presented in Figure 2.1. The availability of high-precision INS systems really allowed for the use of direct georeferencing with centimeter accuracies, which are needed for ALS applications. The integration of dGPS and INS itself is not trivial and is most often achieved by utilizing Kalman filters (Cramer, 1997; Lithopoulos, 1999). The components presented in the last three sections (laser range finder, dGPS and INS) comprise a LIDAR system. In order to obtain an airborne laser scanner, an additional component is needed, which will be presented in the next section.

2.2.4 Scanner

Following the definition presented in Section 2.1, a LIDAR system is turned into an ALS system by adding a method for beam deflection across track. For all LIDAR systems, the progression of the measurement platform enables a scan along a line in flight direction. There are LIDAR systems available that sample only a single spot beneath the measurement platform at a time (e.g. SLICER, see Harding et al. (2001)) and through progression of the platform a line scan is generated.

In order for the ALS to be able to scan a rectangular area (which is rectangular only in the coordinate system of the ALS) with one flight track, the laser beam needs to be deflected across track. This is in most cases achieved through the use of oscillating or rotating mirrors. In Fig. 2.2 this process is illustrated for a rotating polygon of mirror facets. A motor (blue) rotates the cylinder with the mirrors (grey) to deflect the laser beam (red) originating from a laser source (green). Since the rotary motion of such a mirror is constant, the spacing of points on the scanned surface across track will not be constant, but modulated by a sine function.

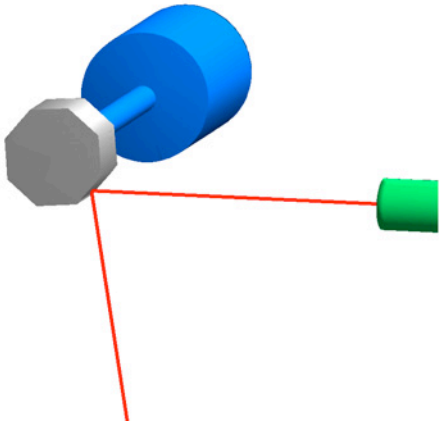

Figure 2.2: Illustration of beam deflection through the use of a rotating polygon with mirror facets.

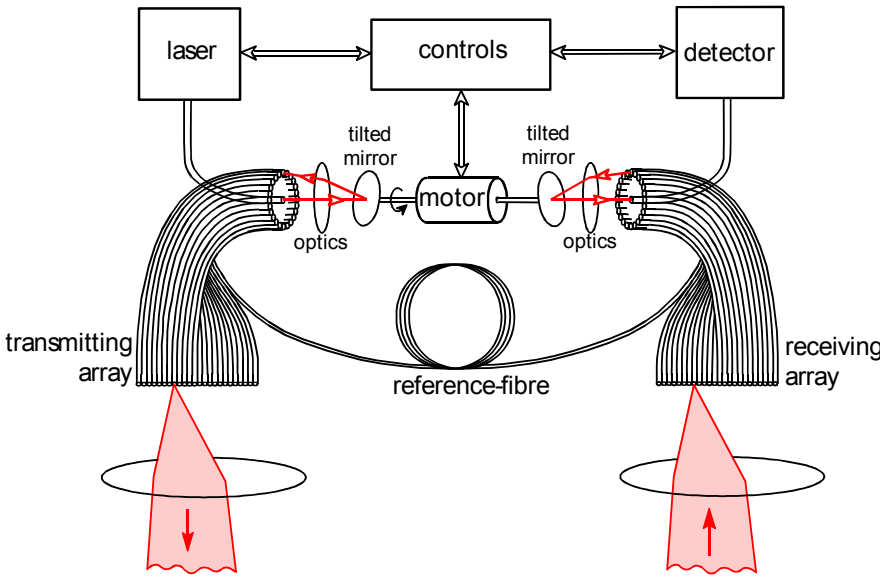

Figure 2.3: Illustration of beam deflection through the use of a fibre array. (Image from www.toposys.com)

Another method of beam deflection is the use of fibre-arrays. For instance, the German company Toposys[1] builds and maintains ALS systems that use a fixed number of fibers for beam deflection. In Fig. 2.3 such an array of fibers is shown. A rotating mirror is only used for distributing the laser beam to the fibre-array, thus errors in beam positioning due to vibration are eliminated. For the array used in the Toposys FALCON II sensor, the maximum scanning angle is ± 7.15 degrees, while the angular resolution in-between the fibers is 1.96 mrad. Systems with rotating/oscillating mirrors have the advantage that the maximum scan angle might be configured for different acquisition settings, offering higher flexibility over systems that use fibre-arrays. On the

[1] www.toposys.com

other hand, systems with fibre-arrays should be less susceptible to errors induced by vibrations and or imprecise facet alignment (Katzenbeisser, 2003a).

2.3 Laser Signal

In most applications of ALS data the measured distance of an echo is considered as corresponding to a specific object at the location of the echo. This is not always correct, and a number of studies (Axelsson, 1999; Hofton et al., 2000; Jutzi and Stilla, 2003; Wagner et al., 2003; Katzenbeisser, 2003b) have shown that the interaction of complex scatterers and the laser pulse is not yet well enough understood. But it is well acknowledged that these interactions can have a substantial influence on the measured distance of an object to the laser emitter. In the following section we will explore how the laser pulse and the scatterer(s) interact. This can be considered as a one-dimensional problem, with the relevant axis being either time or range, with both being equivalent due to the constant speed of light. The underlying relation describing the measured signal strength is the same for airborne laser scanning and radar remote sensing (Wagner et al., 2003). Thus, the radar equation can as well be used for computing signal strengths for LIDAR systems. In the following section an adapted version of the radar equation especially for ALS is presented, as it was presented in Wagner et al. (2006).

2.3.1 Return Power

If a target can be detected by an ALS system is a question of return energy contained in the reflected pulse. Several factors influence the return energy, and for simple targets this energy can be computed, if properties such as beam divergence, distance target-sensor, emitted pulse energy and target properties (geometry and reflectivity) are known. The laser beam is widened with the distance from the sender based on optical beam divergence. Beam widening due to atmospheric divergence can in most cases be neglected (Baltsavias, 1999a). Under the assumptions of a diffuse target that reflects uniformly into the hemisphere, Baltsavias (1999a) computed the energy of the return signal as

$$P_r = \rho \frac{M^2 A_r}{\pi R^2} P_t \tag{2.2}$$

P_r is the power at the receiver, ρ the reflectivity of the target, M is the atmospheric transmission, A_r the illuminated receiver area, R is the distance in-between the laser and the target and P_t the laser pulse energy at the transmitter. Wagner et al. (2006) developed a special form of the radar equation to compute the return power of a laser pulse for a given geometric setting, in which they introduce the cross-section σ of the scatterer and neglect the atmospheric transmittance M:

$$P_r = \frac{P_t D_r^2}{4\pi R^4 \beta_t^2} \sigma \tag{2.3}$$

P_t is the power of the laser pulse leaving the transmitter, R is the distance between laser system and scatterer, D_r the aperture diameter of the receivers optics, while β_t is

the beam divergence. σ is the so-called back scatter cross-section, which is defined as follows:

$$\sigma = \frac{4\pi}{\Omega}\rho A_s \tag{2.4}$$

Ω is the angle defining a back scattering cone due to surface roughness, ρ is the reflectivity of the scatterer and A_s is the illuminated area of the scattering element. Baltsavias (1999a) provided an example computation of the return energy for a standard ALS scenario. The ratio of return energy to transmitted energy was as low as $1.2{*}10^{-9}$. Since the transmitter energy can not be too high due to eye safety constraints, one will need very sensitive detectors with a very good signal-to-noise ratio (SNR). For the transmitter/receiver combination, optics with band-pass properties for the specific laser wavelength are used, since they filter out the background radiation from other wavelengths. One of the main aspects of Equations 2.2 and 2.3 is that target visibility for a LIDAR system not only depends on targets size, but as well on target reflectivity and in some cases even more on the latter than on the first. Thus, if considering the visibility of a specific object, it's reflectivity at the specific wavelength of the laser needs to be known. Wavelengths of ALS systems are typically in the near infrared, with the Optech systems being at 1064 nm, while Falcon II utilizes a laser with 1560 nm wavelength (see Table 2.1 for details). The fourth paper of this thesis (Chapter 7) will, among other subjects, deal with a practical study concerning the effect of object visibility due to size and reflectance of an object.

2.3.2 Waveform

Wagner et al. (2006) presented an equation describing the form of the return signal with time, the so-called waveform. We are going to use this relation to simulate the return signals of some typical scatterers. These simulations should provide some insight into the mathematical expression below. Following Wagner et al. (2006), the power at the receiver over time t can be expressed as

$$P_{r,i}(t) = \frac{D_r^2}{4\pi R_i^4 \beta_t^2} P_t(t) \star \sigma_i(t) \tag{2.5}$$

where D_r is the aperture diameter of the laser receiver and σ_i is the differential cross section of the scatterer. $\star$ is the convolution operator.

This relation was used to simulate the return waveform of some simple objects. In Figure 2.4 a Gaussian shaped laser pulse is used, since this is the shape most often used by commercial systems, while the theoretically nearly rectangle shape used in Figure 2.5 is less commonly used (Jutzi and Stilla, 2005). As scatterer, a sloped plane is used, which has a normalized differential cross-section of one over a range of three meters. This would be equivalent to a sloped object of 45 degrees illuminated by a laser pulse being three meter in diameter. In the bottom panel of Fig. 2.4 the return waveform of this object is displayed. The Gaussian form of the laser pulse leads to sloped signal edges at the beginning and the end of the main peak, while the peak itself remains flat.

Using the superposition of some Gaussian functions, an exemplary vegetation cross-section was set up, as it is shown in Fig. 2.5 (middle panel). This time, a rectangle as

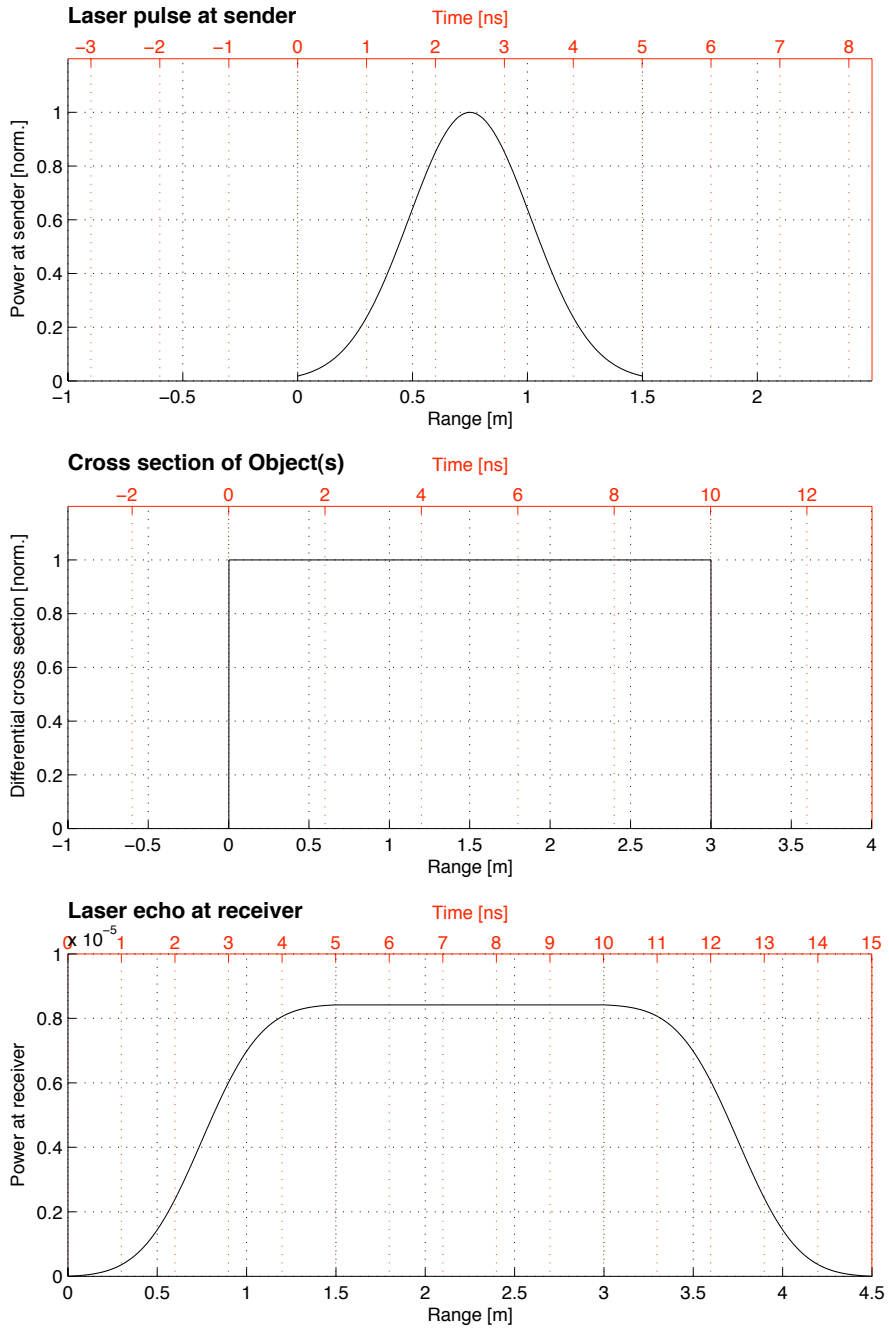

Figure 2.4: Simulation of return waveform for a sloped plane. Top panel displays original laser pulse, middle panel the cross-section of the plane and the bottom panel the waveform as recorded by the receiver.

shape of the emitted laser pulse with a duration of 10 nanoseconds $[ns]$ and an equivalent length of three meters was used. One can note that objects that are separated in the cross-section plot can not be separated in the return waveform, as e.g. the low vegetation close to the ground peak (right-most peak). Another problem arises from the fact that the ground peak might be widened due to the effect of terrain slope or roughness.

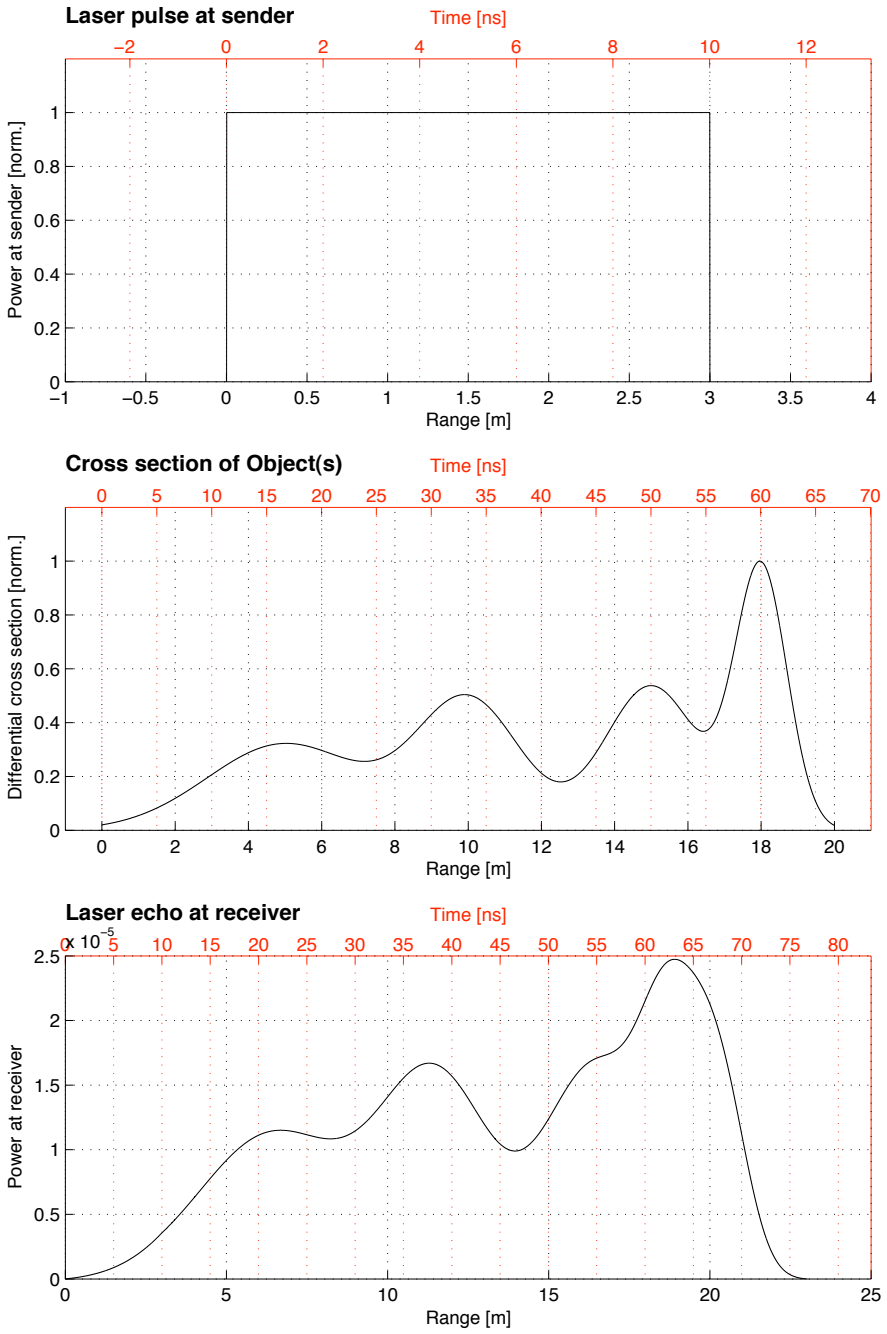

Figure 2.5: Simulation of return waveform for a vegetation scenario. Top panel displays original laser pulse, middle panel the cross-section of the plane and the bottom panel the waveform as recorded by the receiver.

In such cases, the determination of terrain height might contain errors that might be as large as the footprint diameter for a slope of 45 degrees. This leads us to the next section, which will deal with echo detection and separation of scatterers.

2.3.3 Echo detection

A critical part for most commercially available ALS systems is the echo detection. Most systems do not record the full return waveform, but detect in real time a discrete number of echos from the return signal. For most systems, two discrete echos are detected, which are called first and last echo in literature. Some systems allow the detection of up to five echos, with each being stored. Echo detection is most often achieved by thresholds. When the first raising edge of the return signal exceeds a certain intensity, a first echo is triggered. A last echo is triggered as the last raising edge of the return signal. An illustration of how this might work for a tree is given in Figure 2.11. There, a first echo is triggered as soon as the vegetation density inside the tree crown reaches a critical value. A part of the laser pulse moves on to be reflected from the bottom and to trigger a last echo at the receiver. Depending on the final form and amplitude of the return signal, a system that uses a constant threshold for triggering might induce ranging errors, as was stated by Katzenbeisser (2003b). He proposed to use an adaptive threshold, that takes signal intensity into account to correctly trigger first and last echos. The threshold is set to a fraction (e.g. $1/e$ or 0.5 of the peak's amplitude, of which the raising edge is to be detected. Since the amplitude of the peak is not a priori known when detecting the raising edge, this echo triggering will have to be done from a saved version of the return waveform, e.g. by using a buffer. Another critical property related to echo detection is the instrument dead-time, i.e. the time that is needed in-between two echos to be recorded as separated echos. This time manifests the vertical distance that two objects inside the illuminated area of a laser beam must be separated to be recorded as distinct (e.g. first and last echo) returns. This distance is related to the duration of the emitted laser pulse, and is at least half the pulse length of the emitted pulse. For a system using a laser pulse being 10 ns (three meters) in length, the minimum detectable vertical spacing that could be measured by one laser shot would be 1.5 meters. In practice, this distance can be much larger due to the widened returns of single scatterers, which overlap in the time domain and can not be separated by traditional means of echo detection. It is as well suspected that the flight altitude might as well affect this minimum distance of separation, and thus this aspect will as well be subject of Chapters 6 and 7.

2.3.4 Point Spacing

One important property of ALS data acquisition is the so-called point density, which is defined as the number of laser echos per unit area. The point density can be considered in some as the equivalent to resolution for passive imaging sensors. The higher the point density is, the more precise and accurate the ALS data products will be, with a saturation towards very high point densities, when the earth's surface will be oversampled. For instance, for building reconstruction a point density of one to two points per square meter might be sufficient, while for powerline mapping a point density of 10 points per square meter is needed (Maas and Vosselman, 1999).

For a fibre array, the point density is controlled by flight altitude and angular fibre spacing across track and flying speed and scan frequency along track:

$$\Delta y = h * \mu \tag{2.6}$$

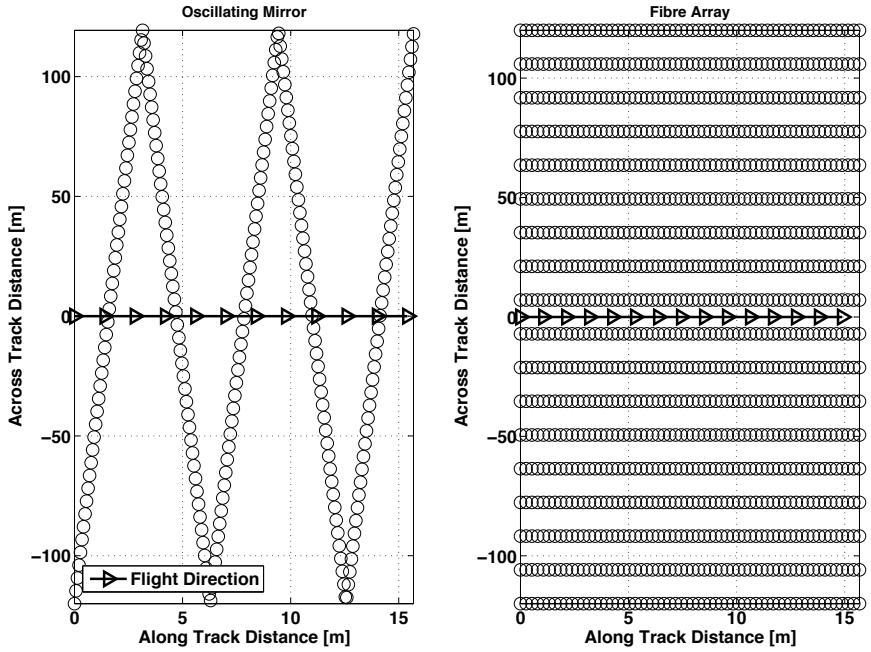

Figure 2.6: Illustration of point spacing for an ALS system using an oscillating mirror (left) and a fibre array for beam deflection (right). Empty circles represent outlines of single laser echos on the reflecting surface.

$$\Delta x = \frac{v}{f_{scan}} \tag{2.7}$$

h is the flight altitude over ground, μ the angular spacing of the fibre array, v the speed of the measurement platform and f_{scan} the line scan frequency. For a typical case of the Toposys system, using $70\ m/s$ for v, $653\ Hz$ for f_{scan}, $900m$ for h and $1.96mrad$ for μ, Δx and Δy are $0.11m$ and $1.76m$, respectively. Together with the footprint size of $0.9m$ at $h = 900m$ AGL, this manifests an oversampling of the earth's surface along track and an under-sampling across track. For systems bearing a rotating or oscillating mirror, the point spacing on the ground is not as easy to compute. It depends furthermore on the scan frequency and the maximum scan angle, which can be varied for most systems. The scan pattern on the ground is either Z-shaped or sinusoidal, depending on the mirror rotating or oscillating with constant speed (Z-shaped) or an oscillating motion modulated with a sine function (Baltsavias, 1999a). In Figure 2.6 the scan patterns of two commonly used beam deflection mechanisms are illustrated. The left panel shows the idealised (no stopping of mirror at edges) Z-shaped scan pattern of a ALS system using an oscillating mirror for beam deflection, while the right panel shows the scan pattern of the fibre-array being part of the Toposys Falcon II system. The oversampling along track and under-sampling across track is clearly visible from this illustration.

2.3.5 Footprint Size

Most commercially available ALS systems are so-called small footprint systems, where the beam diameter on the ground under normal acquisition conditions (e.g. altitudes up to 1000 m AGL) is in the order of about one meter. These systems enable the generation of high resolution terrain and surface models, which is their primary use. The footprint size depends on beam divergence γ and flight altitude h (and in some cases the aperture D of the transmitter/receiver optics):

$$A = D + 2h\,tan(\frac{\gamma}{2}) \tag{2.8}$$

Since D can be neglected in most cases (but not in all, as we will learn in Section 7.5.3), and γ is generally very small, Equation 2.8 can be rewritten to:

$$A = h * \gamma \tag{2.9}$$

It is known that the size of the footprint alters the ability of the laser pulse to penetrate vegetation (Nilsson, 1996; Chasmer et al., 2006). The smaller the footprint is, the larger is the chance of not receiving a last echo from the ground in denser vegetation. Thus, for systems recording first and last echo, the penetration of vegetation will in fact be better for systems using larger footprints (Schnadt and Katzenbeisser, 2004). For some systems, such as the Optech ones, the beam divergence can be set for different acquisitions, allowing to e.g. increase the penetration rate into vegetation. Some systems, such as LVIS (Blair et al., 1999), have much larger footprint diameters (in the order of ten meters). The latter systems should allow for covering larger areas with less cost, but with a lower spatial resolution.

2.4 ALS Systems

A large number of ALS systems is available for either commercial or scientific uses, a comprehensive summary was given by Baltsavias (1999b). A small summary of the most current and most used systems will be provided in Table 2.1, together with the major technological specifications that are needed to infer properties such as the point density on the ground.

2.4.1 Small footprint

ALS systems can be classified by their means of beam deflection, scanning frequency, laser wavelength and beam divergence and the number of echos they record. From these properties, parameters that are more relevant for the user can be computed, as e.g. the point density or the footprint size on the ground. From a technical point of view, it is not mandatory to differentiate between large and small footprint laser scanners, but based on the different implications for vegetation applications that arise from the scale of the footprint this differentiation is reasonable. This will be explained in detail in Section 3.

Another relevant information (characterizing an ALS system) is the length of the laser pulse used, since it controls the minimum distance that two objects need to be

apart to be identified separately by first and last echo. In reality, this distance will as well be influenced by the method of echo detection applied. However, system manufacturers do not always provide this information, thus the most practical test to infer this distance would be using histograms from the difference of first and last echo (see Figure 5.2, top panel for an example).

The most commonly used ALS systems are built by the Canadian company Optech, with the ALTM 3100 being their most recent development. An additional option for the Optech 3100 is the use of a waveform digitizer, that will enable the system to record full return waveforms. We provide as well the technical information for two systems built by the German company Toposys, since the Falcon II system is the sensor that was used during this thesis. It records both first and last echo at the same time. The Falcon III is a very recent development and will only be available in autumn 2006 the earliest. Furthermore, the LMS Q560 built by the Austrian company Riegl is listed, which is the first small footprint sensor capable of recording the full return waveform.

Small footprint							
Company / Instrument	Scan principle / pattern	Wavelength $[\mu m]$	Scan Angle $\theta[^\circ]$	Pulse Rate $[khz]$	Scan rate $[Hz]$	Beam div. $[mrad]$	Pulse length $[ns]$
Optech ALTM 3100	Osc. mirror	1064	$0 - \pm 25$	≤ 100	≤ 70	0.3 (0.8)	10
Riegl LMS Q560	Rot. mirror	1500	± 22.5	50-100	4 ns	≤ 0.5	-
Saab Topeye Mark II	Fibre Array	1064	$\pm 7/10$	50	-	1	4
Toposys Falcon II	Fibre Array	1560	± 7.3	83	653	1	5
Toposys Falcon III	Fibre Array	1560	± 13.5	50-125	165-415	0.7	5-10
Large footprint							
LVIS	Rot. Mirror	1064	± 7	0.1-0.5	-	8	10
GLAS	fixed	1064	fixed	0.4	-	0.11	6

Table 2.1: Listing of commonly used LIDAR systems, separated for small and large footprint systems. For some properties no information is provided by the system manufacturers.

2.4.2 Large footprint

The LVIS system developed and operated by NASA offers the advantage of recording the full return waveform, thus describing the vertical vegetation structure contained in the illuminated area. However, since no horizontal structure information on scales smaller than the footprint diameter can be derived, these systems can only provide terrain models with a spatial resolution in the order of ten meters. Thus, the derivation of vegetation properties is only possible as an average value for stands. Furthermore, at these scales, one has to deal with a widened ground return (in the return waveform) due to terrain undulations or terrain slope, and thus, properties such a tree height might

only be derived with certain errors. The LVIS system is not operated commercially, but only on a scientific basis. In Section 3.8 some approaches deriving vegetation properties based on LVIS data will be presented.

There is even one large footprint system available in space, which is primarily used as an altimeter for the world's ice sheets. This satellite is called ICESat and the instrument aboard GLAS (Geoscience Laser Altimeter System). It has a very large foot print of about 70 m in diameter. There are some newer studies that compare GLAS waveforms of vegetation with those recorded by LVIS (Lefsky et al., 1999b; Harding and Carabajal, 2005) and found quite good agreement for areas without larger topographic undulations.

2.5 ALS Data Products

By default, ALS systems only record the location of each echo in the three dimensional space. These locations are stored as x, y, z triplets in a file and manifest what is often called *raw* laser data in literature. An example data-set of this raw data is displayed in Fig. 2.7. The data in this form is not of great use to most end-users, they are primarily interested in gridded elevation models, be it of the terrain or the surface, including objects such a trees and buildings.

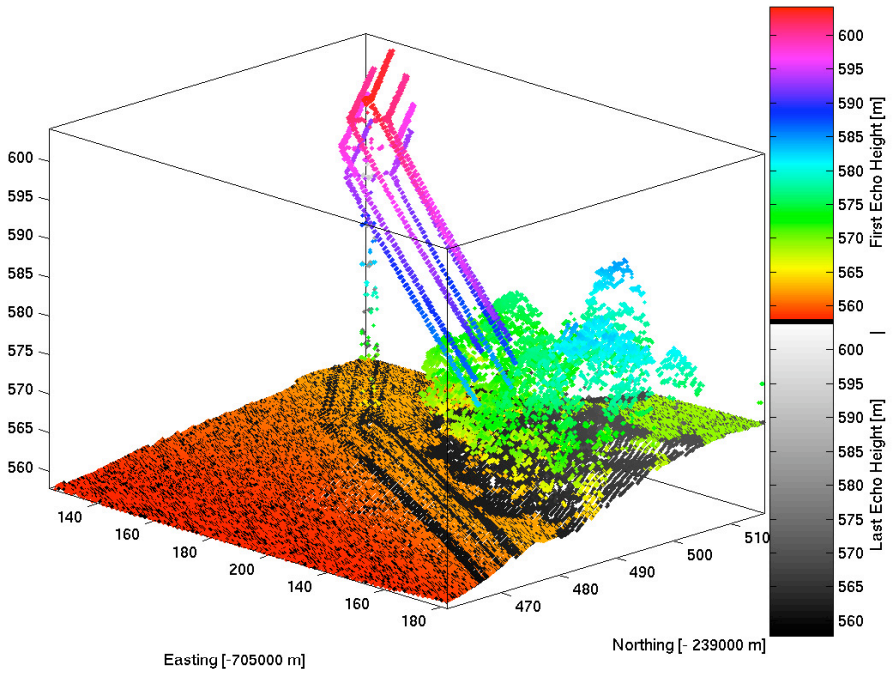

Figure 2.7: A section of ALS raw data colored separately for first and last echo returns. The scene contains bare earth, a powerline and vegetation (from left to right). Data was collected at 500 m AGL with a nominal footprint diameter of 0.5 meters in the area of Hinwil, Switzerland

Thus, the data providers convert the raw data into gridded models of terrain height (digital terrain model, DTM) or surface height (digital surface model, DSM). This is

done by interpolation using either last echo data (DTM) or first echo data (DSM) and special filtering algorithms, which are needed to filter out vegetation and buildings, which are contained as well in last echo data.

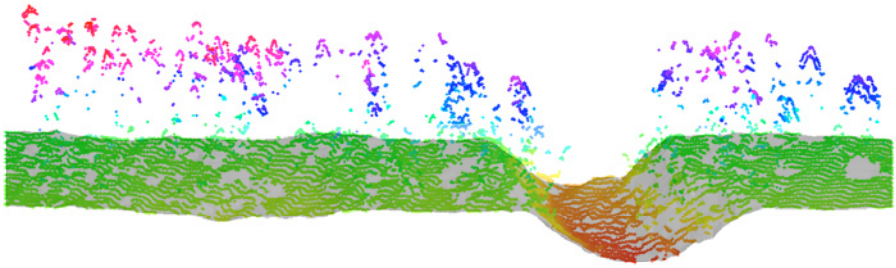

Figure 2.8: Last echo laser raw data superimposed with DTM interpolated from the raw data. Remaining vegetation spikes have been filtered out and the resulting holes are closed by interpolation.

In Figure 2.8 an illustration of DTM generation is given. The laser raw data (colored dots) displayed in the figure are last echo data and one can note that there are still last echos that are triggered inside the vegetation and need to be filtered out to yield the DTM (gray surface). For the generation of a DSM, an example is provided in Fig. 2.9. Here the generation of the model is much easier, since only the highest raw laser echos inside each grid cell need to be used for the DSM (green surface). One can note that there are much less first echos from the ground and much more being triggered inside the vegetation when comparing with Figure 2.8. Data providers in most cases deliver the following products to their customers: DTM, DSM and, if asked for, as well the raw laser data. Although these models surfaces are often considered as the true surface, one

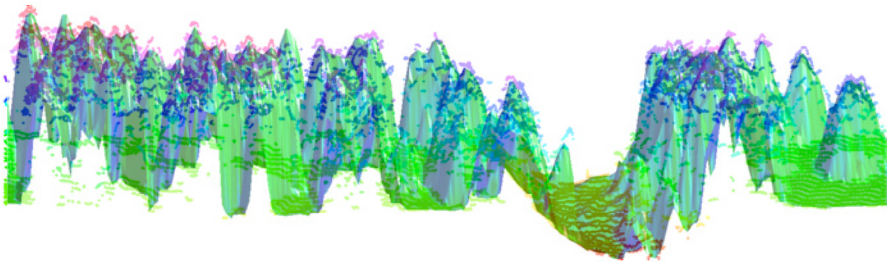

Figure 2.9: First echo laser raw data superimposed with DSM interpolated from the raw data.

still has to consider possible errors that might propagate further into vegetation products. For instance, for very dense vegetation there might not be enough penetration through the canopy in order to get a high number of ground points. Resulting holes in the DTM are closed by interpolation, but for an undulated or sloped terrain this might induce large errors in terrain representation, as was stated by Kraus and Pfeifer (1998). On the other hand, a DSM might be too low in cases were the point spacing is not high enough to sample all tree tops, or the vegetation is not dense enough to trigger first returns.

2.6 Typical Applications of ALS Data

Since the main purpose of ALS systems is generally to generate high quality, high resolution digital raster models, all disciplines that need such models are potential users. Especially hydrology benefits from the ability of ALS to derive terrain models in forested areas, revealing break-lines of the terrain that would not be visible by traditional photogrammetry (Kraus and Pfeifer, 2001; Reutebuch et al., 2003; Clark et al., 2003). A caveat is that for most deciduous canopies, accurate terrain information can only be gained from ALS acquisitions that are carried out in leaf-off conditions, since the tree crowns are generally wider and denser than for conifers such as the ones found in our study area.

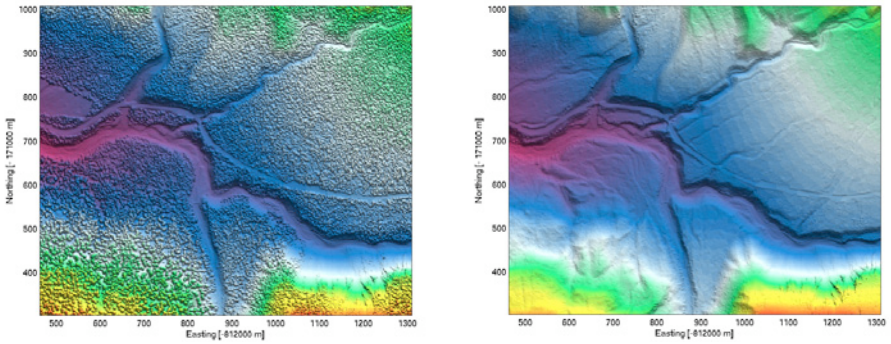

Figure 2.10: Section of DSM (left panel) and DTM (right panel) for the Ofenpass area in the Swiss National Park (SNP). Grid resolution is one meter, height is color-coded, and violet to blue denotes low and orange to red denotes high values

An example of ALS data revealing topographic features, such as riverbeds or even walking paths in a forest can be found in Fig. 2.10. In the left panel, the DSM is displayed, with all areas having a high textural granularity being forest. One can note that no topographic features are visible in these regions in the DSM, while they are clearly visible in the DTM, that does not contain any higher vegetation such as e.g. trees (right panel). Other areas have more interest in the surface models generated by ALS data, especially those using city models for simulation of electromagnetic wave propagation for mobile phone networks. More or less automated algorithms exist that extract building locations and reconstruct buildings by the use of primitives from ALS data (Haala and Brenner, 1998, 1999; Maas, 1999; Maas and Vosselman, 1999; Murakami et al., 1999; Vosselman and Dijkman, 2001; Maas, 2002; Brenner, 2005). A qualitative comparison of these methods regarding accuracies and degree of automation can be found in Kaartinen et al. (2005). Other applications include corridor mapping (power lines), archeology, coastline protection, pits and deposits and forestry. The high potential of ALS data for the last application will be topic of the next section.

2.7 Potential for Vegetation Applications

For the first time, a remote sensing method offers a direct measurement of surface elevations, without the need of error prone matching of stereo pairs as for digital orthophotos, and even with greater accuracies (Schenk et al., 2001). Due to the ability of the laser beam to penetrate the vegetation canopy to some extent, and since most systems record at least first and last echo, a three-dimensional description of the canopy can be provided.

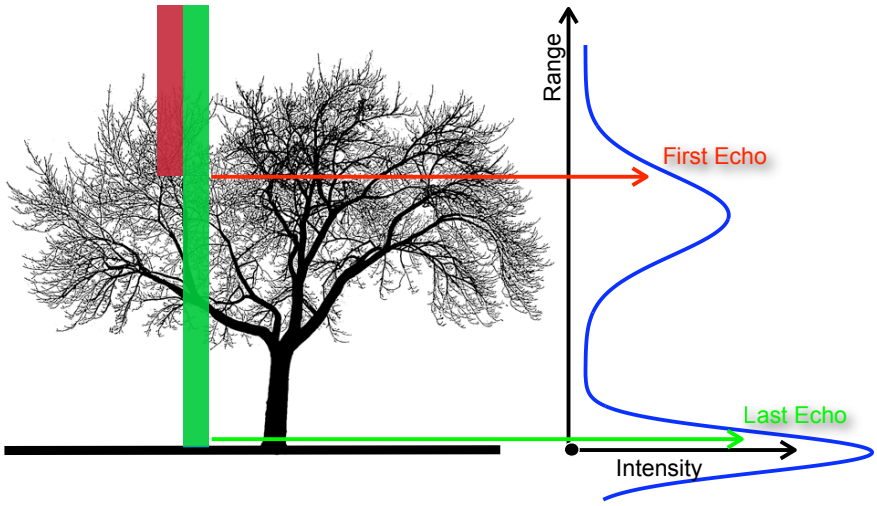

Figure 2.11: Illustration of where first and last echo would be triggered in case of a tree as scattering element.

In Figure 2.11 an illustration of the process of triggering first and last echo for a single return waveform is given. Considering the fact that some ALS systems allow for recording as much as 10 first and last echos per square meter, the high potential of ALS for describing both the horizontal and vertical structure of the vegetation is evident. In Figure 4.3 a section of LIDAR raw data returns is displayed. By looking at the raw data, for the human eye semantic information such as locations of single tree crowns or the form of the terrain can be quite easily deferred. This canopy description has the potential to deliver information on biophysical properties such as tree geometry (including height), biomass or even vegetation density estimations. The interaction of the laser beam with the canopy is based on multiple surface scattering and the intensity of the return signal is higher the larger the amount of scattering elements per unit volume is. This basic relation could be exploited to derive vegetation density estimates from ALS data. However, this relation is not a direct one, since not only the amount of scatterers but as well their orientation and reflectance control the amount of back scattered radiation (see Section 2.3.2).

To further illustrate the information content of first and last echo ALS data, the section of raw data depicted in Figure 2.7 contained a powerline. In order to differentiate between first and last echo, two different colormaps have been used; a gray scaled one for last echo data and a rainbow colored one for first echo data. One can note that in

the first echo data the powerline casts a shadow that is almost twice as wide as the laser footprint diameter. But still, last echo data seems to be triggered in any case from the ground beneath the powerline. This effect is due to the high reflectance of the powerline and manifests a potential error source for object sizes measured by ALS data. The fourth publication (Chapter 7) will deal in more detail with this phenomena.

In the next section previous approaches for derivation of biophysical properties from ALS data will be presented. A special emphasis will be given to whether the methods derive the vegetation properties in direct or indirect fashion and on how much of the derivation is automated.

Chapter 3

State of the Art and Objectives

In the context of vegetation applications based on ALS data, it will be differentiated between small-footprint and large footprint ALS data. As stated before, small-footprint ALS systems have footprint diameters in the order of some decimeters up to three meters, while large footprint systems have diameters of more than 10 meters. Thus, only small footprint systems should allow for a characterization of forest stands at the tree level. Since small-footprint ALS data are much more common in Europe, the main focus will be given to issues related to this kind of data. This is even more so, as all papers in this thesis use data provided by a small-footprint system. That is, all the following sections except Section 3.8) deal with approaches based on small-footprint ALS data, whereas the last section will provide some insight into methods based on the experimental large footprint systems available. Hyyppä et al. (2004) provide a comprehensive summary of algorithms and methods that derive forest measurements based on small-footprint ALS data. The authors classify the approaches into several fields, the presented classification of approaches is loosely following theirs.

3.1 Canopy Geometry

The vegetation property being estimated from ALS data in a most direct fashion is canopy height. Canopy height is in most cases computed as the difference of a DSM and a DTM. For vegetated areas, the resulting model is often called canopy height model (CHM). Though it is easy to manually deduce tree heights from this model, the respective values have to be taken with caution. The quality of the CHM is influenced by errors in both DTM and DSM, with the first being either too high and the latter being too low, thus manifesting a potential underestimation of tree height by ALS. This underestimation is in fact systematic and has been noticed and quantified in a number of studies (Hyyppä et al., 2001; Gaveau and Hill, 2003). Errors that might be induced by slope and terrain roughness (see Section 2.3.2) might further contribute to errors in tree height estimation.

For small-footprint ALS data collected with higher point densities (more than two points per square meter) there exists the potential to derive the geometry of single trees. These algorithms generally segment the CHM into regions that presumably belong to the same tree. Due to the large amount of raw data and since it is easier to implement

algorithms on grids, early approaches used the CHM to delineate single trees and their geometry. Hyyppä and Inkinen (1999); Hyyppä et al. (2001) were the first to present a segmentation algorithm to derive information about single trees. Their method was based on finding local maxima's in the CHM for localizing the tree tops and then using region growing to derive individual tree segments. From these segments, measures such as crown volume and crown diameter could be derived, from which again stand wise attributes, such as basal area or stem volume were computed. The standard errors they found for mean height, basal area and stem volume were all close to 10 percent, which is a quite good value for measures based on a remote sensing system. Popescu et al. (2003) proposed a similar segmentation approach based on the CHM, which used a smoothed version of the CHM; they found for their derivation of crown diameter an RMSE of 1.4 m.

Several other studies were based on a segmentation of the CHM (Andersen et al., 2001; Persson et al., 2002; Schardt et al., 2002), while other authors proposed using the raw ALS data for either segmentation (Andersen et al., 2002) or feature extraction (Pyysalo and Hyyppä, 2002; Holmgren and Persson, 2004). It was expected that the unaltered point cloud would contain additional and more precise information than the CHM, since the interpolation of raw data into models comprises a loss of information. But since the raw ALS data is vector data, special approaches are needed to extract the needed information from the pint cloud. Andersen et al. (2002) used ellipsoidal models of single pine trees and fitted those in a Bayesian framework with raw ALS data of a 0.21 ha test area, minimizing the differences between tree model and ALS data. Since this process is very time consuming, it's application to larger areas is probably not feasible.

Single tree approaches offer the advantage that the needed forest inventory information can be derived from the segmented trees, without the need of establishing a regression model as with the methods presented in Section 3.4. Thus, results based on a tree segmentation approach should be directly comparable from one site to another. However, it is unclear how much different sensor configurations influence the results of single tree extraction methods. To at least test how much variation is introduced by the methods itself, the Finnish Geodetic Institute (FGI, J. Hyyppä) started a project of comparing single tree extraction methods on the same data. The data was provided together with a small training set of field measured tree locations by FGI and each group taking part in the test provided tree locations and geometric properties. Results of this test are yet to be published, but will be published in a form similar to the EuroSDR comparison of building extraction methods (Kaartinen et al., 2005) The method described in Chapter 4 took part in this comparative study and is an automated method to derive the geometric information of single trees directly from the raw data.

3.2 Canopy Density

Due to the ability of the ALS data to reveal an insight into both the vertical and horizontal structure of canopy, interest was high to try to deduce measures of vegetation density, such as biomass, fractional cover or leaf area index. Biomass is an important parameter for ecologists in the framework of carbon uptake studies and is relevant in

the context of the Kyoto protocol. Thus, there has been a large interest into passive remote sensing methods for the retrieval of canopy density related parameters, since some of these passive sensors are space-borne and allow global coverage. Parameters being of high relevance are leaf area index (LAI) and fractional cover (fCover). LAI was first defined as the total one-sided area of photo synthetic tissue per unit ground surface area (Watson, 1947). This definition is only valid for broad leaf forests though, and consequently Myneni et al. (1997) defined the LAI as the maximum projected leaf area per unit ground surface area. fCover is defined as the fraction of ground covered by vegetation over uncovered ground. Both LAI and fCover are dimensionless parameters, even though LAI is often given as meter square per meter square to illustrate it's meaning as an area ratio. For passive optical sensors, there exists a long tradition of deriving LAI by the use of regression models from the reflectance data (Chen and Cihlar, 1996; Carlson and Ripley, 1997; Gower et al., 1999; Weiss and Baret, 1999; Eklundh et al., 2001; Chen et al., 2002; Colombo et al., 2003; Lee et al., 2004; Wang et al., 2004). Since LAI can not be directly estimated from reflectance values, the use of radiative transfer models (that simulate reflectance values) for the estimation of biophysical parameters has been increasing in recent years. Generally, an inversion process is used to derive LAI and other biophysical parameters from the reflectance values measured by the remote sensing systems (Atzberger, 2004; Fang et al., 2003; Haboudane et al., 2004; Koetz et al., 2005, 2004; Meroni et al., 2004; Myneni et al., 1997; Tian et al., 2003). ALS system generally do not provide coverage of large areas, but due to the direct nature of their measurement, effort was put into developing methodologies that could derive canopy density estimates from ALS data. Even though small-footprint ALS systems generally do not record the full waveform of the return signal, which is a quite direct measure of canopy density, a few studies have shown that both LAI and fCover could be derived on stand level from ALS data (Lovell et al., 2003; Hagiwara et al., 2004). Lovell et al. (2003) provided a methodology to derive fCover and LAI based on ALS and ground based LIDAR data. Their computation of LAI was based on a foliage profile. A validation was carried out using hemispherical photographs. They found that the absolute values of fCover are scale dependent; the larger the pixel size, the lower the value of fCover is. This effect is due to averaging out pixels with high fCover by pixels with little or no vegetation (small fCover) when transitioning to higher resolutions. Todd et al. (2003) retrieved the horizontal and vertical distribution of light transmittance inside the canopy through the use of an Optech ALS system. They compared this ALS derived structural information with field measurements of the fraction of photosynthetically active radiation (FPAR) and concluded that discrete return LIDAR data could capture the relevant foliage characteristics needed for development of functional linkages between biophysical and ecological studies.

One of the major difficulties that these approaches face is the lack of high quality ground truth data. The only way of precisely estimating the LAI of a tree is destructive sampling, thus being quite impractical for estimating the LAI of larger areas. Consequently, methods were established that measure some aspect of the light regime inside the canopy and try to infer the LAI e.g. based on measured gap fraction. These methods are basically remote sensing methods of their own, with their own problems and limitations. A comprehensive summary of the underlying theory is given by Jonckheere

et al. (2004), while a comparison of different measurement systems was carried out by Weiss et al. (2004). Today, the most commonly used techniques are either the LAI 2000[1] or hemispherical photographs, with the latter being increasingly popular due to the availability of high resolution CCDs. Furthermore, hemispherical photographs offer the advantage of error tracing, since the image provides as well information on measurement conditions. Thus, images containing direct sunlight can be excluded from a series of ground truth data, as e.g. was done for our second paper presented in Chapter 5. Using precise georeferencing, linking of single hemispherical photographs with areas of laser raw data becomes possible (Riano et al., 2004b), opposed to working on stand or plot level. A similar approach will be presented in the second paper, putting special interest on the scales where ground truth data and ALS data correlate the best.

3.3 Properties Relevant for Fire/Fuel Modeling

ALS data is of special interest for the wildland fire community. Wildland fire is a complex 4-d problem best described by fluid dynamics. Hence, the interest into data about characterizing fuel distribution in three dimensions has been high. Properties being of large relevance are the spatial arrangements of trees, their crown length and their crown density. Especially crown base height and crown bulk density serve as direct input into empirical fire models such as FARSITE (Finney, 1998). Thus, Riano et al. (2003) and Riano et al. (2004a) presented a methodology to gain these parameters from regions of raw ALS data being about 10 by 10 meter in size. Andersen et al. (2005) used regression models to link field measured estimates of crown fuel weight, crown bulk density, crown base height and canopy height with ALS data. This was again done on a larger scale of about 20 meters. While the results of these approaches are directly usable for fire behavior models such as FARSITE, they still lack a more detailed, three dimensional description of the fuel bed, which should become possible with high point density, small footprint ALS data. This kind of data would then fit within the requirements of more sophisticated fire behavior models (Morvan and Dupuy, 2001; Linn et al., 2002; Séro-Guillaume and Margerit, 2002; Margerit and Séro-Guillaume, 2002).

3.4 Statistical Approaches on Stand Scale

For approaches on stand scale, the most common method of deriving vegetation properties is by regression models. These models need to be tuned with field data for each vegetation domain and ALS acquisition setting. An early hint towards this direction was given by Næsset (1997), who correlated forest inventory variables such as mean tree height and stem volume with stand wise statistics (height histograms) of ALS raw data. The potential of this approach to derive forest inventory information was further explored by Means et al. (2000), who derived mean tree height and stem volume for single stands from ALS data. Another approach was presented by Næsset (2002) using a practical two-step procedure. The driving factor behind his approach was the desire to make forest inventory based on ALS data operational. His methodology comprises

[1] www.licor.com

the measurement of the requested forest variables (e.g. mean tree height, stem number, basal area) on a certain amount of test plots in the field, then using multiple regression models to link the field data with so-called ALS predictor variables. These models are then used to derive the forest information for the whole area covered by ALS data. Typical ALS predictor variables are height percentiles based on a statistic of ALS raw data echos for areas of plot size (10-30 meter in diameter). This method provides good results, but since for every vegetation domain and different ALS sensor model new field data needs to be collected, it is quite labour intensive. Furthermore, a quantitative comparison of data from different sites is difficult. Popescu et al. (2002) compared a statistical method for the derivation of tree height with a method based on single trees, and found better results for the single tree method. Whether this finding is robust needs to be tested as well by studies using higher point densities; they were using ALS which had a point density as low as 0.5 points per square meter. Lim et al. (2003) quantitatively analysed the explanatory value of specific LIDAR metrics (e.g. 90% height percentile) for typical forestry parameters. They found that laser height metrics would best explain mean canopy height and stem density, but still could explain a lot of the variation in other properties, such as above-ground biomass and stand volume. Næsset et al. (2005) have compared several kinds of regression techniques for this approach, stating that the choice of the regression method itself does not have a statistical influence on the results. It is well accepted that the statistical methods provide good results for ALS data of lower point densities, for which single tree approaches would not work that well.

3.5 Fusion of ALS data with passive optical imaging sensors

The fusion of ALS with optical imaging sensors is quite promising, since the two instrument types provide different, but still complementary information. Some ALS systems are already operated together with a line scanner, which allows for the generation of true orthophotos (Schnadt and Katzenbeisser, 2004), since a DSM is provided by the ALS. Gougeon et al. (2001) stated that a close to optimal forest inventory system could be built using an ALS system allowing for individual tree recognition (high point density needed) and a multispectral sensor for species recognition of these single trees. Popescu and Wynne (2004) used fusion of ALS and multispectral optical data for differentiating forest types, which improved their ALS based canopy height statistics. Regarding species detection, Holmgren and Persson (2004) state that ALS data alone can be used to differentiate pine and spruce trees, since their spectral signatures do not differentiate enough. Since they used ALS data with a very high point density, they were able to reconstruct the crown shape of single trees to an extent that allowed for discrimination of pine and spruce trees. Newer approaches use radiative transfer models to fuse large footprint LIDAR data and hyper-spectral imagery. Koetz et al. (2006) showed that using a specialized RTM for both LIDAR and imaging spectroscopy would improve the derivation of some of the biophysical parameters being retrieved by model inversion over using solely imaging spectroscopy data. It is well acknowledged that for future approaches a more fundamental understanding of the involved physical processes is needed.

3.6 Effects of Data Acquisition

Based on theory, we can infer that the acquisition conditions should have an influence on the quality of ALS data. For instance, the measured height will be different if a slope is sampled with different scan angles. Point density influences the accuracy to which objects can be reconstructed, and the footprint size influences the penetration of the laser beam into vegetation. It is hard to relate errors to single acquisition properties, since by changing the altitude the maximum scan angle, the point density and footprint size on ground will be altered as well. Thus, some researchers have tried to use simple models of the acquisition geometry to single out the effects on data quality. Holmgren et al. (2003) used such a model to compute the effect scanning angle would have on tree height statistics and canopy closure properties (e.g. fCover). They found that tree height was less affected by scanning angle, while canopy closure measures are affected to a larger extend. This is due to the laser pulse traveling a longer distance through the vegetation for large scan angles, thus the probability of hitting canopy elements is getting higher and the canopies seems to be denser. As acquisition parameters often have to be optimized to be cost effective while still providing accurate data, Ahokas et al. (2005) used a numerical model to find an optimum scanning angle for large area acquisitions. They found a serious degradation of tree height measured by ALS only for scanning angles larger than 15 degrees. They stated as well that flying at higher altitudes increases the standard deviation of height measurements to $\pm$ 20 cm, which is probably sufficient for most applications. Lovell et al. (2005) used a similar model of the canopy to find optimal acquisition parameters for forest height retrieval.

Special interest was given to the effect of point spacing for canopies with different tree spacing. They found as well that height measures would degrade toward the edges of the swath; their conclusion was that it was probably due to lower point spacing. But, this behavior might as well have been an effect of the large scan angle at the edge of the swath. A more empirical study was carried out by Næsset (2004), who compared several first and last echo statistics (ALS predictor variables) for two different flight levels ($\sim$ 500 m and $\sim$ 850 m AGL). Only one out of 54 first echo statistics differed significantly from one flight level to the other. The last echo statistics were more susceptible to the changed altitude, being in general about 50 cm higher for the higher flight altitude. Density measures were as well significantly affected by changing the altitude, with higher values for the higher altitude.

3.7 Full waveform

Due to advances in technology, some system providers (e.g. Riegl and Optech) now offer small footprint ALS systems that record the full-waveform of the return signal. These systems should offer the benefit of revealing physical properties of the scatterers, e.g. their cross-section. First approaches (Persson et al., 2005) used these waveforms to generate additional echos to the two default laser echos (first/last), providing more detail in the vertical dimension. However, when using these additional echos for statistics such as the predictor variables commonly used in the methods described in Section 3.4, the statistics might be altered in an unknown way, since not all the echos would rep-

resent scatterers of equal strength. A solution to this problem would be the approach of Wagner et al. (2006), who uses Gaussian decomposition (as e.g. Hofton et al. (2000) for large footprint sensors) to retrieve the amplitude and half-width of each peak detected in the return waveform. If one stores these values together with the location of the peak, one has all the necessary information to compute the cross-section of the scatterer, which is finally a physical meaningful variable. Since these small footprint, full waveform sensors are just becoming available, there have not been so many applications so far. Some studies point out the potential of the full waveform, be it for classification of echos prior to DTM generation (Ducic et al., 2006) or for a more precise location of building edges (Jutzi et al., 2005).

3.8 Large Footprint

Probably due to the fact that the landmass of the United States is so much bigger than that of European countries and that larger regions have a less complex topography, large footprint systems are primarily used by US research groups. NASA had the plan to launch a space-borne LIDAR system to monitor the earth's vegetation, and as a airborne prototype the LVIS system was developed. It offered a footprint size of 10 to 25 meter while recording the full waveform. Many studies have shown that this system is capable of deriving tree height, biomass and other vegetation parameters at stand level (Lefsky et al., 1999a,b; Means et al., 1999, 2000; Blair et al., 2001; Drake et al., 2002). (Hofton et al., 2000) presented a methodology to derive the height of single scatterers from a return waveform by Gaussian decomposition. A smoothed version of the waveform was searched for local maxima's, who's locations were used as starting points in a least square matching procedure. Peterson et al. (2001) modeled LVIS waveforms using a simple geometric model named GORT (Ni et al., 1999). This model is similar to that of Sun and Ranson (2000), which was used by Koetz et al. (2006) to show that it could be inverted for the retrieval of biophysical parameters. Newer studies showed that LVIS can as well be used for habitat mapping (Hyde et al., 2005) or mapping of fuel properties that might be input into wildland fire behavior models (Peterson et al., 2003). Fusion with other earth observation systems has also been accomplished, as e.g. by Hyde et al. (2006). The advantage of using such a large footprint systems is that it could cover larger areas with lower costs. However, LVIS remains an experimental system that suffers from inaccuracies in sloped or undulated terrain and the anisotropic distribution of energy inside the footprint. All LIDAR systems have a similar energy distribution, but for a large footprint systems it might cause problems due to the lower granularity of the data. For instance, Hyde et al. (2005) noted that their tree height statistics had errors in cases were large trees were close to the edge of the illuminated area (footprint), since they would not reflect enough energy back to be detected in the return waveform. This problem will not arise using small-footprint ALS systems as long as the tree scale is much larger than the footprint scale.

3.9 Objectives and research questions

Advances in navigation technology, namely the combination of dGPS and precise INS systems and their integration with LIDAR nowadays allow for a three-dimensional characterization of the earth's surface with unprecedented precision and resolution. Many variables describing the state of the vegetation canopy that are of high interest to ecologists, but namely foresters and fire researchers are related in some way to the three-dimensional structure of the vegetation canopy. These relations are suspected to be found on all scales that are apparent in a forest environment, be it the scale of the stand, the scale of a single tree or even scales as small as the branch or leaf level. Since small footprint ALS data provides information on scales that are in-between the scale of single trees and the branch scale, one can expect that it is possible to derive information on all scales larger than that in a quite direct fashion, and, since the discrete echos (first/last) provide another information dimension, maybe even on scales smaller than that of the laser footprint. In the last sections, the state of the art regarding the derivation of biophysical vegetation properties from ALS data was presented. There exist approaches on tree scale and stand scale that derive information on both vegetation structure and vegetation density. Some of the vegetation properties relevant for foresters and fire behavior modelers can be derived in a direct fashion from laser data (e.g. canopy height) and others (e.g. canopy density) in a more indirect fashion, e.g. by the use of regression models. There are as well methods available that use technology from image processing or cognitive computing to defer information from the laser point cloud that is already visible to the human eye (e.g. the location of single trees) but can not be extracted in a practical way for larger data sets. However, since laser raw data usually sums up to a large amount of data, algorithms that automatically defer the needed information are needed. Finally, the interaction of the laser pulse itself with the vegetation and how it is altered by different acquisition conditions is not yet well enough understood. Thus, there are several challenges to face when deriving biophysical vegetation properties from airborne laser scanning data:

- How can the three-dimensional structure of the vegetation at the single tree level automatically be extracted from ALS raw data, and what are the accuracies obtained? (first publication, Chapter 4)
- Does discrete return raw ALS data contain information about vegetation density at scales as small as the laser footprint and if so, can that information be extracted in a direct fashion? (second publication, Chapter 5)
- How robust are the derivation methods with respect to acquisition conditions such as flight altitude and scan angle? (third publication, Chapter 6)
- How might different spatial or spectral properties of the targets affect object detectability and measured object dimensions? (fourth publication, Chapter 7)

These research questions are dealt with in four different chapters, with each being a separate publication. Following this, a synopsis presents the research questions again and confronts these with the major findings of the different publications. The next

chapter contains the first publication concerned with the automatic extraction of single tree geometry from ALS raw data.

Bibliography

Ahokas, E., Yu, X., Oksanen, J., Hyyppä, J., Kaartinen, H., Hyyppä, H., 2005. Optimization of the scanning angle for countrywide laser scanning. In: Vosselman, G., Brenner, C. (Eds.), International Archives of Photogrammetry, Remote Sensing and Spatial Information Sciences. Vol. XXXVI, PART 3/W19 of 115-119. ISPRS.

Allgöwer, B., Bur, M., Stähli, M., Koutsias, N., Tinner, W., Conedera, M., Stadler, M., Kaltenbrunner, A., 2003. Can Long-term Wildland Fire History Help to Design Future Fire and Landscape Management? An Approach from the Swiss Alps. 3rd International Wildland Fire Conference and Exhibition, Sydney, Australia, 11.

Allgöwer, B., Harvey, S., Rüegsegger, M., 1998. Fuel Models for Switzerland: Description, Spatial Pattern, Index for Crowning and Torching. 3rd International Conference on Forest Fire Research / 14th Conference on Fire and Forest Meteorology, Luso, Portugal, 2605–2620.

Andersen, H.-E., McGaughey, R. J., Reutebuch, S. E., 2005. Estimating forest canopy fuel parameters using lidar data. Remote Sensing of Environment 94 (4), 441–449.

Andersen, H.-E., Reutebuch, S. E., Schreuder, G. F., 2001. Automated individual tree measurement through morphological analysis of a lidar-based canopy surface model.

Andersen, H.-E., Reutebuch, S. E., Schreuder, G. F., 2002. Bayesian object recognition for the analysis of complex forest scenes in airborne laser scanner data. In: ISPRS Commission III, Symposium 2002 September 9 13, . G. A. (Ed.), ISPRS Commission III, Symposium 2002 September 9 - 13, 2002, Graz, Austria. pp. A–035 ff (7 pages).

Atzberger, C., 2004. Object-based retrieval of biophysical canopy variables using artificial neural nets and radiative transfer models. Remote Sensing of Environment 93 (1-2), 53–67.

Axelsson, P., 1999. Processing of laser scanner data -algorithms and applications. ISPRS Journal of Photogrammetry & Remote Sensing 54 (2-3), 138–147.

Baltsavias, E. P., 1999a. Airborne laser scanning: basic relations and formulas. ISPRS Journal of Photogrammetry & Remote Sensing 54 (2-3), 199–214.

Baltsavias, E. P., 1999b. Airborne laser scanning: existing systems and firms and other resources. ISPRS Journal of Photogrammetry & Remote Sensing 54, 164–198.

Bernard, M. L., Carbonel, M., Nimour, N., 2000. Are large wildland fires - as anomalous ecologic processes - natural hazards. Physics and Chemistry of the Earth, Part A: Solid Earth and Geodesy 25 (12), 763–768.

Blair, J. B., Hofton, M. A., Luthcke, S. B., 2001. Wide-swath imaging lidar development for airborne and spaceborne applications. International Archives of Photogrammetry and Remote Sensing XXXIV-3/W4, 17–20.

Blair, J. B., Rabine, D. L., Hofton, M. A., 1999. The laser vegetation imaging sensor: a medium-altitude, digitisation-only, airborne laser altimeter for mapping vegetation and topography. ISPRS Journal of Photogrammetry & Remote Sensing 54 (2-3), 115–122.

Brenner, C., 2005. Building reconstruction from images and laser scanning. International Journal of Applied Earth Observation and Geoinformation 6 (3-4), 187–198.

Carlson, T. N., Ripley, D. A., 1997. On the relation between NDVI, fractional vegetation cover, and leaf area index. Remote Sensing of Environment 62 (3), 241–252.

Chasmer, L., Hopkinson, C., Treitz, P., 2006. Investigating laser pulse penetration through a conifer canopy by integrating airborne and terrestrial lidar. Canadian Journal of Remote Sensing 32 (2), 116–125.

Chen, J. M., Cihlar, J., 1996. Retrieving leaf area index of boreal conifer forests using Landsat TM images. Remote Sensing of Environment 55 (2), 153–162.

Chen, J. M., Pavlic, G., Brown, L., Cihlar, J., Leblanc, S. G., White, H. P., Hall, R. J., Peddle, D. R., King, D. J., Trofymow, J. A., 2002. Derivation and validation of canada-wide coarse-resolution leaf area index maps using high-resolution satellite imagery and ground measurements. Remote Sensing of Environment 80 (1), 165–184.

Chuvieco, E., 2003. Wildland Fire Danger Estimation and Mapping - The Role of Remote Sensing Data. World Scientific.

Clark, M. L., Clark, D. B., Roberts, D. A., 2003. Small-footprint lidar estimation of sub-canopy elevation and tree height in a tropical rain forest landscape. Remote Sensing of Environment 91, 68–91.

Colombo, R., Bellingeri, D., Fasolini, D., Marino, C. M., 2003. Retrieval of leaf area index in different vegetation types using high resolution satellite data. Remote Sensing of Environment 86 (1), 120–131.

Countryman, C. M., 1972. The fire environment concept. Berkley, CA, Pacific Southwest Forest and Range Experiment Station, 12pp.

Cramer, M., 1997. GPS/INS Integration. Photogrammetric Week Wichmann Verlag, Heidelberg.

Drake, J. B., Dubayah, R. O., Clark, D. B., Knox, R. G., Blair, J. B., Hofton, M. A., Chazdon, R. L., Weishampel, J. F., Prince, S. D., 2002. Estimation of tropical forest structural characteristics using large-footprint lidar. Remote Sensing of Environment 79, 305–319.

Ducic, V., Hollaus, M., Ullrich, A., Wagner, W., Melze, T., 2006. 3d vegetation mapping and classification using full-waveform laser scanning. International Workshop 3D Remote Sensing in Forestry Vienna, Feb., 14-15, 2006, 211–217.

Eklundh, L., Harrie, L., Kuusk, A., 2001. Investigating relationships between landsat etm+ sensor data and leaf area index in a boreal conifer forest. Remote Sensing of Environment 78 (3), 239–251.

Fang, H., Liang, S., Kuusk, A., 2003. Retrieving leaf area index using a genetic algorithm with a canopy radiative transfer model. Remote Sensing of Environment 85 (3), 257–270.

Finney, M., 1998. FARSITE: Fire Area Simulator-Model. Development and Evaluation. USDA Forest Service Research Paper, RMRS-RP-4.

Finney, M. A., Jun. 2005. The challenge of quantitative risk analysis for wildland fire. Forest Ecology and Management 211 (1-2), 97–108.

Forestry Department and FAO of the United Nations, 2001. Global forest fire assessment 1990-2000. Tech. rep., Forest Resources Assessment Programme.

Gaveau, D., Hill, R., 2003. Quantifying canopy height underestimation by laser pulse penetration in small-footprint airborne laser scanning data. Canadian Journal of Remote Sensing 29, 650–657.

Gougeon, F. A., St-Onge, B. A., Wulder, M., Leckie, D. G., 2001. Synergy of Airborne Laser Altimetry and Digital Videography for Individual Tree Crown Delineation. Proc. 23rd Canadian Symposium on Remote Sensing / 10e Congrés de l'Association québécoise de télédétection Sainte-Foy, Qubec, Canada, (CD–ROM).

Gower, S. T., Kucharik, C. J., Norman, J. M., 1999. Direct and indirect estimation of leaf area index, fapar, and net primary production of terrestrial ecosystems. Remote Sensing of Environment 70, 29–51.

Gruen, A., Zhang, L., 2006. Automated Generation of the 3D Structure of Forest Canopy. International Workshop 3D Remote Sensing in Forestry Vienna, Feb., 14-15,, 32–39.

Guyette, R. P., Spetich, M. A., Jul. 2003. Fire history of oak-pine forests in the Lower Boston Mountains, Arkansas, USA. Forest Ecology and Management 180 (1-3), 463–474.

Haala, N., Brenner, C., 1998. Interpretation of urban surface models using 2d building information. Computer Vision and Image Understanding 72 (2), 204–214.

Haala, N., Brenner, C., 1999. Extraction of buildings and trees in urban environments. ISPRS Journal of Photogrammetry & Remote Sensing 54 (2-3), 130–137.

Habeck, J. R., Mutch, R. W., Oct. 1973. Fire-dependent forests in the northern rocky mountains. Quaternary Research 3 (3), 408–424.

Haboudane, D., Miller, J. R., Pattey, E., Zarco-Tejada, P. J., Strachan, I. B., 2004. Hyperspectral vegetation indices and novel algorithms for predicting green lai of crop canopies: Modeling and validation in the context of precision agriculture. Remote Sensing of Environment 90 (3), 337–352.

Hagiwara, A., Imanishi, J., Hashimoto, H., Morimoto, Y., 2004. Estimating leaf area index in mixed forest using an airborne laser scanner. In: International Archives of Photogrammetry, Remote Sensing and Spatial Information Sciences ISSN 1682-1750 VOLUME XXXVI, PART 8/W2.

Harding, D., Lefsky, M., Parker, G., Blair, J., 2001. Laser altimeter canopy height profiles: Methods and validation for closed-canopy, broadleaf forests. Remote Sensing of Environment 76, 283–297.

Harding, D. J., Carabajal, C. C., 2005. Icesat waveform measurements of within-footprint topographic relief and vegetation vertical structure. Geophysical Research Letters 32, L21S10, doi:10.1029/2005GL023471.

Hofton, M. A., Minster, J. B., Blair, J. B., 2000. Decomposition of laser altimeter waveforms. IEEE Transactions on Geoscience and Remote Sensing 38, 1989–1996.

Holmgren, J., Nilsson, M., Olsson, H., 2003. Simulating the effects of lidar scanning angle for estimation of mean tree height and canopy closure. Canadian Journal of Remote Sensing 29, 623–632.

Holmgren, J., Persson, A., 2004. Identifying species of individual trees using airborne laser scanner. Remote Sensing of Environment 90, 415–423.

Hyde, P., Dubayah, R., Peterson, B., Blair, J., Hofton, M., Hunsaker, C., Knox, R., Walker, W., Jun. 2005. Mapping forest structure for wildlife habitat analysis using waveform lidar: Validation of montane ecosystems. Remote Sensing of Environment 96 (3-4), 427–437.

Hyde, P., Dubayah, R., Walker, W., Blair, J. B., Hofton, M., Hunsaker, C., May 2006. Mapping forest structure for wildlife habitat analysis using multi-sensor (lidar, sar/insar, etm+, quickbird) synergy. Remote Sensing of Environment 102 (1-2), 63–73.

Hyyppä, J., Hyyppä, H., Litkey, P., Yu, X., Haggrén, H., Rönnholm, P., Pyysalo, U., Pitkänen, J., Maltamo, M., 2004. Algorithms and methods of airborne laser scanning for forest measurements. In: International Archives of Photgrammetry, Remote Sensing and Spatial Information Sciences, Vol. XXXVI - 8/W2.

Hyyppä, J., Inkinen, M., 1999. Detecting and estimating attributes for single trees using laser scanner. Photogrammetric Journal of Finland 16, 27–42.

Hyyppä, J., Kelle, O., Lehikoinen, M., Inkinen, M., 2001. A segmentation-based method to retrieve stem volume estimates from 3-d tree height models produced by laser scanners. IEEE Transactions on Geoscience and Remote Sensing 39, 969–975.

Jonckheere, I., Fleck, S., Nackaerts, K., Muys, B., Coppin, P., Weiss, M., Baret, F., 2004. Review of methods for in situ leaf area index determination: Part i. theories, sensors and hemispherical photography. Agricultural and Forest Meteorology 121 (1-2), 19–35.

Jutzi, B., Neulist, J., Stilla, U., 2005. Sub-pixel edge localization based on laser waveform analysis. International Archives of Photogrammetry and Remote Sensing XXXVI, 109–115.

Jutzi, B., Stilla, U., 2003. Laser pulse analysis for reconstruction and classification of urban objects. International Archives of Photogrammetry and Remote Sensing 34, Part 3/W8, 151–156.

Jutzi, B., Stilla, U., 2005. Erfassung und Analyse der zeitlichen Signalform bei gepulsten Lasersystemen. pers. Mitteilung, 11.

Kaartinen, H., Hyyppä, J., Gülch, E., Vosselman, G., Hyyppä, H., Matikainen, L., Hofmann, A., Mäder, U., Persson, Å., Söderman, U., Elmqvist, M., Ruiz, A., Dragoja, M., Flamanc, D., Maillet, G., Kersten, T., Carl, J., Hau, R., Wild, E., Frederiksen, L., Holmgaard, J., Vester, K., 2005. Accuracy of 3D City Models: EuroSDR comparison. International Archives of Photogrammetry and Remote Sensing XXXVI, 227–232.

Katzenbeisser, R., 2003a. About the calibration of lidar sensors. ISPRS Workshop 3-D Reconstruction form Airborne Laser-Scanner and InSAR data" Dresden.

Katzenbeisser, R., 2003b. Echo detection. Technical Note.

Koetz, B., Baret, F., Poilve, H., Hill, J., 2005. Use of coupled canopy structure dynamic and radiative transfer models to estimate biophysical canopy characteristics. Remote Sensing of Environment 95 (1), 115–124.

Koetz, B., Morsdorf, F., Sun, G., Ranson, K. J., Itten, K., Allgower, B., 2006. Inversion of a lidar waveform model for forest biophysical parameter estimation. IEEE Geoscience and Remote Sensing Letters 3, 49–53.

Koetz, B., Schaepman, M., Morsdorf, F., Itten, K., Allgöwer, B., 2004. Radiative transfer modeling within a heterogeneous canopy for estimation of forest fire fuel properties. Remote Sensing of Environment 92 (3), 332–344.

Kraus, K., Pfeifer, N., 1998. Determination of terrain models in wooded areas with airborne laser scanner data. ISPRS Journal of Photogrammetry & Remote Sensing 53, 193–203.

Kraus, K., Pfeifer, N., 2001. Advanced DTM Generation from LIDAR Data. International Archives of Photogrammetry and Remote Sensing XXXIV-3/W4, 23–35.

Lee, K.-S., Cohen, W. B., Kennedy, R. E., Maiersperger, T. K., Gower, S. T., 2004. Hyperspectral versus multispectral data for estimating leaf area index in four different biomes. Remote Sensing of Environment 91 (3-4), 508–520.

Lefsky, M. A., Cohen, W. B., Acker, S. A., Parker, G. G., Spies, T. A., Harding, D., 1999a. Lidar remote sensing of the canopy structure and biophysical properties of douglas-fir western hemlock forests. Remote Sens. Environ. 70, 339–361.

Lefsky, M. A., Harding, D., Cohen, W. B., Parker, G., Shugart, H. H., 1999b. Surface lidar remote sensing of basal area and biomass in deciduous forests of eastern maryland, usa. Remote Sensing of Environment 67, 83–98.

Lim, K., Treitz, P., Baldwin, K., Morrison, I., Green, J., 2003. Lidar remote sensing of biophysical properties of tolerant northern hardwood forests. Canadian Journal of Remote Sensing 29 (5), 658–678.

Linn, R., Reisner, J., Colman, J. J., Winterkamp, J., 2002. Studying wildfire behavior using FIRETEC. International Journal of Wildland Fire 11, 233–246.

Lithopoulos, E., 1999. The Applanix Approach to GPS/INS Integration. Photogrammetric Week Wichmann Verlag, Heidelberg.

Lovell, J., Jupp, D., Culvenor, D., Coops, N., 2003. Using airborne and ground-based ranging lidar to measure canopy structure in Australian forests. Canadian Journal of Remote Sensing 29 (5), 607–622.

Lovell, J., Jupp, D., Newnham, G., Coops, N., Culvenor, D., Aug. 2005. Simulation study for finding optimal lidar acquisition parameters for forest height retrieval. Forest Ecology and Management 214 (1-3), 398–412.

Maas, H.-G., 1999. The potential of height texture measures for the segmentation of airborne laserscanner data. Fourth International Airborne Remote Sensing Conference and Exhibition 21st Canadian Symposium on Remote Sensing, Ottawa, Ontario, Canada.

Maas, H.-G., 2002. Methods for measuring height and planimetry discrepancies in airborne laserscanner data. Photogrammetric Engineering & Remote Sensing 68 (9), 933–940.

Maas, H.-G., Vosselman, G., 1999. Two algorithms for extracting building models from raw laser altimetry data. ISPRS Journal of Photogrammetry & Remote Sensing 54 (2-3), 153–163.

Margerit, J., Séro-Guillaume, O., 2002. Modeling forest fires. Part II: Reduction to two-dimensional models and simulation of propagation. International Journal of Heat and Mass Transfer 45, 1723–1737.

Mbow, C., Goita, K., Benie, G. B., May 2004. Spectral indices and fire behavior simulation for fire risk assessment in savanna ecosystems. Remote Sensing of Environment 91 (1), 1–13.

Means, J. E., Acker, S. A., Fitt, B. J., Renslow, M., Emerson, L., Hendrix, C., 2000. Predicting forest stand characteristics with airborne scanning lidar. Photogrammetric Engineering & Remote Sensing 66 (11), 1367–1371.

Means, J. E., Acker, S. A., Harding, D. J., Blair, J. B., Lefsky, M. A., Cohen, W. B., Harmon, M. E., McKee, W. A., 1999. Use of Large-Footprint Scanning Airborne Lidar To Estimate Forest Stand Characteristics in the Western Cascades of Oregon. Remote Sensing of Environment 67, 298–308.

Meroni, M., Colombo, R., Panigada, C., 2004. Inversion of a radiative transfer model with hyperspectral observations for LAI mapping in poplar plantations. Remote Sensing of Environment 92 (2), 195–206.

Miller, J. D., Yool, S. R., Aug. 2002. Modeling fire in semi-desert grassland/oak woodland: The spatial implications. Ecological Modelling 153 (3), 229–245.

Morvan, D., Dupuy, J. L., Oct. 2001. Modeling of fire spread through a forest fuel bed using a multiphase formulation. Combustion and Flame 127 (1-2), 1981–1994.

Murakami, H., Nakagawa, K., Hasegawa, H., Shibata, T., Iwanami, E., 1999. Change detection of buildings using an airborne laser scanner. ISPRS Journal of Photogrammetry & Remote Sensing 54 (2-3), 148–152.

Myneni, R., Nemani, R., Running, S., 1997. Estimation of global leaf area index and absorbed PAR using radiative transfer models. IEEE Transactions on Geoscience and Remote Sensing 35, 1380–1393.

Næsset, E., 1997. Estimating timber volume of forest stands using airborne laser scanner data. Remote Sensing of Environment 61 (2), 246–253.

Næsset, E., 2002. Predicting forest stand characteristics with airborne scanning laser using a practical two-stage procedure and field data. Remote Sensing of Environment 80 (1), 88–99.

Næsset, E., 2004. Effects of different flying altitudes on biophysical stand properties estimated from canopy height and density measured with a small-footprint airborne scanning laser. Remote Sensing of Environment 91 (2), 243–255.

Næsset, E., Bollandsas, O. M., Gobakken, T., 2005. Comparing regression methods in estimation of biophysical properties of forest stands from two different inventories using laser scanner data. Remote Sensing of Environment 94 (4), 541–553.

Ni, W., Li, X., Woodcock, C., Caetano, M., Strahler, A., 1999. An analytical hybrid gort model for bidirectional reflectance over discontinuous plant canopies. IEEE Transactions on Geoscience and Remote Sensing 37, 987–999.

Nilsson, M., 1996. Estimation of tree heights and stand volume using an airborne lidar system. Remote Sensing of Environment 56, 1–7.

Pedlosky, J., 1992. Geophysical Fluid Dynamics. Springer.

Persson, A., Holmgren, J., Söderman, U., 2002. Detecting and measuring individual trees using an airborne laser scanner. Photogrammetric Engineering & Remote Sensing 68 (9), 925–932.

Persson, A., Söderman, U., Töpel, J., Ahlberg, S., 2005. Visualization and analysis of full-waveform airborne laser scanner data. International Archives of Photogrammetry and Remote Sensing XXXVI.

Peterson, B., Hyde, P., Hofton, M., Dubayah, R., Fites-Kaufman, J., Hunsaker, C., Blair, J., 2003. Deriving canopy structure for fire modeling from lidar. EARSEL - 4th International Workshop: Remote Sensing and GIS applications for Forest Fire Management, Ghent.

Peterson, B., Ni-Meister, W., Blair, J., Hofton, M., Hyde, P., Dubayah, R., 2001. Modeling lidar waveforms using a radiative transfer model. International Archives of Photogrammetry and Remote Sensing XXXIV-3/W4, 121–124.

Popescu, S. C., Wynne, R. H., 2004. Seeing the Trees in the Forest: Using Lidar and Multispectral Data Fusion with Local Filtering and Variable Window Size for Estimating Tree Height. Photogrammetric Engineering & Remote Sensing 70, 589–604.

Popescu, S. C., Wynne, R. H., Nelson, R. F., Dec. 2002. Estimating plot-level tree heights with lidar: local filtering with a canopy-height based variable window size. Computers and Electronics in Agriculture 37 (1-3), 71–95.

Popescu, S. C., Wynne, R. H., Nelson, R. F., 2003. Measuring individual tree crown diameter with lidar and assessing its influence on estimating forest volume and biomass. Canadian Journal of Remote Sensing 29, 564–577.

Pyne, S., Andrews, P., Laven, R. (Eds.), 1996. Introduction to Wildland Fire. Wiley, New York.

Pyysalo, U., Hyyppä, H., 2002. Reconstructing tree crowns from laser scanner data for feature extraction. In: ISPRS Commission III, Symposium 2002 September 9 - 13, 2002, Graz, Austria. pp. B–218 ff (4 pages).

Reutebuch, S. E., McGaughey, R. J., Andersen, H.-E., Carson, W. W., 2003. Accuracy of a high-resolution lidar terrain model under a conifer forest canopy. Canadian Journal of Remote Sensing 29, 527–535.

Riano, D., Chuvieco, E., Condes, S., Gonzalez-Matesanz, J., Ustin, S. L., 2004a. Generation of crown bulk density for pinus sylvestris l. from lidar. Remote Sensing of Environment 92 (3), 345–352.

Riano, D., Meier, E., Allgöwer, B., Chuvieco, E., Ustin, S. L., 2003. Modeling airborne laser scanning data for the spatial generation of critical forest parameters in fire behavior modeling. Remote Sensing of Environment 86 (2), 177–186.

Riano, D., Valladares, F., Condes, S., Chuvieco, E., 2004b. Estimation of leaf area index and covered ground from airborne laser scanner (lidar) in two contrasting forests. Agricultural and Forest Meteorology 124 (3-4), 269–275.

Rothermel, R. C., 1972. A mathematical model for predicting fire spread in wildland fuels. Research Paper INT- 115 Ogden, UT: U.S. Department of Agriculture, Forest Service, Intermountain Forest and Range Experiment Station., 40p.

Russell, W. H., McBride, J. R., Aug. 2003. Landscape scale vegetation-type conversion and fire hazard in the San Francisco bay area open spaces. Landscape and Urban Planning 64 (4), 201–208.

Schardt, M., Ziegler, M., Wimmer, A., Wack, R., Hyyppä, J., 2002. Assessment of forest parameters by means of laser scanning. In: ISPRS Commission III, Symposium 2002 September 9 - 13, 2002, Graz, Austria. pp. A–302 ff (8 pages).

Schenk, T., Seo, S., Csatho, B., 2001. Accuracy study of airborne laser scanning data with photogrammetry. International Archives of Photogrammetry and Remote Sensing XXXIV-3/W4, 113–118.

Schnadt, K., Katzenbeisser, R., 2004. Unique airborne fiber scanner technique for application-oriented lidar products. International Archives of Photogrammetry and Remote Sensing XXXVI - 8/W2, 19–23.

Séro-Guillaume, O., Margerit, J., 2002. Modeling forest fires. part i: a complete set of equations derived by extended irreversible thermodynamics. International Journal of Heat and Mass Transfer 45, 1705–1722.

St-Onge, B., Hu, Y., Véga, C., 2006. Reconstruct Forest Canopy Height Using Stereo-Ikonos Panchromatic Images and a LIDAR DTM. International Workshop 3D Remote Sensing in Forestry , Vienna, Feb. 14-15, 2006, 97–102.

Stephens, S. L., Jun. 1998. Evaluation of the effects of silvicultural and fuels treatments on potential fire behaviour in Sierra Nevada mixed-conifer forests. Forest Ecology and Management 105 (1-3), 21–35.

Sun, G., Ranson, K., 2000. Modeling lidar returns from forest canopies. IEEE Transactions on Geoscience and Remote Sensing 38 (6), 2617–2626.

Tian, Y., Wang, Y., Zhang, Y., Knyazikhin, Y., Bogaert, J., Myneni, R. B., 2003. Radiative transfer based scaling of lai retrievals from reflectance data of different resolutions. Remote Sensing of Environment 84 (1), 143–159.

Todd, K. W., Csillag, F., Atkinson, P. M., 2003. Three-dimensional mapping of light transmittance and foliage distribution using lidar. Canadian Journal of Remote Sensing 29 (5), 544–555.

Vosselman, G., Dijkman, S., 2001. 3d building model reconstruction from point clouds and ground plans. International Archives of Photogrammetry and Remote Sensing XXXIV-3/W4, 37–43.

Wagner, W., Ullrich, A., Briese, C., 2003. Der Laserstrahl und seine Interaktion mit der Erdoberfläche. Österreichische Zeitschrift für Vermessung & Geoinformation 4, 223–235.

Wagner, W., Ullrich, A., Ducic, V., Melzer, T., Studnicka, N., Apr. 2006. Gaussian decomposition and calibration of a novel small-footprint full-waveform digitising airborne laser scanner. ISPRS Journal of Photogrammetry and Remote Sensing 60 (2), 100–112.

Wang, Y., Woodcock, C. E., Buermann, W., Stenberg, P., Voipio, P., Smolander, H., Hame, T., Tian, Y., Hu, J., Knyazikhin, Y., Myneni, R. B., May 2004. Evaluation of the MODIS LAI algorithm at a coniferous forest site in Finland. Remote Sensing of Environment 91 (1), 114–127.

Watson, D. J., 1947. Comparative physiological studies in the growth of field crops. i. variation in net assimilation rate and leaf area between species and varieties, and within and between years. Annals of Botany 11, 41–76.

Wehr, A., Lohr, U., 1999. Airborne laser scanning - an introduction and overview. ISPRS Journal of Photogrammetry & Remote Sensing 54 (2-3), 68–82.

Weiss, M., Baret, F., 1999. Evaluation of canopy biophysical variable retrieval performances from the accumulation of large swath satellite data. Remote Sensing of Environment 70 (3), 293–306.

Weiss, M., Baret, F., Smith, G. J., Jonckheere, I., Coppin, P., 2004. Review of methods for in situ leaf area index (LAI) determination: Part II. Estimation of LAI, errors and sampling. Agricultural and Forest Meteorology 121 (1-2), 37–53.

Zoller, H., 1995. Vegetationskarte des Schweizerischen Nationalparks. Erläuterungen. National Park Forschung, 108.

Chapter 4

LIDAR Based Geometric Reconstruction of Boreal Type Forest Stands at Single Tree Level for Forest and Wildland Fire Management

This chapter has been published as: F. Morsdorf, E. Meier, Benjamin Kötz, K.I. Itten, M. Dobbertin, and Britta Allgöwer. *LIDAR Based Geometric Reconstruction of Boreal Type Forest Stands at Single Tree Level for Forest and Wildland Fire Management* **Remote Sensing of Environment, Volume 92, Issue 3, Pages 353-362**, 30. August 2004
Reprinted with Permission.

Abstract

Vegetation structure is an important parameter in fire risk assessment and fire behavior modeling. We present a new approach deriving the structure of the upper canopy by segmenting single trees from small-footprint LIDAR data and deducing their geometric properties. The accuracy of the LIDAR data is evaluated using 6 geometric reference targets, with the standard deviation of the LIDAR returns on the targets being as low as 0.06 m. The segmentation is carried out by using cluster analysis on the LIDAR raw data in all three coordinate dimensions. From the segmented clusters, tree position, tree height, and crown diameter are derived and compared with field measurements. A robust linear regression of 917 tree height measurements yields a slope of 0.96 with an offset of 1 m and the adjusted R^2 resulting at 0.92. However, crown diameter is not well matched by the field measurements, with R^2 being as low as 0.2, which is most certainly due to random errors in the field measurements. Finally, a geometric reconstruction of the forest scene using a paraboloid model is carried out using values of tree position, tree height, crown diameter, and crown base height.

4.1 Introduction and Problem Statement

Forest Fires are biogeophysical processes controlled by physical properties such as weather, fuel, and topography Countryman (1972); Pyne et al. (1996). Deriving robust estimates of these parameters has always been an important task in wildland fire risk assessment. As the weather can be described by a combination of forecast models and station measurements and as the topography is not time-dependent, the fuel complex is probably the most difficult to estimate due to its higher temporal and spatial variability. The physical fuel properties include quantity, size, compactness, and arrangement, and can be estimated for each of the fuel components as ground, surface, and crown fuel Pyne et al. (1996). The role of remote sensing in estimating these properties has been increasing in recent years Chuvieco (2003), with special emphasis on new high resolution active and passive optical sensors. Airborne laser scanning offers a great potential for deriving physical fuel properties, and algorithms deriving structural forest parameters (such as tree height, tree position, crown diameter, crown base height) in a spatial context have been successfully implemented by a number of researchers Means et al. (2000); Drake et al. (2002a); Næsset and Okland (2002). As this structural information relates to arrangement, quantity, and size, it is relevant for wild-land fires and can be used as input for existing fire behavior models such as FARSITE and BEHAVE Finney (1998). New thermodynamic fire models have been developed that are not based on empirical equations (such as for FARSITE or BEHAVE), but on a closed set of physical laws and equations describing most of the relevant chemical and physical processes in wild-land fire behavior Séro-Guillaume and Margerit (2002); Margerit and Séro-Guillaume (2002). These models need input data on higher spatial scales (since they for instance explicitly model combustion at the sub-tree scale) and can use structural information based on single tree metrics.

Two different types of laser scanners are most commonly used: small- and large-footprint laser scanners Lefsky et al. (2002). Most of the large footprint laser scanners are able to record the full continuous waveform of the return signal, as for instance LVIS Drake et al. (2002b), whereas the small footprint laser scanners record only discrete returns; in the case of the TopoSys system used in this study these are the first and the last pulse of the signal. The input for fire behavior models that can be derived from large-footprint LIDAR data are: elevation, slope, aspect, canopy height, canopy cover, and canopy bulk density, with a spatial scale in the order of 15 to 25 m Peterson et al. (2003). All the parameters that can be derived from large footprint systems can be derived from small footprint systems as well, if the single returns are used to model a waveform as done by Riano et al. (2003). However, the small footprint data contains valuable structural information on smaller scales (about 1 m) that is not used when modeling the waveform on scales of about 10 to 15 m. As small-footprint LIDAR systems with high point density ($> 10\, points/m^2$) are now available Baltsavias (1999), the derivation of these geometric properties on a single tree basis has been subject to recent research, but mainly applied for standard forestry applications Næsset and Bjerknes (2001). Previous approaches mostly focused on segmentation of the Digital Surface Model (DSM) for the detection of single trees Hyyppä et al. (2001); Persson et al. (2002); St-Onge and Achaichia (2001). Since the processing step from the LIDAR point cloud

to a DSM always includes loss of information, working with the LIDAR raw data has been increasing Pyysalo and Hyyppä (2002); Brandtberg et al. (2003), even though the sheer amount of data makes it hard to handle on larger scales. Andersen et al. (2002) for instance have proposed fitting ellipsoid crown models in a Bayesian framework to the raw LIDAR data, including a probabilistic modeling of the crown - laser pulse interaction. Clustering in raw data has been used for terrain, vegetation and building detection Roggero (2001), but to our knowledge not for segmenting single trees. We will present a practical two stage procedure for segmenting single trees from the LIDAR raw data itself. Our objective is to derive geometric properties from segmented clusters of laser points belonging to a specific tree, without altering the original data. Finally, a geometric reconstruction of the forest scene should become possible that can be used in physically based fire behavior models.

4.2 Data and Test Site

4.2.1 Test Site and Field Data

The study area for the acquisition of the field data is located in the eastern Ofenpass valley, which is part of the Swiss National Park (SNP). The same area has been used as test site in the study of Koetz et al. (2004). The Ofenpass represents a dry inner-alpine valley with rather little precipitation (900-1100 mm/a). Surrounded by 3000 meter peaks, the Ofenpass valley starts at about 1500 m a.s.l. in the west and quickly reaches an average altitude of about 1900 m a.s.l towards the east. Embedded in this environment are boreal type forests where few, but very impacting (stand-replacing) fires besides frequent fire scares were observed. The ecology of these stands and their long-term fire history were subject of ongoing studies in the same area Allgöwer et al. (2003). The south-facing Ofenpass forests, the location of the field measurement, are largely dominated by mountain pine (Pinus montana ssp. arborea) and some stone pine (Pinus cembra) as a second tree species, being of interest for natural succession Zoller (1992); Lauber and Wagner (1996). These forest stands can be classified as woodland associations of Erico-Pinetum mugo Zoller (1995). The understory is characterized by low and dense vegetation composed mainly of Vaccinium, Ericaceae, and Seslaria species. The study area has also been subject to previous fuel modeling studies where three main fuel models could be identified through extensive field studies Allgöwer et al. (1998). Therein model A 'mixed conifers' equals the association Rhodendro ferruginei-Laricetum, Model B 'mountain pine' the Erico-Pinetum mugo and model C 'dwarfed mountain pine' the Erico-Pinetum mugo prostratae. In the present study the field measurements were taken within forest stands corresponding to the model B since this is the dominant fuel type of the area. On a small subset of the test region, the Swiss Federal Institute for Forest, Snow and Landscape Research (WSL) maintains a long-term forest monitoring site. This site contains about 2000 trees with diameter at breast height (DBH) larger than 0.12 m, which have been geolocated and whose geometric properties including tree height, crown diameter, and stem diameter have been measured using standard forestry tools. Crown diameter was estimated using a compass and by calculating the crown diameter from the included angle. In Figure 4.1 an overview of the

test site is given. More than 20 % of the stand are upright standing dead trees, with the minimum tree age being 90 years, the mean and maximum being 150 and 200 years respectively. The whole stand has regenerated after a period of clear cutting in the 18th and 19th century, and has been without any management since the foundation of the Swiss National Park in 1914. The main cause for dying of the trees is the root rot fungi, as described in Dobbertin et al. (2001).

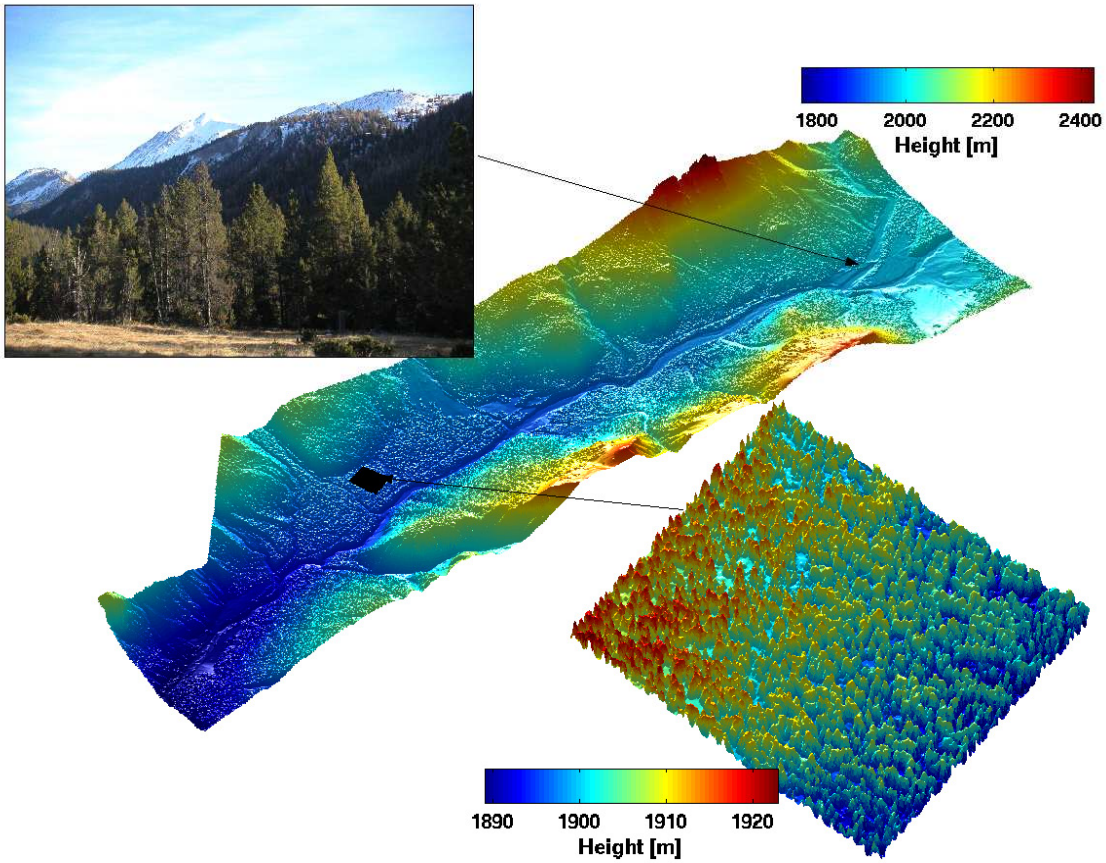

Figure 4.1: The Digital Surface Model (DSM) of the Ofenpass area in the Swiss National Park. The area containing the long-term monitoring site of the WSL is enlarged. The photograph was taken on the day of the LIDAR flight.

4.2.2 Laser Scanning Data

In October 2002 a helicopter based LIDAR flight was carried out over the test area, covering a total area of about 14 km^2. The LIDAR system used was the Falcon Sensor developed and maintained by the German company TopoSys. The system is a push-broom laser altimeter recording both first and last reflection from the laser signal on the ground (first/last pulse). The flight was conducted with a nominal height over ground of 850 m, leading to an average point density of more than 10 points per square meter (p/m^2). A smaller subset of the area (0.6 km^2) was overflown with a height of 500 m above ground, resulting in a point density of more than 20 p/m^2, thus combining the

two datasets yields to a point density of more than 30 p/m^2 for both first and last pulse. This density has been used in this study. The footprint sizes were about 30 cm in diameter for 850 m flight altitude and about 20 cm in diameter for 500 m altitude. The raw data delivered by the sensor (x,y,z - triples) was processed into gridded elevation models by TopoSys using the company's own processing software. The DSM was processed using the first pulse reflections, the Digital Terrain Model (DTM) was constructed using the last returns and filtering algorithms. The grid spacing was 1 m for the large area and 0.5 m for the smaller one, with a height resolution of 0.1 m in both cases.

4.2.3 Quality Assessment

The quality of the LIDAR data was assessed using 6 geometric reference targets being 3 m by 3 m in size. The targets were leveled to less than 0.5 degrees, using a digital angle meter. The positions of the 4 corners of each target (see Fig. 4.2) were determined using a GPS and theodolite measurements resulting in an internal accuracy of less than 2 cm. Regarding the models (DSM/DTM), the absolute positional accuracy was determined by Toposys (using the target positions) to be similar to or less than the resolution of the models, with horizontal positional accuracy being below 0.5 m and vertical accuracy better than 0.15 m.

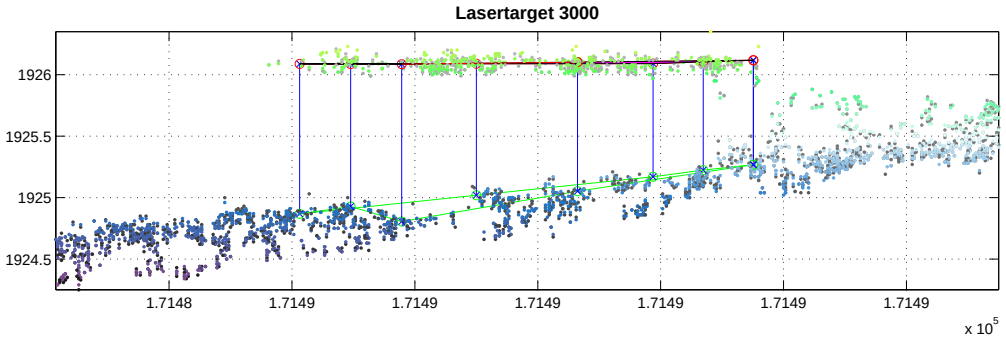

Figure 4.2: Side view of one of the 6 geometric reference targets with the LIDAR raw data points superimposed. The color denotes height. The points being beneath the target are in front and behind the target in three-dimensional space.

Furthermore, we used the reference targets to infer the noise of the sensor on a plain, homogeneously reflecting surface, which is the best case reflecting scenario. To estimate the sensors noise, we calculated the standard deviation of all points reflected from the target, as can be seen in Figure 4.2. A positional offset was calculated using the center of gravity (COG) derived from the laser points being on the targets with the COG of the targets themselves. The center of gravity is derived according to Equation 4.1.

$$COG = [\overline{x}; \overline{y}]; \tag{4.1}$$

These offsets only account for the internal accuracy of the adjusted laser-strips, since a previously found translational offset of 3.5 m in easting and 1 m in northing had been

ID	points	$\Delta\ height$	$\sigma\ height$	$\Delta\ x$	$\Delta\ y$
1000	215	3	6.8	9	7
2000	266	-2	5.9	24	-11
3000	151	-2	6.6	6	6
4000	381	1	5.6	15	-3
5000	302	-2	5.8	4	15
6000	276	2	5.2	25	-18

Table 4.1: Using the reference target data, we calculated the mean height difference of all points ($\Delta\ height$) on the laser target with the mean target height, the standard deviation of the points on the laser target ($\sigma\ height$), and the differences of the positions of the centers of gravity ($\Delta\ x$ and $\Delta\ y$). The second column gives the number of points on a reference target , with first *and* last pulse being counted. The values in the last four columns are given in centimeter.

applied by Toposys to all of the data. The values for offsets and noise are listed in Table 4.1.

4.3 Segmentation Through k-Means Clustering

As we did not want to lose any of the information contained in the three-dimensional point cloud, we decided to do a cluster analysis of the raw x,y,z - triples in all three coordinate dimensions, opposed to working on the gridded DSM. Cluster analysis is a well known statistical tool for dividing feature spaces into areas containing values similar to each other, with this similarity being determined by a specific metric. In our case, the feature space is spanned by the coordinate axes x, y, and z and we use a simple Euclidean distance metric. The *k*-means clustering algorithm itself tries to minimize the overall sum of distances of the points in feature space to their so-called cluster centroids or buoys. This happens in a iterative manner, where, as a first step, the initial centroids are most often randomly chosen with the convergence of the clustering to a global minimum being heavily dependent on these starting locations. So the success of using cluster analysis boils down to a clever or exhaustive determination of these starting positions. Since pine tree crowns are of a general ellipsoidal shape, with the treetops being horizontally centered, we propose the use of local maxima derived from the DSM as starting positions (*seed points*). This can be achieved using a simple filter on the depth image, and is thus much easier to implement than a determination of the seed points in the raw data itself. Hence, the first stage of the segmentation process will be the seed point extraction from the DSM, the second the cluster analysis starting off these locations.

For the detection of local maxima in a DSM Hyyppä et al. (2001) proposed applying a smoothing filter on the DSM for smoothing out the tree tops (the 'hat' formed by the upper part of the tree crown), followed by a morphological operation for finding pixels having all 8 neighbors smaller than the center pixel. The kernel size and weights of the smoothing filter are important parameters since they have to be tuned for each DSM

resolution and expected crown diameters. For our data, having a grid resolution of 0.5 m and mean crown diameters of 1.7 m, we have chosen a 3×3 kernel filter with the following weights: $[1\ 2\ 1; 2\ 4\ 2; 1\ 2\ 1]/16$.

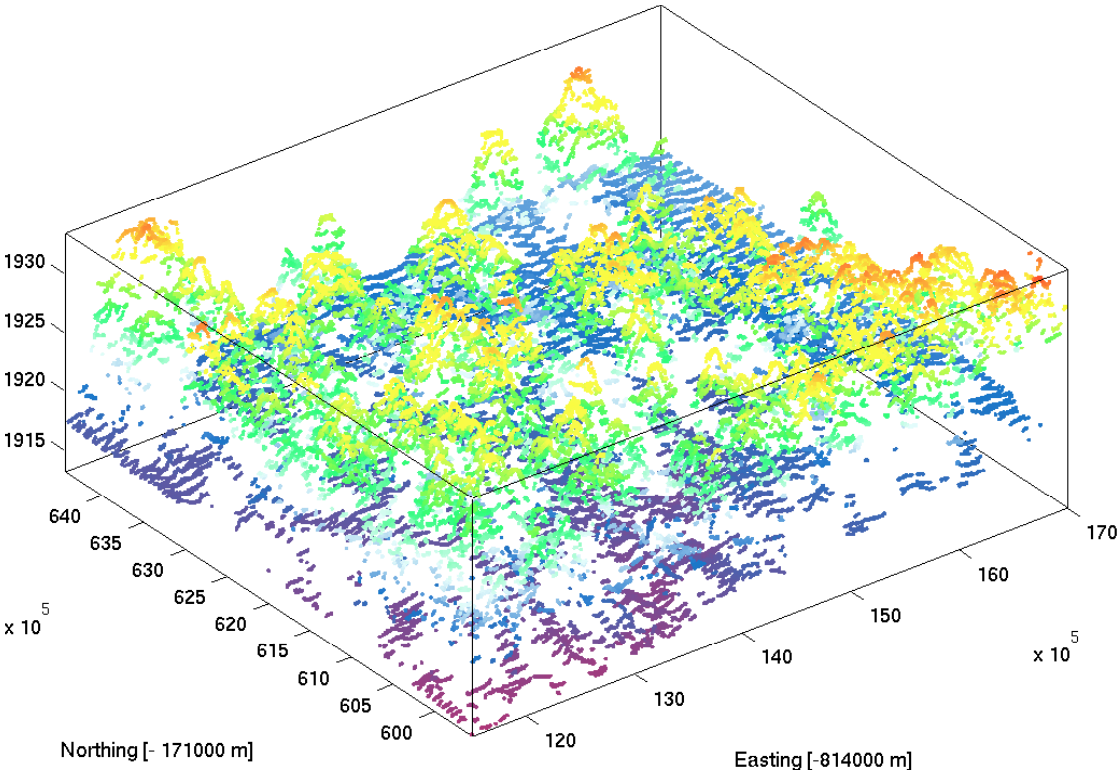

Figure 4.3: The LIDAR raw data (x,y,z - triples) as seen from the side, combined from the two overflights. Yellow and red represent high z-values, while blue and violet colors are low values.

Since clustering with an Euclidean metric favors ball shaped clusters in a three dimensional feature space, we introduce a scaling argument for the z-coordinate. This is done to accommodate for the aspect ratio of pine tree crowns, which in our case ranges from 3 to 6, hence the height of the tree crown is 3 to 6 times larger than the crown diameter. Based on the field data, we have chosen a value of 3 as a starting point and have found good results using this scaling number for the z-axis. For clustering, both, first and last pulse data is being used without differentiation of the two. The k-means clustering algorithm used is the one implemented in the Statistics Toolbox in MATLAB, using the information from Spath (1985). The algorithm clusters the data in an iterational process divided into two steps. The first step uses so called *batch updates*, where each iteration consists of reassigning points to their nearest cluster centroid all at once, which is followed by a recalculation of the cluster centroids. During the second step of *online updates* points are individually reassigned if that reduces the sum of distances and the cluster centroids are recomputed after each assignment. As we did not want to cluster ground returns as well, a cutoff distance of 1 m above ground was applied, derived from the DTM. A sample of the raw data used is depicted in Figure 4.3. We combined the data from the two overflights, resulting in an extremely high point den-

sity ($> 30\, p/m^2$). However tests have shown that the segmentation works as well using only the data from the higher over flight, with only the feature extraction suffering due to the lower point density. Features such as tree height and crown volume are biased towards lower values with reduced sampling density due to under-sampling. It should be noted that the pine tree crowns in the test area are rather small in diameter (1.5 to 3 m), so that the high point density would compare to a normal point density in areas with larger tree crowns.

As small-footprint LIDAR raw data can sum up to about 400 MB per km^2 this results in a large amount of time consuming processing. But none of the steps described in this processing scheme does need human interaction: the processing can be done automatically. As clustering a larger area all at once is not feasible, we used 50×50 m windows with an overlap of 50%. The clustered data was joined automatically afterwards, eliminating double clusters in the overlapping parts and partial clusters at the edges. For the smaller subset of about 0.6 km^2 the clustering took about two days on a state-of-the-art PC, with still some redundancy due to the 50% overlapping clustering window, resulting in clustering the whole area twice.

The outcome of the clustering is depicted in Figure 4.4. The raw data points have been projected in the x, y - plane for better visibility of the horizontal boundaries. The numbers (as well as the colors) represent cluster identifiers assigned during the segmentation process.

4.4 Results

4.4.1 Derivation of Geometric Properties

After clustering, a single cluster will presumably consist only of LIDAR returns from a single tree *crown*. Hence all information relating to crown geometry will be contained in these returns. The most important geometric properties (tree height, position) can be derived directly from these returns by finding the maximum value of z or by computing the center of gravity as described in Equation 4.1. However, other properties such as crown diameter or crown base height need a more sophisticated treatment of the point cloud. Crown diameter d was estimated from the segmented point cloud by dividing the number of returns contained in a cluster by the mean point density, thus yielding an area covered by the crown. From this area a diameter A was derived using the relation for a circle $d = 2 * \sqrt{\frac{A}{\pi}}$. Using the convex hull for estimating the area of the crowns was not feasible, since crowns are not necessarily of convex shape. Wether a more sophisticated algorithm determines the outline of the crown superiorly is subject of recent work. Crown base height is computed using 95 $\%$ percentile of the z - values contained in a cluster. Using this value, crown height can be computed as tree height minus the height of the base of the crown. These values can then be used with a simple geometric tree model to reconstruct the forest stand as seen in Fig. 4.9 .

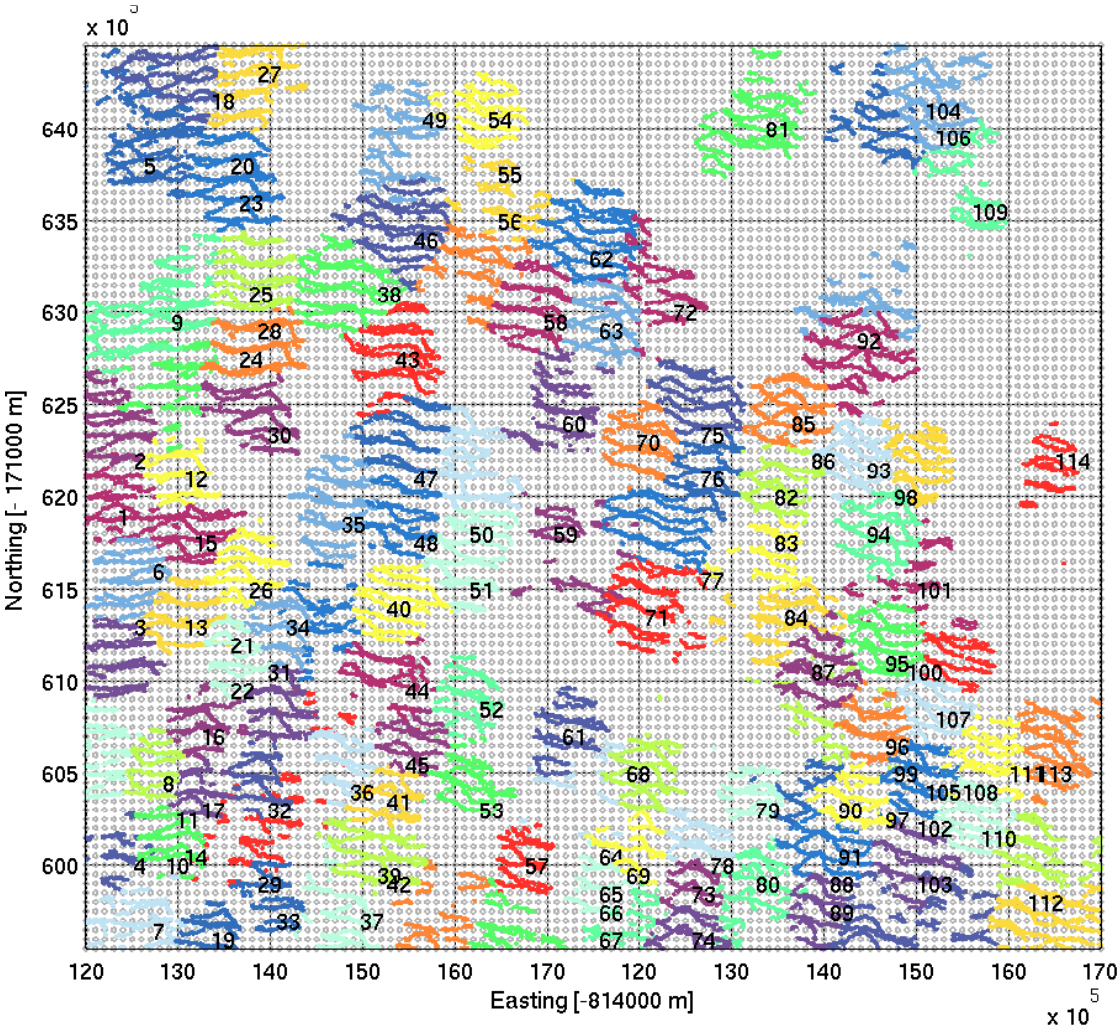

Figure 4.4: The segmented LIDAR points projected in the x, y- plane, the different colors represent the cluster assignment and are randomly chosen for each cluster for better visibility of cluster boundaries.

4.4.2 Matching the Field Data with the Tree Clusters

Since we had to deal with about 2000 trees residing in the database of WSL we had to come up with an automatic matching of field tree data with cluster data. The total number of segmented clusters was considerably less than the number of field inventory trees (about 1200 compared to 1984). This was due to the fact that in the field inventory groups of trees standing very close ($< 1m$) to each other, they are identified as several single trees, whereas the LIDAR derived clusters of returns were composed of all of these trees.

Having several stems very close to each other is a typical feature of the pine vegetation in the Swiss National Park. We solved this problem by assigning each field tree with the closest LIDAR derived cluster, using distance and tree height as matching criteria. This way, a cluster could be assigned to more than one field measurement, compensating for areas with several trees in a very small radius (typically less than 1

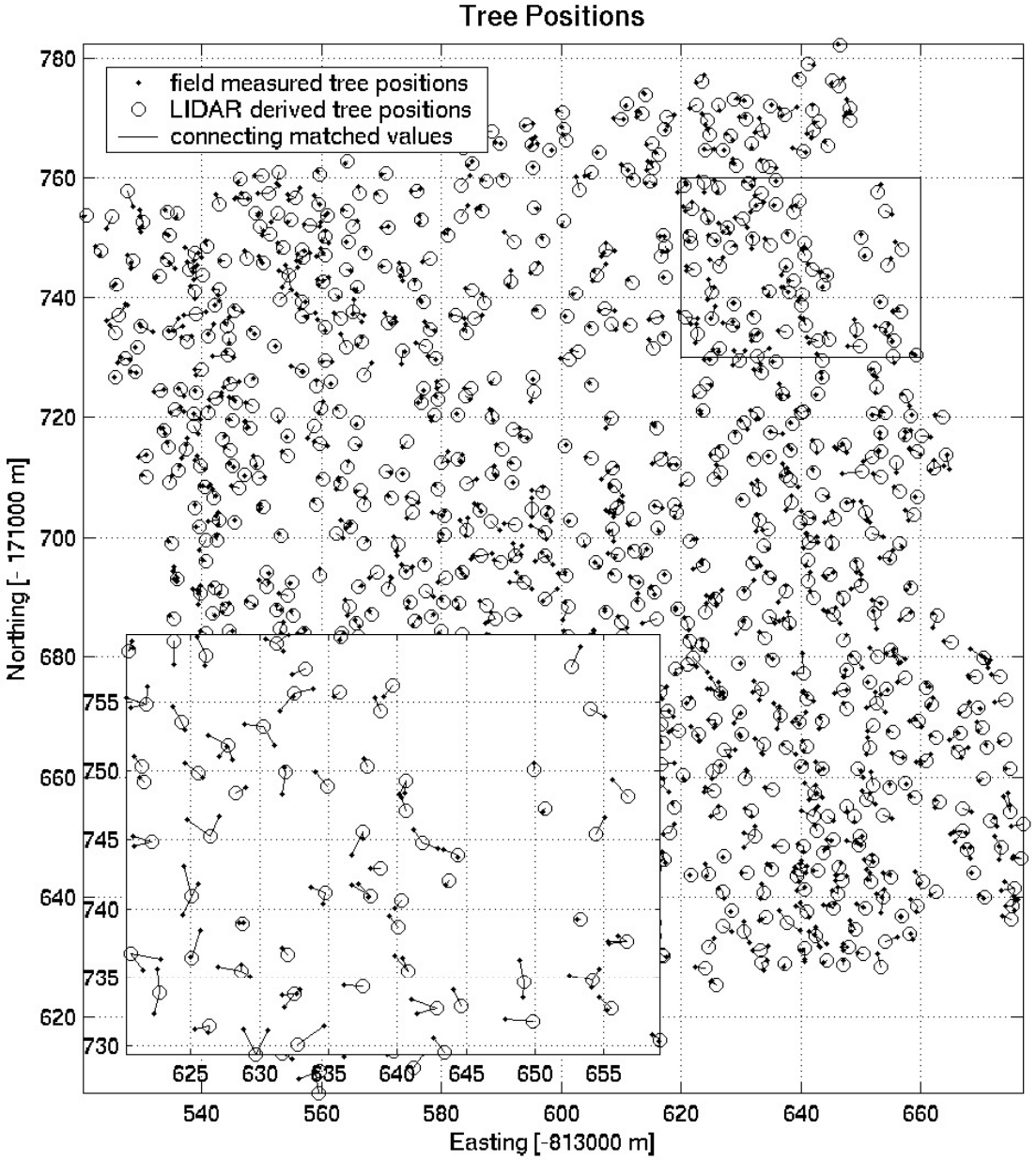

Figure 4.5: The matching of the field measured tree positions (dots) and the LIDAR determined (circles) positions is done automatically. The lines connect the matched tree locations. A LIDAR tree can be matched with more than one field data tree to overcome the effect of tree clumping. The area contained in the rectangle in the upper right is enlarged in the lower left.

m). The outcome of this matching can be seen in Figure 4.5. Furthermore, it is visible from Figure 4.5 that the matching is quite good for the middle and top-left region, while being considerably inferior for the top-right and bottom-left region of the image. At these locations the WSL intensified their field work and added understory trees into their monitoring scheme and trees with a DBH (diameter at breast height) of less than 0.12 m. Hence we do have more field data trees being assigned to one LIDAR derived

tree height in these regions. If more than one field measurement was assigned to a cluster, only the tallest tree was chosen for the robust regression in Fig. 4.6, since the highest point in the LIDAR cluster would belong to that tree. It should be noted that the automatic matching may introduce mismatch, and thus some tree height estimations are way off, as can be seen in Fig. 4.6

4.4.3 Validation with field data

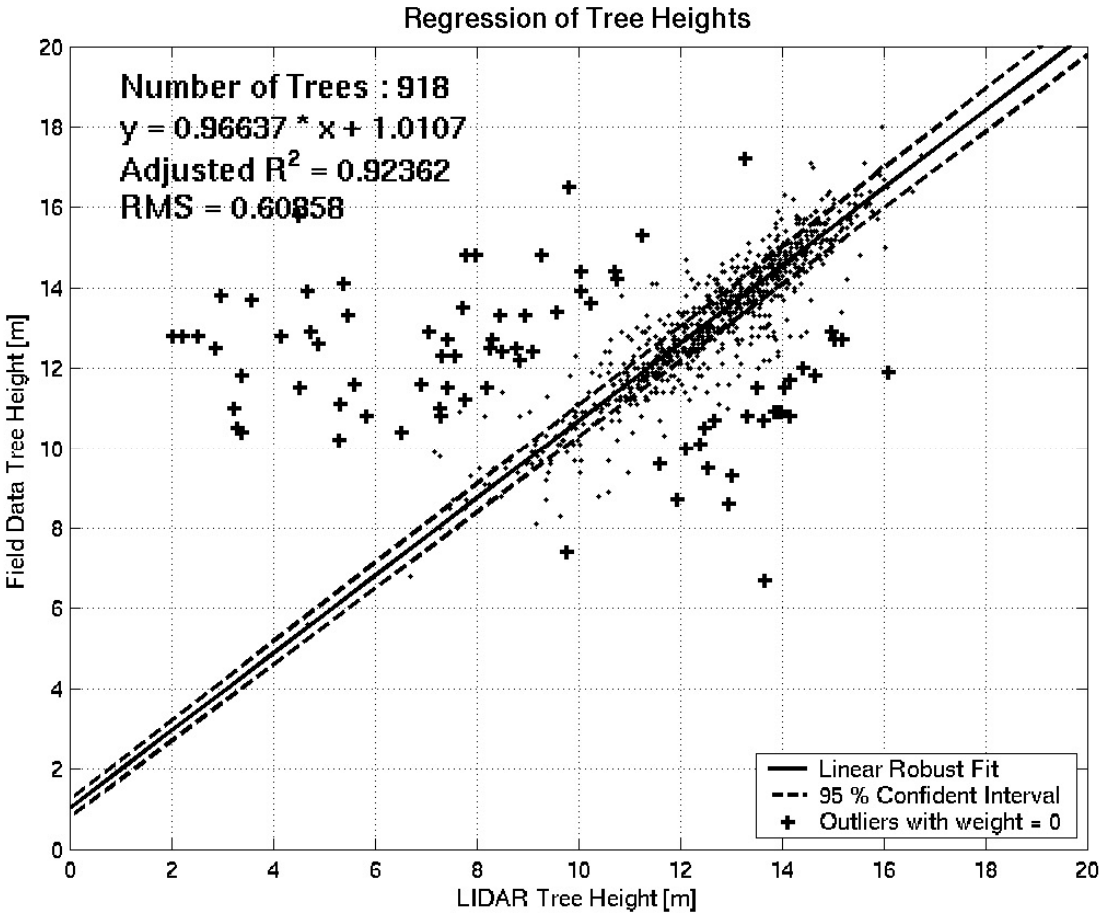

Figure 4.6: A robust regression of the field measured tree heights against LIDAR derived tree heights is carried out, which uses weights on outliers from the linear model to reduce their influence in the fit. Errors for the linear's model coefficients are derived and included as green dashed lines in the graph.

Having matched the clustered data with the field data, we can carry out a robust regression of LIDAR derived tree heights and field data tree heights. The tree height is derived as the maximum height of the LIDAR points belonging to a specific cluster. In Fig. 4.6, we chose to use a robust regression Huber (1981) over a normal linear regression, because of outliers introduced through the automated matching process; these are due to mismatch. This can be done since far the most of the data points reveal the linear relationship (as inferred from the histogram of the weights used on

the data values), and furthermore, we have more than 900 data points allowing such a statistical approach. This robust regression calculates iteratively bisquare weights on those data points that do not fit the linear model to reduce their influence on the fit. The calculated errors for the linear model's coefficients are included in the graph. The linear fit reveals a slope close to 1 (0.96) and an offset of 0.98; this manifests a systematic underestimation of tree heights by the LIDAR data, which is consistent with previous work Næsset (2002); Hyyppä et al. (2001) and due to the fact that the treetop is not necessarily sampled by the laser scanner. This underestimation will get smaller with higher point density. Gaveau and Hill (2003) have quantified this effect for small footprint LIDAR data and have as well found another source of underestimation. The vegetation needs a critical density to trigger a first pulse reflection and thus, even if the tree top is sampled, the LIDAR pulse penetrates the vegetation to a certain distance. This distance depends on vegetation density and footprint size.

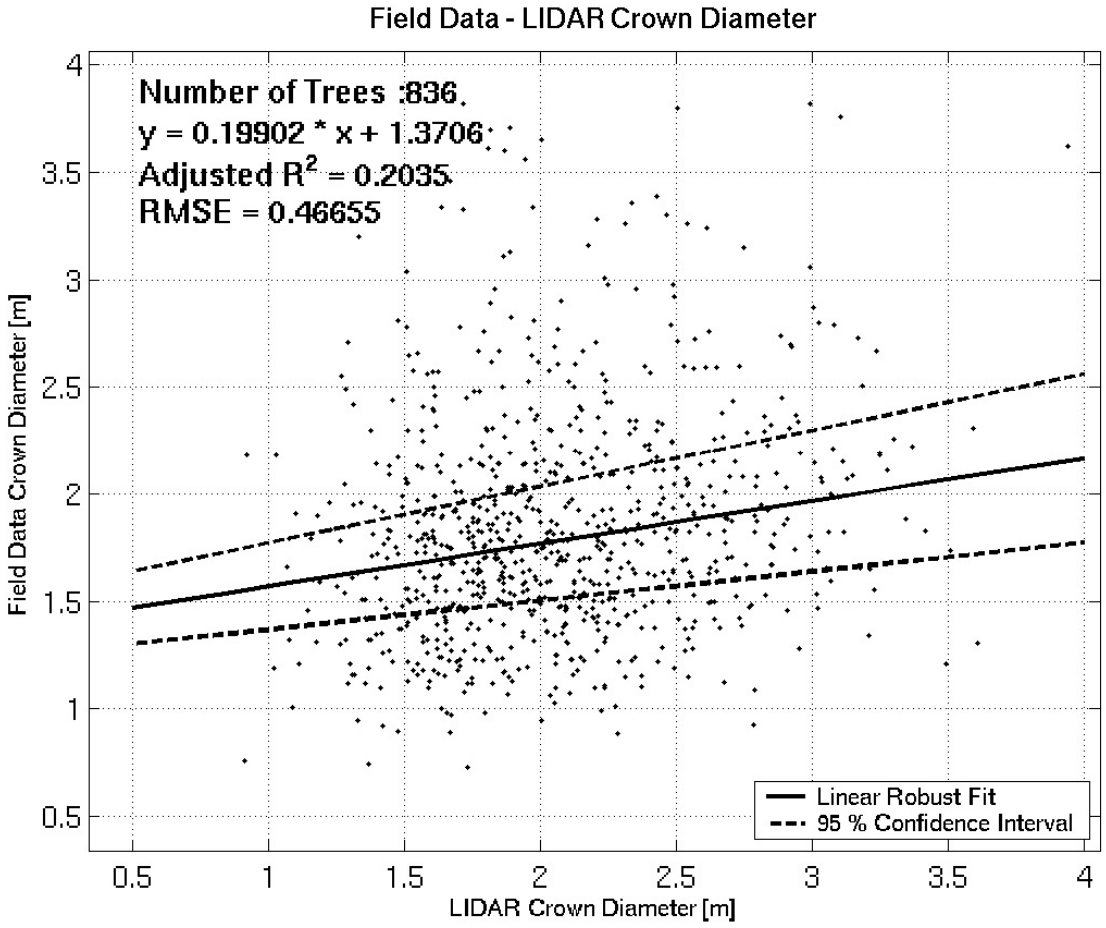

Figure 4.7: A robust regression of the field measured crown diameters against LIDAR derived crown diameters is carried out. Only the values with the weight being larger than zero (Fig. 4.6) have been used.

A problem validating the values of crown diameter with the field data arises again from the tree clumping. Solving this problem by taking only the value of the dominant

tree, as we did with the height measurements, does not work for the crown diameter. In the case of tree clumping, the LIDAR values will reflect the diameter of *all* of the trees standing in a group, and not only that one of the dominant tree. Hence, if there was more than one field tree assigned to a LIDAR cluster in the matching process, we derived an artificial diameter from the field measurements by computing the convex hull of the tree group. From this convex hull, a diameter was estimated in the same way as for the LIDAR clusters in Section 4.4.1. Then, these values were used for the regression shown in Fig. 4.7. Unfortunately, there is only a weak linear relationship visible. There seems to be some connection between field measurements and LIDAR derived crown diameters since the values are in the same range in both cases, but inside this range the distribution of values seems to be more or less random, as expressed by the low value of adjusted R^2 of 0.2 and the coefficient determining the slope of the regression being only 0.2. Thus, there seem to be quite large random errors associated with either the LIDAR derived crown diameters or with the field measurements of crown diameters. A systematic under- or overestimation is not visible in our dataset.

4.4.4 Allometric Relationship

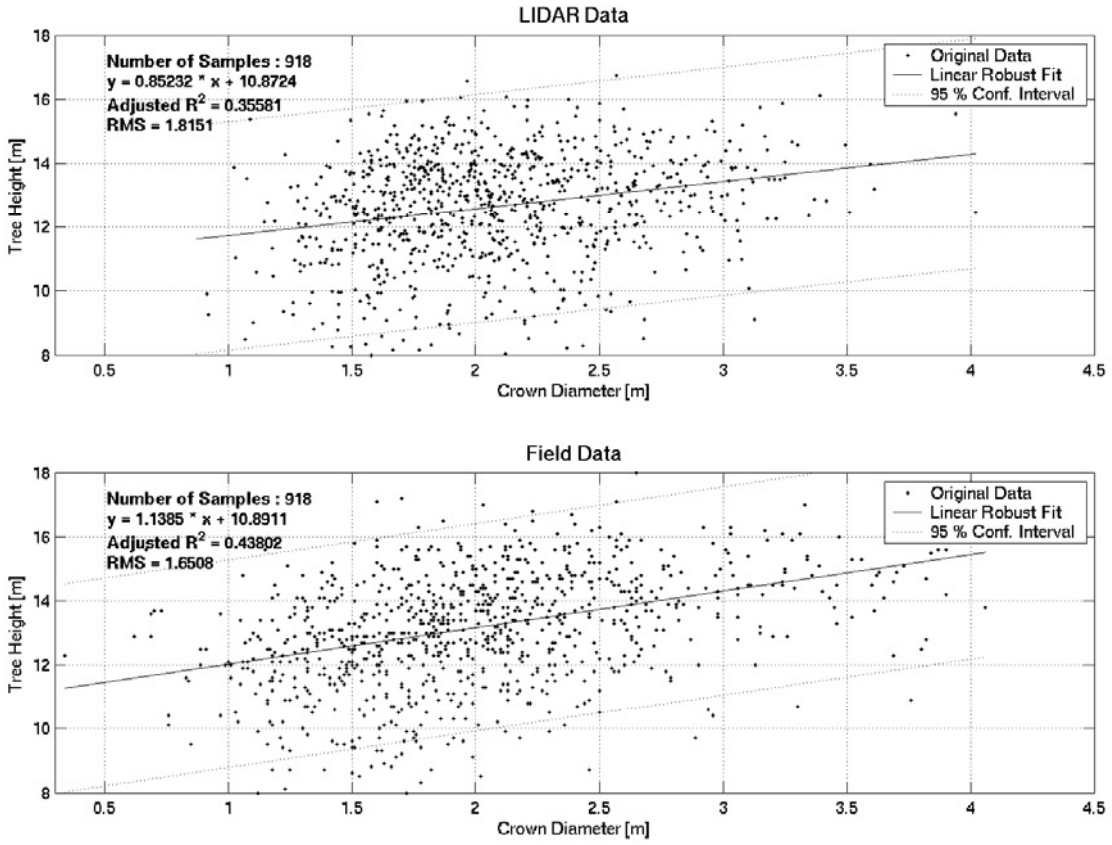

Figure 4.8: Relation of tree height to crown diameter for LIDAR (top) and field data (bottom). A robust regression has been carried out as in Figure 4.7 and 4.6.

Another way of assessing the feasibility of clustering results is the derivation of allo-

metric relationships from the segmented tree clusters. Here we can use a large number of trees, which would be very time (and cost) consuming with traditional field work. We utilize the LIDAR derived values of tree height and crown diameter, as well as the matched field measurements. In Fig. 4.8 (top) we show a regression of LIDAR derived crown diameter and tree height revealing a slope of 0.8 and an offset of 10.9 m, with the adjusted R^2 being at 0.35. The slope is a little less then in Fig. 4.8 (bottom). There, the same regression is shown for the field data, with a positive slope of 1.1 and a slightly larger R^2 of 0.43. The offset is as large as for the LIDAR data, being at 10.9 m. This is the kind of relation one would expect with larger trees having larger crowns. The two images in Fig. 4.8 reveal that the relation of tree height and crown diameter is quite similar for the LIDAR derived values and the field measurements. It might be that the problems that the crown diameter regression suffers from in Fig. 4.7 are not so predominant in these allometric relationships. However, the low R^2 are probably due to the fact that the stands are not healthy and heterogeneous regarding their age distribution.

4.4.5 Geometric Reconstruction

Using the derived values of tree height, tree position, crown diameter, and crown base height, it becomes now possible to reconstruct the forest scene using a simple geometric model. We used a rotational paraboloid for the tree crown and a cylinder for the trunk, with the height of these two parts being determined trough crown base height. In Fig. 4.9 we show the same area as in Fig. 4.3 and 4.4. The LIDAR raw data is superimposed on the reconstructed scene and might be obscured by the tree models in some cases.

4.5 Discussion and Conclusion

We have shown that it is feasible to segment single trees in LIDAR raw data using cluster analysis, choosing local maxima as starting positions (seed points). Opposed to previous stand wise approaches, we can now derive geometric properties on a single tree basis, which will be necessary for future fire behavior modeling. If a stand-wise approach is desired for a specific application (as for the empirical fire models), these values can be aggregated to a larger scale. The original raw data is not altered in any way and no information is lost. Tree heights derived from the segmented clusters are in good agreement with the field data, whereas the diameter of the trees do not match as well, which might be due to random errors in the field measurements and the way the crown diameter is derived from the LIDAR data; the field crown diameter are only measured from on side, which might generate errors for asymmetric crowns. A systematic error measuring crown diameter cannot be inferred from our dataset. However, a larger number of field inventory trees have not been detected by the automated segmentation. This is due to the special vegetation in the Swiss National Park bearing a lot of "tree clusters", with several stems inside a radius of about one meter. This fact will definitely cause trouble for correct biomass estimations, as some stems are not detected, which should however not be severe to our approach as we currently only aim to estimate vegetation structure. The group of trees will act in most physical processes

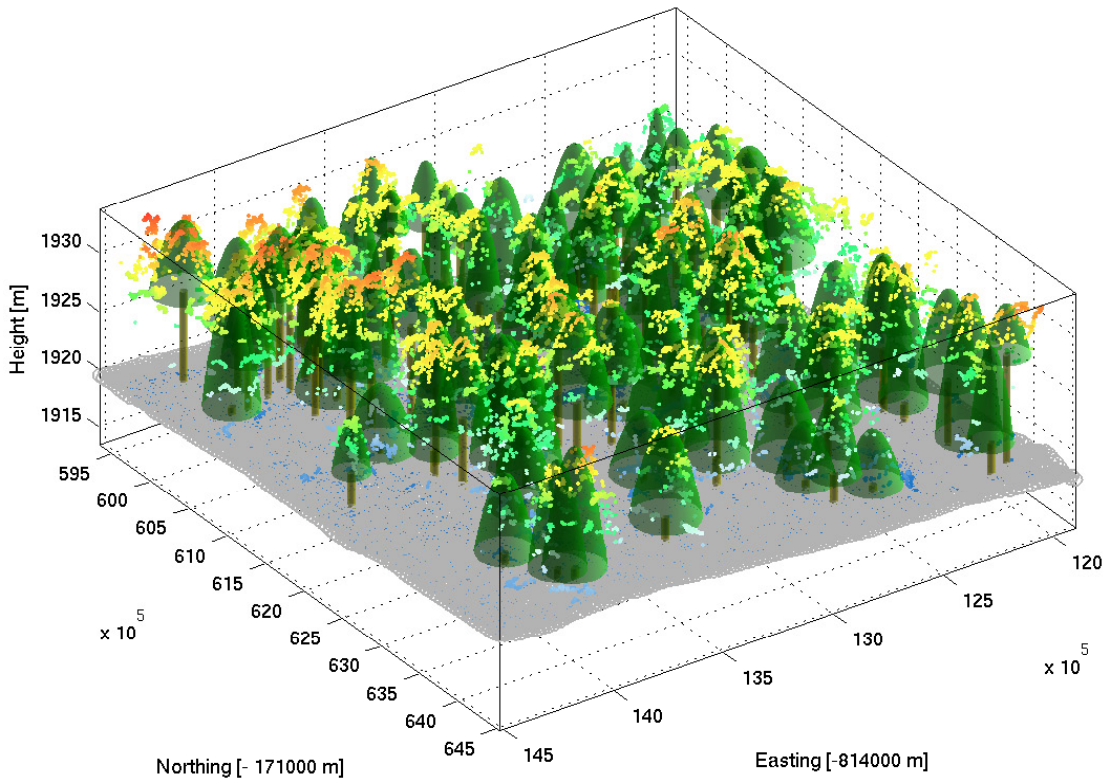

Figure 4.9: Reconstruction of the forest scene using a simple geometric model. The LIDAR raw data is superimposed as colored dots, different colors represent different heights. The tree models are transparent to allow better visibility of laser points.

almost as a single tree, as for instance in radiative transfer modeling. It should be noted that the technique will very probably not work as well with deciduous trees, since the seedpoint extraction relies on the fact that the trees have only *one* well defined local maximum, which might not always be the case for deciduous trees. The age of the stands with a lot of trees at the end of their lifetime bearing only partial crowns is a problem for the derivation of allometric relationships. Future work will include developing a seed point algorithm working on the raw data and the derivation of further geometric crown properties as for instance crown density. As the segmented crown clusters contain an average of about 350 returns (both first and last pulse), one could try to look a the vertical distribution of points inside the cluster to infer a measure of crown density. Especially helpful for this would be a small footprint being capable of recording several returns in between first and last pulse or even the full waveform. Then the estimation of crown density at the tree level would become easier. We will further need to determine the source of the discrepancy in the crown diameter measurements, probably through additional field work; a survey of the study site with a terrestrial laser scanner is already planned. Interfacing the derived structural information with the thermodynamic fire behavior models Séro-Guillaume and Margerit (2002); Margerit and Séro-Guillaume (2002) is already subject of ongoing work.

Bibliography

Allgöwer, B., Bur, M., Stähli, M., Koutsias, N., Tinner, W., Conedera, M., Stadler, M., Kaltenbrunner, A., 2003. Can Long-term Wildland Fire History Help to Design Future Fire and Landscape Management? An Approach from the Swiss Alps. 3rd International Wildland Fire Conference and Exhibition, Sydney, Australia, 11.

Allgöwer, B., Harvey, S., Rüegsegger, M., 1998. Fuel Models for Switzerland: Description, Spatial Pattern, Index for Crowning and Torching. 3rd International Conference on Forest Fire Research / 14th Conference on Fire and Forest Meteorology, Luso, Portugal, 2605–2620.

Andersen, H.-E., Reutebuch, S. E., Schreuder, G. F., 2002. Bayesian object recognition for the analysis of complex forest scenes in airborne laser scanner data. In: ISPRS Commission III, Symposium 2002 September 9 13, . G. A. (Ed.), ISPRS Commission III, Symposium 2002 September 9 - 13, 2002, Graz, Austria. pp. A–035 ff (7 pages).

Baltsavias, E. P., 1999. Airborne laser scanning: existing systems and firms and other resources. ISPRS Journal of Photogrammetry & Remote Sensing 54, 164–198.

Brandtberg, T., Warner, T. A., Landenberger, R. E., McGraw, J. B., 2003. Detection and analysis of individual leaf-off tree crowns in small footprint, high sampling density lidar data from the eastern deciduous forest in north america. Remote Sens. Environ. 85 (3), 290–303.

Chuvieco, E., 2003. Wildland Fire Danger Estimation and Mapping - The Role of Remote Sensing Data. World Scientific.

Countryman, C. M., 1972. The fire environment concept. Berkley, CA, Pacific Southwest Forest and Range Experiment Station, 12pp.

Dobbertin, M., Baltensweiler, A., Rigling, D., 2001. Tree mortality in an unmanaged mountain pine (pinus mugo var. uncinata) stand in the swiss national park impacted by root rot fungi. Forest Ecology and Management 145, 79–89.

Drake, J. B., Dubayah, R. O., Clark, D. B., Knox, R. G., Blair, J. B., Hofton, M. A., Chazdon, R. L., Weishampel, J. F., Prince, S. D., 2002a. Estimation of tropical forest structural characteristics using large-footprint lidar. Remote Sensing of Environment 79, 305–319.

Drake, J. B., Dubayah, R. O., Knox, R. G., Clark, D. B., Blair, J. B., 2002b. Sensitivity of large-footprint lidar to canopy structure and biomass in a neotropical rainforest. Remote Sensing of Environment 81 (2-3), 378–392.

Finney, M., 1998. FARSITE: Fire Area Simulator-Model. Development and Evaluation. USDA Forest Service Research Paper, RMRS-RP-4.

Gaveau, D., Hill, R., 2003. Quantifying canopy height underestimation by laser pulse penetration in small-footprint airborne laser scanning data. Canadian Journal of Remote Sensing 29, 650–657.

Huber, P., 1981. Robust Statistics. Wiley, New York.

Hyyppä, J., Kelle, O., Lehikoinen, M., Inkinen, M., 2001. A segmentation-based method to retrieve stem volume estimates from 3-d tree height models produced by laser scanners. IEEE Transactions on Geoscience and Remote Sensing 39, 969–975.

Koetz, B., Schaepman, M., Morsdorf, F., Itten, K., Allgöwer, B., 2004. Radiative transfer modeling within a heterogeneous canopy for estimation of forest fire fuel properties. Remote Sensing of Environment 92 (3), 332–344.

Lauber, K., Wagner, G., 1996. Flora helvetica. flora der schweiz. Bern, Stuttgart, Wien, Paul Haupt Verlag, 1613.

Lefsky, M. A., Cohen, W. B., Parker, G. G., Harding, D. J., 2002. Lidar remote sensing for ecosystem studies. BioScience 52 (1), 19–30.

Margerit, J., Séro-Guillaume, O., 2002. Modeling forest fires. Part II: Reduction to two-dimensional models and simulation of propagation. International Journal of Heat and Mass Transfer 45, 1723–1737.

Means, J. E., Acker, S. A., Fitt, B. J., Renslow, M., Emerson, L., Hendrix, C., 2000. Predicting forest stand characteristics with airborne scanning lidar. Photogrammetric Engineering & Remote Sensing 66 (11), 1367–1371.

Næsset, E., 2002. Predicting forest stand characteristics with airborne scanning laser using a practical two-stage procedure and field data. Remote Sensing of Environment 80 (1), 88–99.

Næsset, E., Bjerknes, K.-O., 2001. Estimating tree heights and number of stems in young forest stands using airborne laser scanner data. Remote Sensing of Environment 78 (3), 328–340.

Næsset, E., Okland, T., 2002. Estimating tree height and tree crown properties using airborne scanning laser in a boreal nature reserve. Remote Sensing of Environment 79 (1), 105–115.

Persson, A., Holmgren, J., Söderman, U., 2002. Detecting and measuring individual trees using an airborne laser scanner. Photogrammetric Engineering & Remote Sensing 68 (9), 925–932.

Peterson, B., Hyde, P., Hofton, M., Dubayah, R., Fites-Kaufman, J., Hunsaker, C., Blair, J., 2003. Deriving canopy structure for fire modeling from lidar. EARSEL - 4th International Workshop: Remote Sensing and GIS applications for Forest Fire Management, Ghent.

Pyne, S., Andrews, P., Laven, R. (Eds.), 1996. Introduction to Wildland Fire. Wiley, New York.

Pyysalo, U., Hyyppä, H., 2002. Reconstructing tree crowns from laser scanner data for feature extraction. In: ISPRS Commission III, Symposium 2002 September 9 - 13, 2002, Graz, Austria. pp. B–218 ff (4 pages).

Riano, D., Meier, E., Allgöwer, B., Chuvieco, E., Ustin, S. L., 2003. Modeling airborne laser scanning data for the spatial generation of critical forest parameters in fire behavior modeling. Remote Sensing of Environment 86 (2), 177–186.

Roggero, M., 2001. Airborne laser scanning: Clustering in raw data. International Archives of Photogrammetry and Remote Sensing XXXIV-3/W4, 227–232.

Séro-Guillaume, O., Margerit, J., 2002. Modeling forest fires. part i: a complete set of equations derived by extended irreversible thermodynamics. International Journal of Heat and Mass Transfer 45, 1705–1722.

Spath, H., 1985. Cluster Dissection and Analysis: Theory, FORTRAN Programs, Examples. Halsted Press,New York, 226 pp.

St-Onge, B. A., Achaichia, N., 2001. Measuring forest canopy height using a combination of lidar and aerial photography data. International Archives of Photogrammetry and Remote Sensing XXXIV-3/W4, 131–137.

Zoller, H., 1992. Vegetationskarte des schweizerischen nationalparks und seiner umgebung. Bern, Hallwag AG.

Zoller, H., 1995. Vegetationskarte des Schweizerischen Nationalparks. Erläuterungen. National Park Forschung, 108.

Chapter 5

Estimation of LAI and fractional cover from small footprint airborne laser scanning data based on gap fraction

This chapter has been published as: F. Morsdorf, Benjamin Kötz, E. Meier, K.I. Itten, and Britta Allgöwer. *Estimation of LAI and fractional cover from small footprint airborne laser scanning data based on gap fraction* **Remote Sensing of Environment, Volume 104, Issue 1, Pages 50-61**, 15. September 2006
Reprinted with Permission.

Abstract

We evaluate the potential of deriving fractional cover (fCover) and leaf area index (LAI) from discrete return, small footprint airborne laser scanning (ALS) data. fCover was computed as the fraction of laser vegetation hits over the number of total laser echos per unit area. Analogous to the concept of contact frequency, an effective LAI proxy was estimated by a fraction of first and last echo types inside the canopy. Validation was carried out using 83 hemispherical photographs georeferenced to centimeter accuracy by differential GPS, for which the respective gap fractions were computed over a range of zenith angles using the Gap Light Analyzer (GLA). LAI was computed by GLA from gap fraction estimations at zenith angles of 0 to 60 degrees. For ALS data, different data trap sizes were used to compute fCover and LAI proxy, the range of radii was 2 to 25 m. For fCover, a data trap size of 2 m radius was used, whereas for LAI a radius of 15 provided best results. fCover was estimated both from first and last echo data, with first echo data overestimating field fCover and last echo data underestimating field fCover. A multiple regression of fCover derived from both echo types with field fCover showed no increase of R^2 compared to the regression of first echo data, and thus, we only used first echo data for fCover estimation. R^2 for the fCover regression was 0.73, with an RMSE of 0.18. For the ALS LAI proxy, R^2 was lower, at 0.69, while the RMSE was 0.01. For LAI larger radii ($\sim$ 15 m) provided best results for our canopy types, which is due

to the importance of a larger range of zenith angles (0-60 degrees) in LAI estimation from hemispherical photographs. Based on the regression results, maps of fCover and LAI were computed for our study area and compared qualitively to equivalent maps based on imaging spectrometry, revealing similar spatial patterns and ranges of values.

5.1 Introduction

Robust estimates of vegetation density such as fCover and LAI are critical for a number of applications. They serve as input parameters for biosphere modeling (Bonan, 1993) and play an important role in fire behavior models (Finney, 1998), since they both contain information about a number of relevant ecological processes. LAI was first defined as the total one-sided area of photo synthetic tissue per unit ground surface area (Watson, 1947). This definition is only valid for broad leaf forests though, and consequently Myneni et al. (1997) defined the LAI as the maximum projected leaf area per unit ground surface area. fCover is defined as the fraction of ground covered by vegetation over uncovered ground. Both LAI and fCover are dimensionless parameters, even though LAI is often given as meter square per meter square to illustrate it's meaning as an area ratio. Remote sensing has always been assigned a major role in deriving these measures. Many approaches were focused on the retrieval of these parameters from passive optical systems, often by the use of regression models (Cohen et al., 2003; Colombo et al., 2003), and in some cases by using radiative transfer modeling (Koetz et al., 2004; Schlerf and Atzberger, 2006). One limitation of these approaches is the limited characterization of canopy structure, in both horizontal and vertical dimension. Airborne laser scanning (ALS) systems can overcome this shortcoming by penetrating the canopy and revealing the vertical stratification of the canopy, as well as the horizontal structure in case of small-footprint systems providing high point densities. Thus, ALS systems have been widely used for stand-wise derivation of structural parameters (Lovell et al., 2003; Means et al., 2000; Lefsky et al., 1999), often by means of regression methods choosing some ALS predictor variables (e.g. height percentiles) for ground based measures of structural information (Næsset, 2002, 2004; Cohen et al., 2003; Andersen et al., 2005). Using small footprint laser data with high point density, the derivation of single tree metrics becomes possible. Its feasibility has been shown by a number of studies (Hyyppä et al., 2001; Andersen et al., 2002; Morsdorf et al., 2004). Some previous studies have already derived LAI and fCover from laser scanning data. Riano et al. (2004) used a relation from Gower et al. (1999) to compute LAI from the gap fraction distribution derived by means of airborne laser scanning, whereas Lovell et al. (2003) used ground based laser range finder information to model LAI using canopy profiles. Koetz et al. (2006) have used a LIDAR waveform model to invert fCover and LAI from large footprint LIDAR data.

Many small footprint sensors are capable of recording discrete returns (e.g. first and last return, or up to five returns), but not the entire waveform. Small footprint, full waveform sensors are just becoming commercially available. Still, discrete returns contain valuable information about the vegetation density and structure at a high spatial resolution, usually in the order of less than one meter. It has been shown in a number of studies that first and last returns can be used to model stand properties such as basal

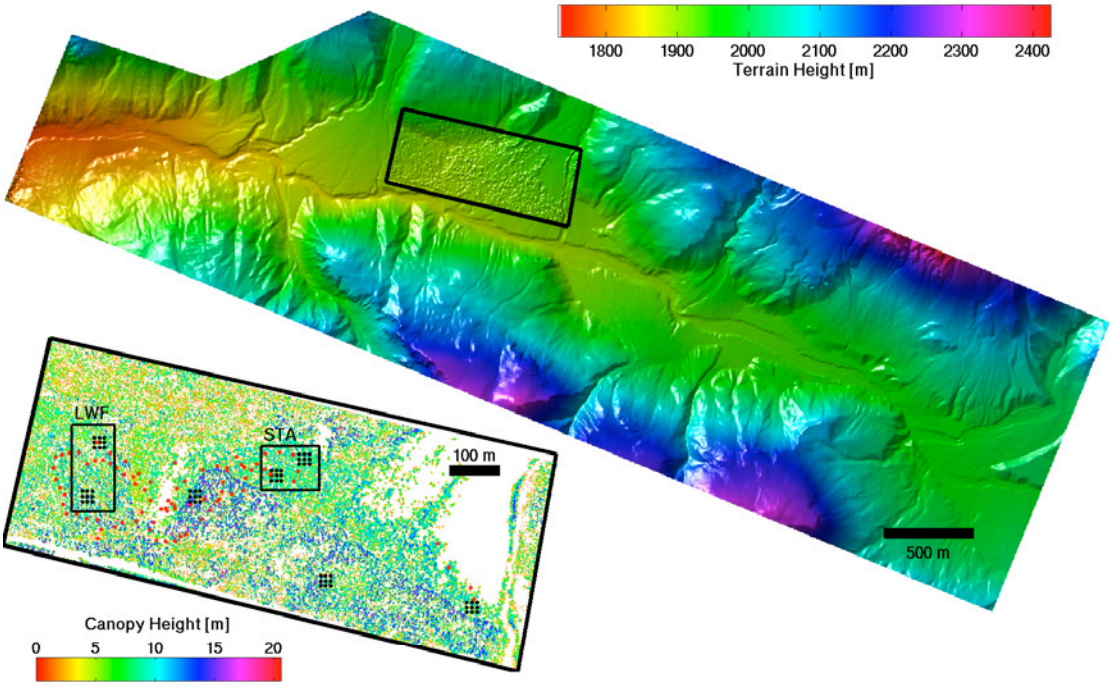

Figure 5.1: The Digital Terrain Model (DTM) of the Ofenpass area in the Swiss National Park. The smaller area marked by the black box was sampled with higher point density due to the lower flying height of 500 m above ground. A canopy height map of that area is displayed in the lower left. Black dots mark positions of hemispherical photographs that were taken in 2002 using a handheld GPS for georeferencing. Red dots indicate positions were hemispherical photographs were taken using differential GPS for georeferencing (2005). Black squares mark areas where the histograms in Figures 5.2 and 5.3 were computed from.

area, biomass and LAI. White et al. (2000) have compared different methods for field LAI estimation with airborne laser altimetry, but for a completely different ecosystem compared to the boreal vegetation found in our study area. Our objective is to evaluate the potential of deriving fCover and LAI from discrete return (first and last), small footprint laser data exploiting the information contained in both return types. Our aim is to establish physically meaningful predictor variables and to evaluate their performance with indirect field measurements based on high-precision georeferencing. Emphasis will be placed on differences in viewing geometry between field based methods and airborne laser scanning. Furthermore, special regard will be paid to the fact that the indirect methods used as ground truth are themselves essentially remote sensing methods.

5.2 Data

5.2.1 Site description

The study area for the acquisition of field data is located in the eastern Ofenpass valley, which is part of the Swiss National Park (SNP). The Ofenpass represents a dry inner-alpine valley with rather little precipitation (900-1100 mm per year). Surrounded by 3000 meter high peaks, the Ofenpass valley starts at about 1500 m a.s.l. in the west and quickly reaches an average altitude of about 1900 m a.s.l towards the east. The south-facing Ofenpass forests, the location of the field measurements, are largely dominated by mountain pine (*Pinus mugo* ssp. *uncinata*) and some stone pine (*Pinus cembra*), which are of interest for natural succession (Zoller, 1992; Lauber and Wagner, 1996). These forest stands can be classified as woodland associations of Erico-Pinetum mugo (Zoller, 1995).

In Figure 5.1 an overview of the test site is given. More than 20 $\%$ of the stand consists of upright standing dead trees, having a minimum age of 90 years, and mean and maximum ages of 150 and 200 years, respectively.

5.2.2 Laser Scanning Data

In October 2002 a helicopter based ALS flight was carried out over the test area, covering a total area of about 14 km^2. The ALS system used was the Falcon II Sensor developed and maintained by the German company TopoSys. Its sensor specifications are given in Table 7.1.

Falcon II Specifications	
Maximum Range	1600 m
Range Resolution	2 cm
Scanning Angle	$\pm 7.15°$
Line-scan Frequency	653 Hz
Pulse Frequency	83 kHz
Laser Wavelength	1560 nm
Number of Fibers	127
Beam Divergence	1 mrad

Table 5.1: Specifications of Falcon II Sensor Platform

The system is a fiber-array laser altimeter recording both first and last intensity peaks from the laser return signal (first/last echo FE/LE). The flight was conducted with a nominal height over ground of 850 m, leading to an average point density of more than 10 points per square meter (p/m^2). A smaller subset of the area (0.6 km^2) was flown at a height of 500 m above ground, resulting in a point density of more than 20 p/m^2, thus combining the two data-sets yielded to a point density of more than 30 p/m^2 for both first and last echo. We only used data from the lower over-flight in this study. The footprint sizes were about 0.9 m in diameter for 850 m flight altitude and about 0.5 m in diameter for 500 m altitude. The raw data delivered by the sensor (x,y,z -

triplets) was processed into gridded elevation models by TopoSys using the company's own processing software. The Digital Surface Model (DSM) was processed using the first pulse reflections, the Digital Terrain Model (DTM) was constructed using the last returns and filtering algorithms. The grid spacing was 1 m for the large area and 0.5 m for the smaller one, with a height resolution of 0.1 m in both cases. A quality analysis of the raw data was done using six artificial reference targets and is described in detail in Morsdorf et al. (2004). The standard deviations of height estimates based on raw echos on these targets were as low as 6 cm, with the internal accuracy of the ALS data well below the pixel size of 0.5 m.

5.2.3 Field inventory

On one hand the definition of LAI is quite simple, but on the other hand its estimation in the field is not trivial at all. There are various ways of determining LAI, a comprehensive summary is given by Jonckheere et al. (2004). Methods can be categorized in two classes, direct and indirect. Direct methods generally use destructive sampling to estimate the total number of leaves on a tree and their area, included angles and distribution to estimate LAI. Indirect methods mostly measure some aspect of the radiative regime and infer the LAI from the distribution of light inside the canopy. Even though the definition of both LAI and fCover is quite different, they are often estimated by the same measurement principle, e.g. LAI2000 or hemispherical photographs, which both can be used to compute LAI and fCover (Jonckheere et al., 2004). We took hemispherical photographs as field samples using a Nikon Coolpix 4500 with a fish-eye lens. The small plot in Figure 5.1 shows a canopy height model (CHM) of the area over flown with the lower altitude. Black dots indicate positions where hemispherical photographs were taken in 2002. In 2005, another data collection was carried out at locations marked by red dots. In 2005, a total of 83 hemispherical photographs was taken, and the location of each image was measured using differential GPS equipment. We used three Trimble Total (one 5700 receiver and two 4700 receiver types) stations for GPS measurements. One 4700 receiver was set up as base station on a known fixed point of surveying quality inside the study area. The resulting baselines were rather short, between 10 to 600 meters in length. The 5700 receiver was used together with a data display (TSCE) to carry out fast static point measurements. A surveying tripod was set up at and leveled at each location, with the GPS antenna placed on top. Succeeding the GPS measurement, the hemispherical photographs were taken. GPS occupation times at each location varied according to satellite availability from 3 to 30 minutes, and the resulting accuracies based on GPS RMS are in the range of 0.5 to 5.4 centimeters with a mean of 1.84 centimeters. The canopy in our study area was not too dense (medium fCover values of about 40 $\%$), thus in most cases occupation times of about 5 minutes were enough (> 5 satellites tracked during measurement), but in the denser parts longer occupation times of up to half an hour were needed to achieve centimeter accuracy.

5.2.4 Processing of field data

The hemispherical photographs were analyzed using the Gap Light Analyzer (GLA, (Frazer et al., 1997)) software. Gap fractions were computed for zenith angles from 0 to 90 degrees with 5 degree spacing, and averaged over all azimuth angles. Areas with sun light (in about 20 images) were treated separately by a local threshold, before applying a global threshold, as was done for the rest of the images containing no illumination effects due to direct sunlight. LAI was computed for each photograph by GLA's own routines. In coniferous canopies, clumping of small scale canopy elements (e.g. needles, twigs) into shoots of some centimeters to some decimeters in size manifests an underestimation of LAI that needs to be corrected (Smolander and Stenberg, 2003). Clumping at shoot scale can be addressed by correcting the indirect LAI estimates (often called effective LAI, LAI_{eff}) with a factor depending on the projection function of canopy elements (Weiss et al., 2004). We decided to derive only LAI_{eff}, since a simple coefficient does not alter the quality of our regression. If one needs values for true LAI, one would have to multiply our values by 1.75 (Chen, 1997; Koetz et al., 2004). We applied this correction factor for generating the maps presented in Section 5.4.5. fCover was derived from the canopy openness measure $CO[\%]$ of GLA, which is based on the fraction of sky pixels weighted with hemispherical area by Eq. 6.4

$$fCover = 1 - CO \tag{5.1}$$

Only pixels from zenith angles smaller than 10 degrees were used for the estimation of fCover, as was proposed by Weiss et al. (2004).

5.3 Methods

5.3.1 Derivation of fractional cover from laser data

The Toposys Falcon II system is capable of recording a first and a last echo of the return signal. A first echo will be triggered if the return signal reaches a certain intensity, hence the vegetation cover reaches a critical density and/or reflectivity. If the vegetation is not too dense, a part of the beam can further penetrate the canopy, until the threshold for the intensity is surpassed a second time and the so called last echo is triggered. Depending on the vegetation openness and density this can be on the ground or inside the vegetation. A minimum distance needs to be in between first and last echo for their separation, which depends on the pulse duration of the laser emitter. With a system recording first and last echo, three types of returns scenarios are possible:

- first echo
- last echo
- single echo, first echo = last echo

The term *single echo* describes the case where only one echo is triggered from a return signal, resulting in both values having the same height. Most single echos will come

from plain surfaces such as roads or generally from the ground, but there are some in the vegetation, as will be discussed in the Section 5.4.1.

For each of the three return classes, we computed fCover according to Eq. 6.1 and Eq. 6.2.

$$\mathbf{fCover} = \frac{\sum E_{vegetation}}{\sum E_{total}} \tag{5.2}$$

with

$$E_{vegetation} = E_{total} > 1.25m \tag{5.3}$$

$E_{vegetation}$ and E_{total} denotes vegetation echos and all (ground and vegetation) echos respectively. We chose a height threshold of 1.25 m, since this was the height at which the lens was placed when taking the hemispherical photographs.

The value of fCover for first pulse data is larger than that for single echos, which in turn is larger than the value for last echos, as can be seen in Figures 5.2 (b) and 5.3 (b). Lovell et al. (2003) concluded from similar findings that the *real* value of fCover must satisfy the following condition:

$$fCover_{FE} > fCover > fCover_{LE} \tag{5.4}$$

FE and LE denote first echo and last echo respectively. Based on Eq. 5.4 one can state that using first pulse information for fCover estimation will overestimate the true fCover value, whereas using last pulse information will underestimate true fCover. The value of true fCover lies somewhere in between, but where exactly is difficult to ascertain, as it will depend on vegetation type/condition and sensor specifications. Many studies deriving stand level indices have only used first pulse data (Yu et al., 2004), since the separation mechanism is not well understood, and still the most significant information is contained in a first pulse histogram. As e.g. Holmgren and Persson (2004) we compute fCover from first and last returns separately by thresholding vegetation heights according to Eq. 6.1 and 6.2. Following this, we use single and multiple regressions of these two fCover values to determine their influence on true fCover as determined by field measurements. Furthermore, we will compute fCover for circular ALS raw data patches (*data traps*) of 2 to 25 m in diameter.

5.3.2 Derivation of LAI from laser data

Our goal is to establish a predictor variable of LAI that is closely linked to the way LAI is estimated using the indirect methods in the field. Following Weiss et al. (2004), the LAI can be expressed through the following equation. The leaf area index, L, at a level H in the canopy is related to the leaf area density $l(h)$ through:

$$L = \int_0^H l(h)dh \tag{5.5}$$

If we introduce the contact frequency $N(H, \theta_v, \phi_v)$ we can write Equation 5.5 as follows:

$$N(H, \theta_v, \phi_v) = \int_0^H G(h, \theta_v, \phi_v) \frac{l(h)}{cos\ \theta_v dh} \tag{5.6}$$

θ_v and ϕ_v denote viewing zenith and azimuth angle respectively and $G(h, \theta_v, \phi_v)$ the projection function. If leaf area density and projection function are considered independent of the level h in the canopy Eq. 5.6 can be simplified into Eq. 5.7

$$N(L, \theta_v, \phi_v) = G(h, \theta_v, \phi_v) \frac{L}{cos\ \theta_v} \tag{5.7}$$

Considering the Falcon II system with its maximum scanning angle of 7.1 degrees, $cos\ \theta_v$ is only changing up to 0.75% from 1 and can thus be neglected. As we have solely conifers in our study area, the projection function is set to 0.5 assuming a spherical foliage distribution (as in Sun and Ranson (2000) and Koetz et al. (2004)), thus we yield a direct proportional relationship of contact frequency to LAI:

$$N(L) = 0.5 * L \tag{5.8}$$

The contact frequency itself should be linearly related to the distribution of first, single and last echos inside the canopy. We still need to account (calibrate) for specific instrument characteristics, which will be footprint size (depends on beam divergence and flying height) and the thresholding algorithm for detection of first and last pulse, as well laser beam attenuation through the atmosphere. In this study, we are using a linear regression model to do so.

Based on the concept of contact frequency we propose to compute a LAI proxy from ALS data by:

$$N_{LAI} = \frac{\sum E_{FE}}{\sum E_{LE} + \sum E_{SE}} \tag{5.9}$$

E_{FE}, E_{SE} and E_{LE} denote the three types of returns described in detail in Section 5.3.1, but only for crowns. The vegetation returns are classified by thresholding the height over terrain of the raw laser hits with a value of 1.25 m, according to the estimation of fCover in Eq. 6.2. The hypothesis for this proxy is as well based on results displayed in Figures 5.2 (b) and 5.3 (b). As for fCover, we will compute this LAI proxy for circular ALS *data traps* of 2 to 25 m in diameter.

Dispersion of crowns inside the canopy is not an issue for our approach, since we only compute the fraction of returns from greater than 1.25 m above the ground, thus inside the canopy. This is a valid approach, since our study site is a single layered and almost a single species canopy type. Thus, our contact frequency measure is only derived from crowns, due to the ability of high point density, small footprint laser scanner data of spatially resolving single tree crowns (Morsdorf et al., 2004). In order to compare these ALS derived estimates of canopy LAI with indirect field measurements, we need to correct for the distribution of canopy elements (e.g. trees) in the scene, which will be done by using the ALS derived fCover values. Since the LAI estimated by ALS is only estimated for the canopy, we need to multiply that LAI value with the respective value of ALS derived fCover in order to yield an LAI estimation for the whole data trap. For instance, if the *canopy* LAI (LAI only computed from canopy elements) was 4 and the fCover value of that respective scene 0.5, then the real LAI for the scene would be 2. Hemispherical photographs only measure the scene LAI and fCover, since they can not discriminate between gaps within crowns and gaps between neighboring crowns.

$$N_{LAI,scene} = N_{LAI,canopy} * fCover_{scene} \tag{5.10}$$

Still, we need to assume horizontal and vertical uniform leaf angle and leaf property distribution. One leaf property that could alter this way of LAI estimation is leaf reflectance. The difference of reflectance between ground and canopy needs to be considered as well. This reflectance difference reveals a major caveat regarding the comparability of laser based vegetation indices from different stands and possibly even different sites. We will discuss its influence in greater detail in the following section.

5.3.2.1 Vegetation reflectance considerations

Based on field measurements, the foliage reflectance at 1560 nm (wavelength of laser beam) is 21.5 %, whereas the background reflectance of the under-story is 15.2 %, making up for a ratio of 1.4. This ratio is specific for our study area, and can be considered a constant for our area, due to the homogeneity of the canopy and under-story in respect to plant species. In order to assess the feasibility of our approach regarding the assumption on spatially uniform reflectance of the canopy, we conducted some tests using PROSPECT (Jacquemoud and Baret, 1990), modeling the reflectance of the green canopy elements in our study site using average leaf parameters from field measurements collected at different sites (Koetz et al., 2004). We varied the moisture content within a range observed in the field, as at 1560 nm absorption due to moisture is the dominant effect. Simulated leaf reflectance yielded 20.8 % reflectance for the lowest values of moisture and 19.2 % for the highest value observed, making up for an absolute difference of only 1.6 %. This is small enough to be neglected, considering results from a practical test using artificial targets on object visibility using different reflectances (Wotruba et al., 2005). All other parameters of PROSPECT were left constant, since our test site is predominantly covered by only one tree type, which is mountain pine.

5.3.3 Regression Methods

For all regressions in this paper, adjusted R^2 and RMSE were computed by the following equations (see Kvalseth (1985) for details):

$$R^2 = 1 - \frac{n-1}{n-p} \frac{\sum(y-\hat{y})^2}{\sum(y-\bar{y})^2} \tag{5.11}$$

n is the number of samples, p is the number of parameter in the regression model (which is two for all our presented regressions), $\hat{y}$ is the fitted value of a sample y (e.g. LAI) and $\bar{y}$ is the mean of all ys. The root mean square error is calculated as:

$$RMSE = \sqrt{\frac{\sum(y-\hat{y})^2}{n-p}} \tag{5.12}$$

For each of the regressions, we excluded outliers in a first linear regression, where the 5% confidence interval for the residuals was estimated and values not enclosing zero were flagged (see Chatterjee and Hadi (1986) for details). We still include them in the regression graphs as empty circles, in order to illustrate that they are real outliers. These outliers may originate from temporal differences between LIDAR flight and data collection, but more likely is that they originate from errors in the acquisition/processing chain of hemispherical photographs, be it by thresholding errors or illumination differences.

5.4 Results

5.4.1 Height histograms

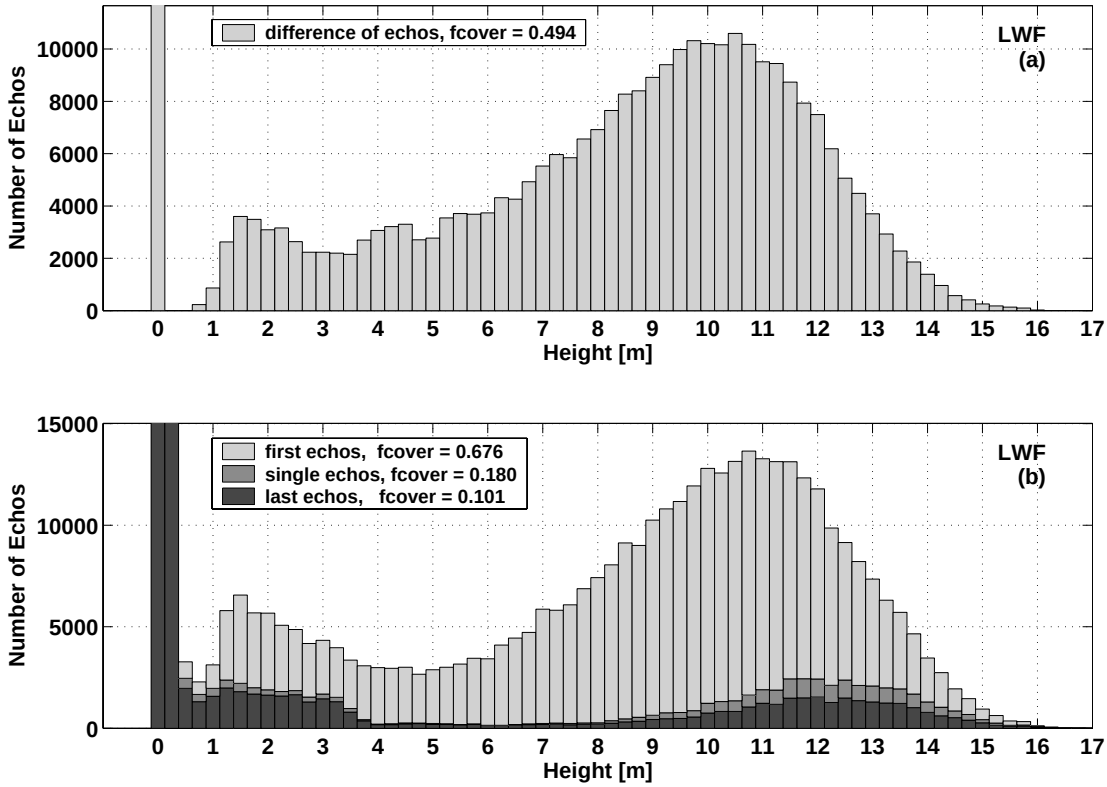

Figure 5.2: Histogram of difference of first and last pulse (a), histogram of first, last and single echos (b) for site LWF. Note that limits of the y-axis have been lowered for better visibility of the vegetation part of the histogram, and thus, the percentage of last/single echos to first echo and the absolute number of ground echos can not be drawn from this graph.

In Figures 5.2 and 5.3 are large area histograms of the measured vegetation heights of three echo types depicted. These height distributions are either called *modeled waveform* in literature (Riano et al., 2003) or canopy density, as in many other studies. Colored in medium and darker gray, the last and single echos are (if not on ground) mostly concentrated in the upper canopy, with their maximum just before the maximum of total echos. Histograms have been derived from areas with different vegetation densities called LWF (Fig. 5.2) and STA (Fig. 5.3). Their geographical extent is marked by black rectangles in Fig. 5.1.

When comparing the two sites LWF and STA, one can note that the fraction of last and single echos in the upper canopy and lower canopy is higher for STA than for LWF, with the mean LAI from field measurements equaling about 1 at LWF and about 2 at STA. This supports our hypothesis that LAI can be estimated by the fraction of different return types inside the canopy. From the upper panels of these figures we can also read off the approximate instrument dead-time, which is the minimum vertical

distance required between two objects to be separately detected by first and last echo. This minimum distance is approximately 1 meter, which can be seen in Figures 5.2 (a) and 5.3 (a). There, a height distribution of the difference of first and last echo is shown, and one can clearly notice the gap from zero to near the 1 m bin. This minimum distance is due to the laser pulse duration. As our typical crown height is between $\sim$ 3-8 m, we should be able to receive separated echos (first/last) from the crowns in most cases.

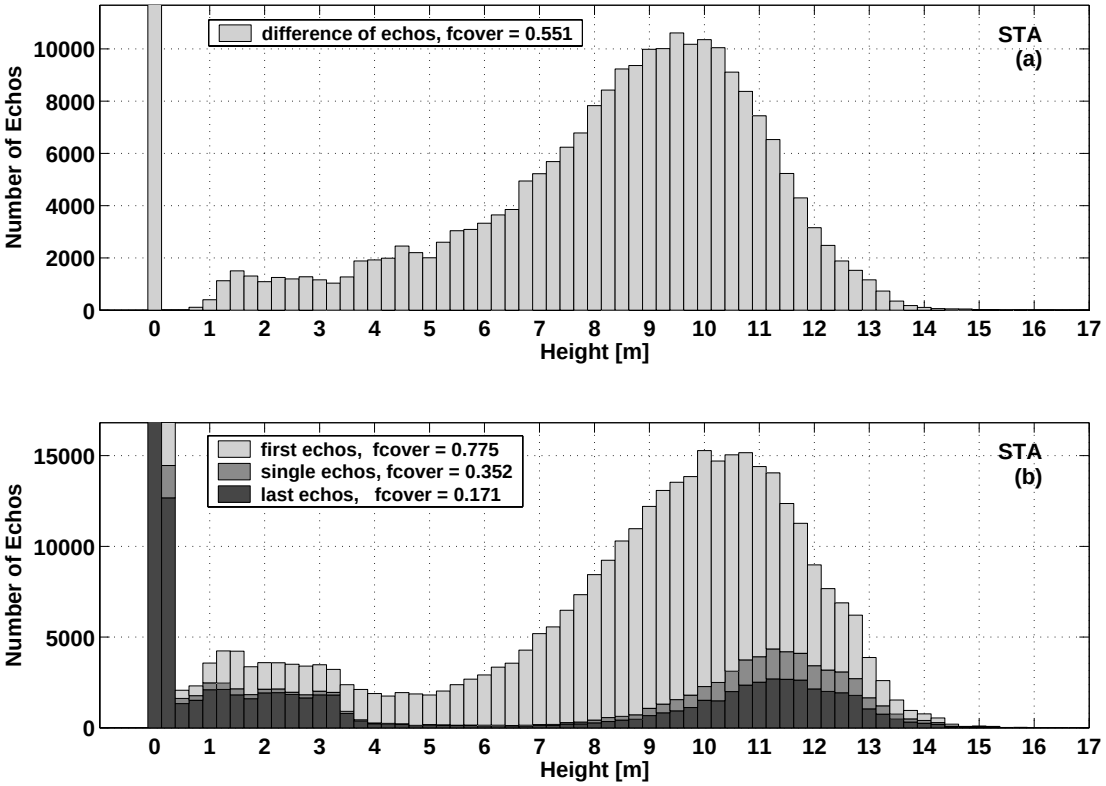

Figure 5.3: Histogram of difference of first and last pulse (a), histogram of first, last and single echos (b) for site STA. The heights have been subtracted by terrain heights interpolated to raw data coordinates from the digital terrain model Toposys provided.

5.4.2 Scales of correlation

If both ground measurements and airborne data are georeferenced to within less than 1 meter, one can assign each hemispherical photograph an area of ALS raw data for the LAI and fCover derivations. Since one does not know how far the hemispherical photograph can "see", we needed to have an estimate of how large the diameter of ALS data has to be chosen around the position of the hemispherical photograph in order to get good agreement of field estimates and the respective ALS ones. Thus, we computed fCover for patches (or traps) from 4 to 50 meters diameter according to Eq. 6.1. These patches have also been called data *traps* in literature (Lovell et al., 2003). We varied also the zenith angles, since we did not really know which zenith angles of hemispherical photographs would capture the information contained in these patches. The distance range that the hemispherical photographs can sample will depend on the vegetation

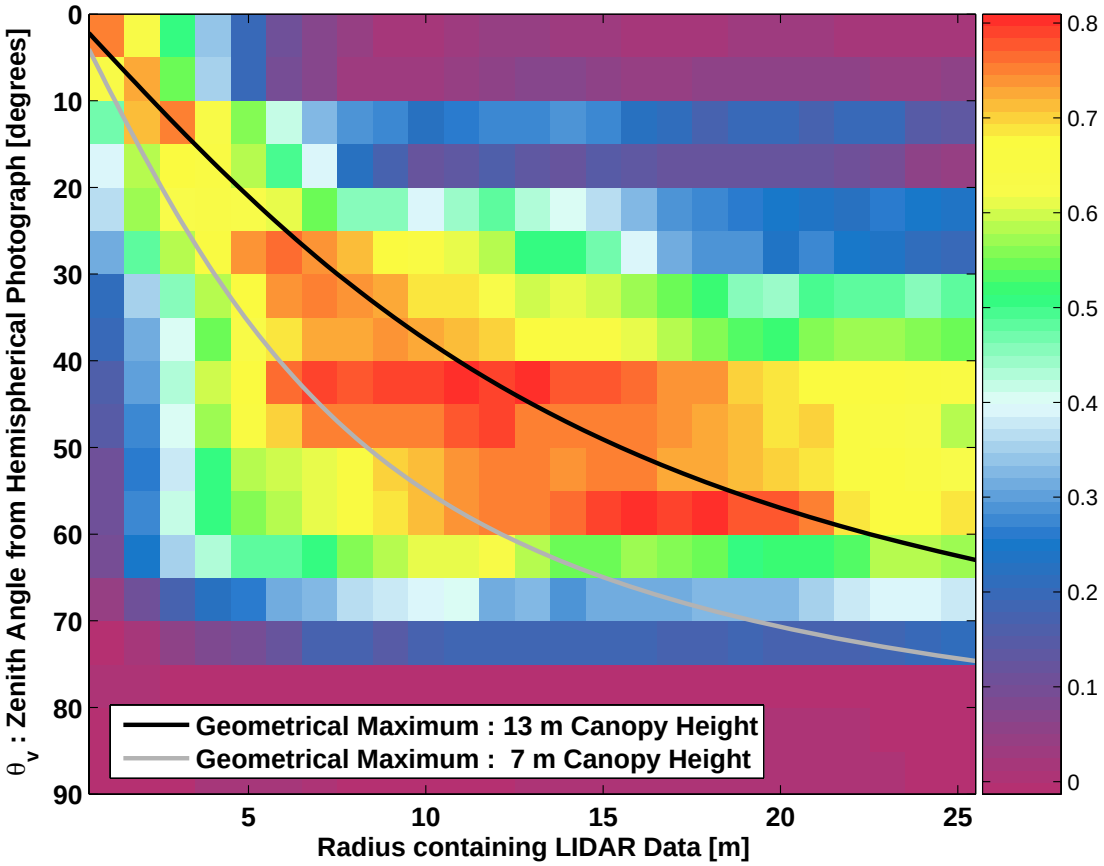

Figure 5.4: Matrix of coefficients of determination (R^2) for regression of gap fraction and ALS derived fCover for a range of zenith angles and ALS raw data patch sizes. The theoretical line of maximum correlation was plotted as well for two different canopy heights.

density in the horizontal dimension and on vegetation density and canopy height in the vertical dimension.

In Fig. 5.4 we display a matrix containing the R^2 values for each regression of field and ALS estimates of gap fraction (which in case of ALS is fCover), varying ALS data trap size (x-axis) and zenith angle of hemispherical photograph (y-axis). From this figure it is evident that significant correlation (as denoted by R^2 values $>$ 0.6) occur for all zenith angles from 0 to 65 degrees and for 1 to 25 meter in radius of ALS raw data patch. For smaller zenith angles, the correlation is high only for small data trap sizes, whereas for larger trap sizes there is only high correlation for large zenith angles. Especially, at very small zenith angles of less than 10 degrees, there is a significant linear relationship of gap fraction with ALS data at trap sizes of up to 2 meter in diameter. This shows that the georeferencing was sufficient in order to link the data at such small scales. For each zenith angle, we computed the required data trap size to capture the complete field of view of a hemispherical photograph for a defined canopy height. This should work under the assumption that the canopy is not too dense, and thus limit the distance a hemispherical photograph will be able to ”look”. Using the values of 6 m

and 13 m as lower respective upper bounds for canopy height, a trigonometric curve was computed and included in the Figure 5.4 as black and grey lines. The maxima of correlation ($R^2 > 0.6$) are in good agreement with these lines, with some regression models having an R^2 as high as 0.8.

5.4.3 fCover

For the derivation of fCover from hemispherical photographs only the innermost zenith angles up to 10 degrees should be used according to Weiss et al. (2004). The zenith angles up to 10 degrees have the highest correlation with data trap sizes of radii up to 2 meters, as can be seen at the axis-crossing in the upper-left corner of Fig. 5.4. Thus, we computed fCover from ALS data traps sized 4 m in diameter for each first and last echo data seperately. Figure 5.5 contains the regressions of these ALS derived fCover values with the respective field measurements. The upper panel contains the fCover value computed from first echo data, the lower the respective one for last echo data. The R^2 for the first echo data is 0.73, with the RMS of 0.18. The R^2 for the last echo regression is lower than that for the first echo data (0.36, with an RMS of 0.11). By comparing the regression lines with the one to one line (thick black one), one can note as well that first echo data will overestimate true fCover, whereas last echo data will underestimate. A multiple regression for both last echo and first echo based fCover against field measured values was carried out as well. There was no increase of R^2 (remained at 0.73) over the solely first echo based regression. Thus, we used the regression model based on first echo data for the computation of fCover values in Fig. 5.8. There seems to be more noise attributed to the lower values, especially in the regression of first echo derived fCover. Higher values are generally less distributed about the regression line. It is also evident that a lot of last echo derived fCover values are zero, while the hemispherical photographs still produced values greater than zero. This is an effect of vegetation being transparent in respect to last echo returns to some extent, depending on vegetation density.

5.4.4 LAI

The same procedure was carried out for the LAI proxy, but we could not vary the zenith angles GLA uses to compute LAI from. GLA offers either an *LAI 5 Ring* value, integrated from zenith angles of 0 to 75 degrees or an *LAI 4 Ring* value, which is integrated from zenith angles of 0 to 60 degrees. We used the latter for the regressions presented in this paper. Thus, we can only provide the dependency of the LAI regression relative to the size of laser raw data patch, which is depicted in Fig. 5.6. The values of R^2 are as low as 0.1 for patches of 2 m in radius and reaches a maximum of about 0.65 at about 15 m in diameter. For larger radii than that, R^2 decreases to values below 0.5. Thus, we chose a diameter of 30 m for the LAI regression in Fig. 5.7.

In Fig. 5.7 the regression of ALS derived LAI and field measured (hemispherical photographs) is depicted. R^2 is 0.69, with an RMS of 0.01. The regression model coefficients are used to compute LAI for the maps in the following section. The number of samples used for the LAI regression is 52, since we excluded all images where the influence of direct sunlight was visible. It is also visible that the spread of values (hence

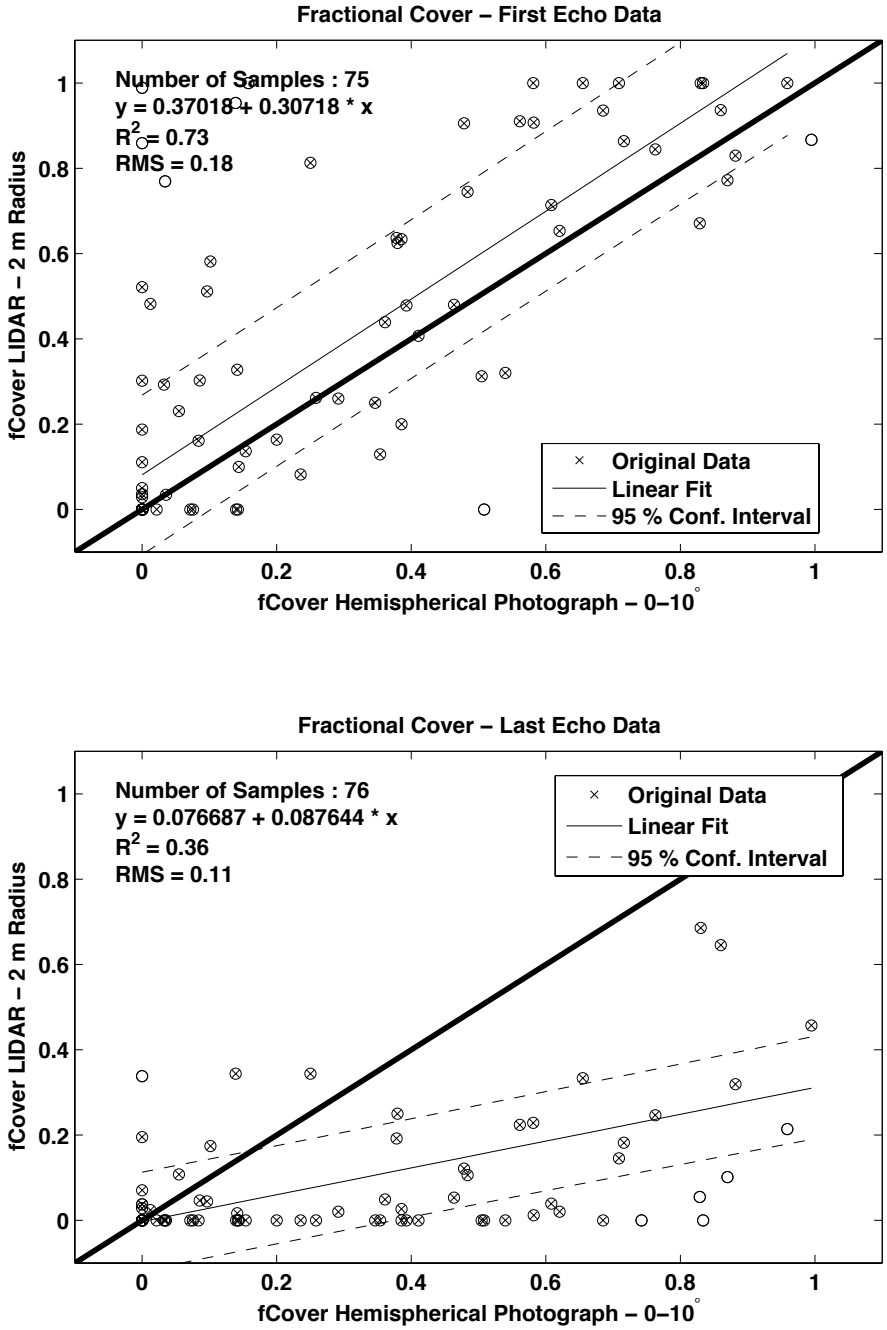

Figure 5.5: Regression of ALS derived fCover with respective values computed from hemispherical photographs. Upper panel shows regression for first echo data, lower shows regression for last echo data. Red circles denote outliers, which have not been used for the statistic computations.

noise) about the one-on-one relation is higher for larger LAI values, resulting in a behavior opposite of what was observed for fCover in Figure 5.5.

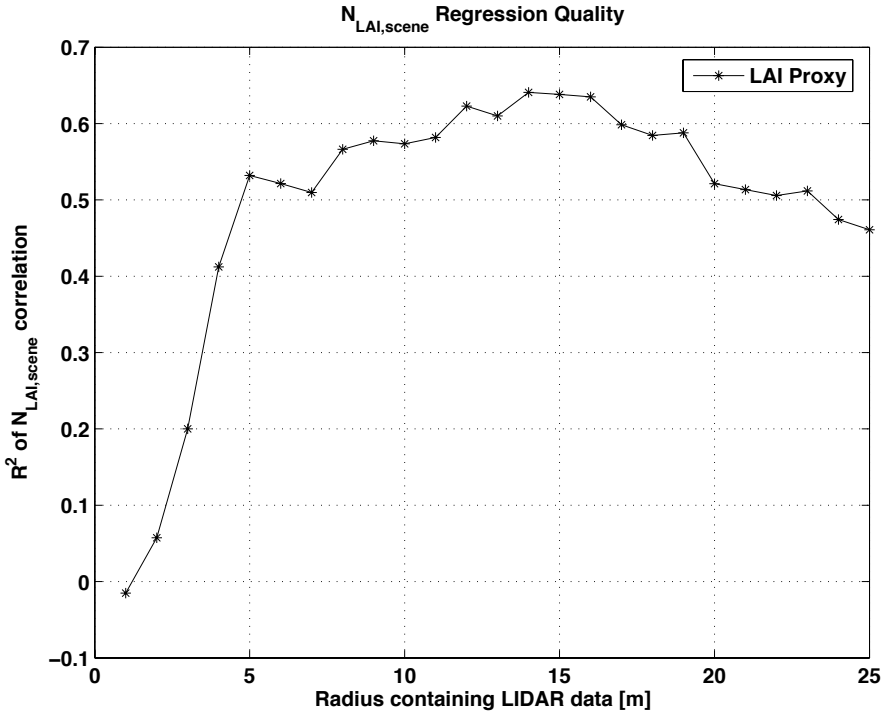

Figure 5.6: Coefficient of determination (R^2) for LAI proxy regression for a range of ALS raw data patches.

5.4.5 Maps of LAI and fCover

Using the regression models, we computed maps for both LAI and fCover for the small study area. For a qualitative comparison, we placed these maps side-by-side with maps derived by imaging spectroscopy using radiative transfer modeling (Koetz et al., 2004). The imaging spectrometer data set has been acquired by the sensor DAIS7915 in the summer 2002 over SNP in a geometric resolution of 10 meters matching the one of the ALS (Chang, 1993). The inversion of the coupled radiative transfer models PROSPECT and GeoSAIL provided biophysical vegetation properties including LAI and fCover (Jacquemoud and Baret, 1990; Huemmrich, 2001). The maps are depicted in Fig. 5.8, with the results from ALS on the left side and the respective results from imaging spectrometry on the right side. The LAI in the lower left plot is the unclumped, true LAI, which was calculated by multiplying the values of LAI_{eff} (as estimated using our regression model) by 1.75 (Koetz et al., 2004). One can note that values appear to be in the same range for both LAI and fCover as derived by both methods. The spatial patterns are more or less the same for both methods, with high LAI and fCover values towards the large alpine meadow on the right hand side. There are some differences, though. For ALS, the alpine meadow, road or river-bed areas are correctly assigned a tree LAI and fCover of 0. For the imaging spectroscopy approach forest and meadow areas would need to be identified and separated a priori since the employed radiative transfer model can not distinguish between these surface types. A standard land surface type classification based on the spectral information content of the imaging spectrome-

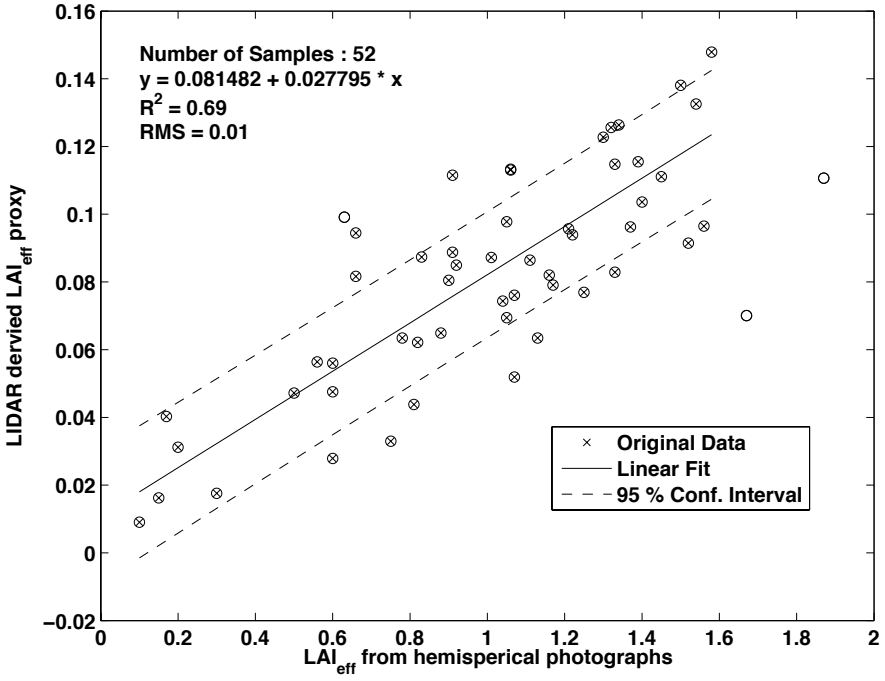

Figure 5.7: Regression of ALS derived LAI Proxy $N_{LAI,scene}$ with LAI_{eff} from hemispherical measurements. Processing of hemispherical photographs was done using GLA. Red circles denote outliers, which have not been used for the statistic computations.

ter data could be used to mask out non-forest surface types.

Comparing fCover and LAI, high LAI values are visible especially at the edges of forest or close to gaps, where the vegetation has better environmental conditions. However, the larger spatial patterns are similar to the map of fCover. This is due to the fact that other ecological parameters control the healthiness and distribution of the vegetation. The spatial patterns of these parameters and processes are then *masked* into the maps of LAI and fCover.

5.5 Discussion and Conclusions

In the past years, airborne laser scanning has been established as a valuable tool for forest structural analyses. Algorithms for the derivation of properties such as tree height, biomass and basal area have been implemented and evaluated on various study sites using laser data from both small and large footprint systems. Our aim was to show the potential of small footprint laser data for the derivation of fCover and LAI, using only single and possibly physical meaningful ALS predictor variables. As was found in previous studies, we could show that it is possible to estimate fCover from ALS data by using the fraction of vegetation echos over ground echos as a predictor variable. fCover was computed from both first and last echos using a data trap size of 2 m radius, with R^2 higher for first echo data (0.73) and lower for last echo data (0.36). First echo based

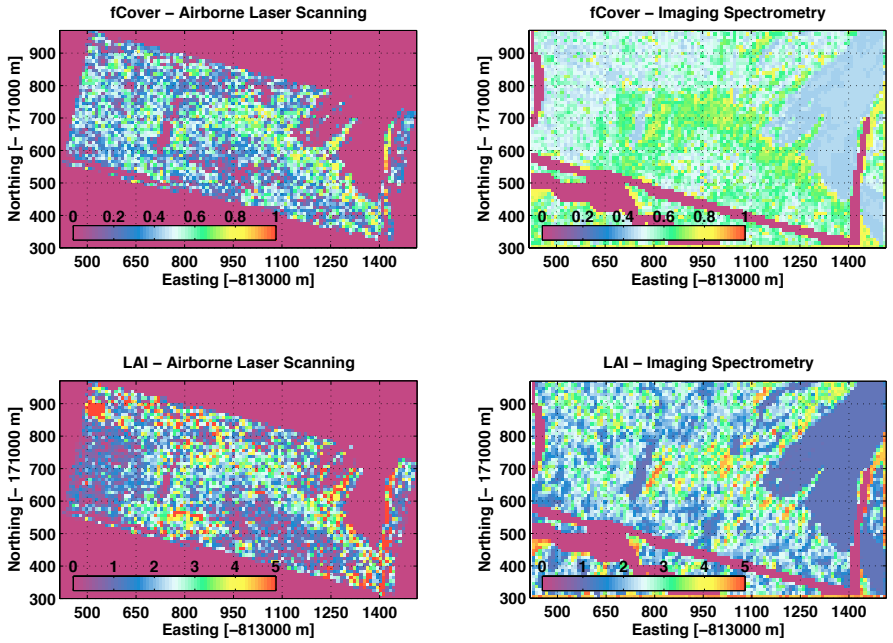

Figure 5.8: Maps of fCover and LAI for the small study area (black square in Fig. 7.1) derived both from airborne laser scanning and imaging spectrometry. The pixel size in each case is 10 meters. Note that for imaging spectrometry areas containing non vegetated surfaces (road, river bed) have been masked out.

fCover values will overestimate field measured values, whereas last echo based fCover values will underestimate them. However, we found that first echo based fCover data is sufficient in establishing a link with field data, and that adding the last echo based fCover values into a multiple regression did not improve R^2. Thus, an overestimation of ALS data is visible and needs to be corrected, e.g. through the use of a regression model as was done in our study. It is known that fCover estimates by hemispherical photographs are biased upwards due to the viewing geometry (Weiss et al., 2004; Lovell et al., 2003), which will produce a lot of vegetation pixels by stems. Thus, one could argue that the ALS would provide a truer estimate of fCover, based on its nearly optimal viewing geometry (near-nadir view). It should be noted that because of our scanner's small scanning angle of 7.15 degrees, we were able to neglect its influence on our results. For larger scanning angles (up to 30 degrees) our findings may not be valid. Significant noise was visible in our regression, leading to somewhat lower R^2 values. One source of this noise could be attributed to the difference in viewing geometry of ALS data and hemispherical photographs. For the lower values the noise is more prevalent than for the higher values, which could be explained by heterogeneity effects in the lower-density canopy of the STA site. This is where most of the lower values originate from. There are also many high laser values assigned with hemispherical values of zero. A high spatial sampling density is needed to get robust fCover estimates in medium dense and heterogeneous canopies, since the area up to 10 degrees off nadir will in most cases contain sky. This is probably due to the sampling strategy, where the camera is not placed too close to a tree to avoid overestimation due to stems and for

practical considerations. For sparse coniferous canopies such as those present on our test site, there is a high proportion of sky within the first 10 degrees of zenith angle. However, ALS systems can provide a much better horizontal sampling of the forest canopy than field inventory methods such as hemispherical photographs.

We have tried to show that the fraction of different return types inside the canopy acts as a new and direct predictor variable for LAI. Regression of the ALS estimates with field data from hemispherical photographs showed moderate to good agreement, with an R^2 of 0.69 and an RMS of 0.01. For LAI, the ALS data trap size showing best correlation with hemispherical photographs was 15 m in diameter, much larger than the one used for fCover. This is explained by GLA using all zenith angles from 0 to 60 degree for it's LAI_{eff} computation.

However, an instrument and vegetation type specific calibration parameter will have to be applied to the ALS derived estimates in any case. The vegetation specific parameter will probably be influenced by two factors, i.e. reflectance differences and clumping of canopy elements at smaller scales than footprint size. Clumping is a well studied phenomenon, since it needs to be corrected for most field based methods as well (e.g. LAI2000, hemispherical photographs, ceptometer, (Jonckheere et al., 2004)). Correction factors have been derived for various canopy types, that are used in day to day field work. Hence, it would not be too big of a problem to extend their use to ALS data. Canopy reflectance, though, is an issue that requires a more complicated procedure. For ALS - LAI_{eff} estimates to be inter-comparable, the reflectance of canopy elements in the wavelength of the laser (the ALS system used provides 1560 nm) should be roughly the same. Modern ALS systems allow as well the recording of the intensity of the returned signal, so this information could be used for assessing effects of canopy reflectance differences. Unfortunately, this option was not yet available in 2002 when our flight campaign was carried out. The processing of hemispherical photographs involves the process of manually thresholding images, a potential source for biases and random noise. Nobis and Hunziker (2005) have tried to overcome this by using automatic thresholding. A very common feature of LAI derived from passive remote sensing data is the saturation for high values (Colombo et al., 2003; Koetz et al., 2005). Our approach seems to be capable of returning effective LAI values above 4 (see Fig. 5.8). Further research is needed to determine whether this finding is robust.

A systematic error that could also explain the noise present in our regressions may be the inability of the hemispherical photographs to separate between-crown and within-crown gap probabilities, which they can not discriminate. By comparison, the small-footprint ALS can do this to an certain extent. There is some ambiguity regarding laser returns from the edges of trees, which could be misclassified as full crown hits. Their ratio of first to single/last echos would not be representative for the within-crown-gap probability. A more sophisticated treatment of the three return classes to retrieve LAI, instead than just taking the fraction of first to single and last returns could also improve the results. It might be that the single returns are more sensitive to LAI changes and vice versa, depending on vegetation type and thresholding used. It would be beneficial to have instruments that deliver inter-comparable results for LAI and fCover from very different areas. This can only be achieved by taking the radiative regime and the associated physical processes into account. We have tried to take a step in that direction by

choosing direct, physically meaningful metrics of ALS raw data for LAI and fCover.

Comparing our results with findings from imaging spectrometry from the same test area, we found good agreement in spatial patterns, but also a systematic overestimation of canopy fCover by imaging spectrometry in areas were only few to no trees were situated. Thus, ALS does provide a truer estimate of canopy fCover in these regions. Furthermore, areas which do **not** contain vegetation of a certain height do not need to be masked out manually; a simple threshold will do. The high resolution maps of fCover and LAI could have a great potential for forest structural analysis, but so far they have not been applied to tasks such as habitat analysis or other ecological problems, with exception of the work of Hill et al. (2004), where the potential of ALS data for bird habitat quality assessment was studied.

We have found that the absolute values of fCover are highly dependent on the size of lidar raw data trap, similar to findings by Lovell et al. (2003). This effect is dependent on the size and spatial distribution of canopy elements (e.g. trees). For a completely homogeneous canopy there should be no scale dependency of fCover above a certain granularity scale, e.g. in case of a corn field data traps larger than about one meter should not vary significantly in their fCover values. Combined with methods for single tree extraction (Hyyppä et al., 2001; Morsdorf et al., 2004), the work we presented would allow the direct retrieval of a close to "true" foliage profile from airborne laser scanning data (Ni-Meister et al., 2001; Lovell et al., 2003). This is due to the fact that between-crown and within-crown-gap probability can be discriminated. This combination of the two approaches will be a subject of future work. Only the small scale clumping on scales smaller than footprint size needs to be corrected, whereas crown dispersion is actually known due to high point density and small footprint size of the laser scanner used in this study. The downside of small footprint laser scanning are its relatively high costs, which would impede a campaign over a greater area only for e.g. LAI retrieval. But since these systems offer many other benefits (e.g. precise terrain models, forest boundaries, the ability of deriving single tree characteristics), the cost per feature will decrease. Currently, the country of Switzerland is being scanned by a small footprint laser scanner up to heights of 2000 m AGL. This will be a valuable multi-purpose data-set, where LAI and fCover could be additional features. Further studies, possibly including radiative transfer modeling of single scenes could aid in further investigating the relationships we established and how robust they are with respect to different site conditions and sensor specifications. Of special interest would be differences in canopy reflectance and different ALS system configurations. Some of these ALS specific parameters that most probably have an influence on the metrics we used are flying height (footprint size, point spacing), laser wavelength and incidence angle.

5.6 Acknowledgments

This project is funded by the EC project "Forest Fire Spread and Migitation" (SPREAD), EC-Contract Nr. EVG1-CT-2001-00027 and the Federal Office for Education and Science of Switzerland (BBW), BBW-Contract Nr. 01.0138.

Bibliography

Andersen, H.-E., McGaughey, R. J., Reutebuch, S. E., 2005. Estimating forest canopy fuel parameters using lidar data. Remote Sensing of Environment 94 (4), 441–449.

Andersen, H.-E., Reutebuch, S. E., Schreuder, G. F., 2002. Bayesian object recognition for the analysis of complex forest scenes in airborne laser scanner data. In: ISPRS Commission III, Symposium 2002 September 9 13, . G. A. (Ed.), ISPRS Commission III, Symposium 2002 September 9 - 13, 2002, Graz, Austria. pp. A–035 ff (7 pages).

Bonan, G. B., Mar. 1993. Importance of leaf area index and forest type when estimating photosynthesis in boreal forests. Remote Sensing of Environment 43 (3), 303–314.

Chang, S.-H., M. J. W. e. a., 1993. 79-channel airborne imaging spectrometer. Im. Spec. of the Terr. Env., SPIE 1937, 164–172.

Chatterjee, S., Hadi, A., 1986. Influential observations, high leverage points, and outliers in linear regression. Statistical Science 1 (3), 379–416.

Chen, J. M., P. M. R. e. a., 1997. Leaf area index of boreal forests: Theory, techniques, and measurements. Journal of Geophysical Research-Atmospheres 102 (D24), 29429–29443.

Cohen, W. B., Maiersperger, T. K., Gower, S. T., Turner, D. P., 2003. An improved strategy for regression of biophysical variables and landsat etm+ data. Remote Sensing of Environment 84 (4), 561–571.

Colombo, R., Bellingeri, D., Fasolini, D., Marino, C. M., 2003. Retrieval of leaf area index in different vegetation types using high resolution satellite data. Remote Sensing of Environment 86 (1), 120–131.

Finney, M., 1998. FARSITE: Fire Area Simulator-Model. Development and Evaluation. USDA Forest Service Research Paper, RMRS-RP-4.

Frazer, G., Trofymow, J., Lertzman, K., 1997. A method for estimating canopy openess, effective leaf area index and photosynthetically active photon flux density using hemispherical photography and computerized image analysis techniques. Tech. rep., Information Report BC-X-373, Natural Resources Canada, Canadian Forest Service, Pacific Forestry Centre, Victoria, BC.

Gower, S. T., Kucharik, C. J., Norman, J. M., 1999. Direct and indirect estimation of leaf area index, fapar, and net primary production of terrestrial ecosystems. Remote Sensing of Environment 70, 29–51.

Hill, R., Hinsley, S., Gaveau, D., Bellamy, P., 2004. Predicting habitat quality for great tits (parus major) with airborne laser scanning data. International Journal of Remote Sensing 25, 4851–4855.

Holmgren, J., Persson, A., 2004. Identifying species of individual trees using airborne laser scanner. Remote Sensing of Environment 90, 415–423.

Huemmrich, K. F., 2001. The geosail model: a simple addition to the sail model to describe discontinuous canopy reflectance. Remote Sensing of Environment 75 (3), 423–431.

Hyyppä, J., Kelle, O., Lehikoinen, M., Inkinen, M., 2001. A segmentation-based method to retrieve stem volume estimates from 3-d tree height models produced by laser scanners. IEEE Transactions on Geoscience and Remote Sensing 39, 969–975.

Jacquemoud, S., Baret, F., Nov. 1990. Prospect: A model of leaf optical properties spectra. Remote Sensing of Environment 34 (2), 75–91.

Jonckheere, I., Fleck, S., Nackaerts, K., Muys, B., Coppin, P., Weiss, M., Baret, F., 2004. Review of methods for in situ leaf area index determination: Part i. theories, sensors and hemispherical photography. Agricultural and Forest Meteorology 121 (1-2), 19–35.

Koetz, B., Baret, F., Poilve, H., Hill, J., 2005. Use of coupled canopy structure dynamic and radiative transfer models to estimate biophysical canopy characteristics. Remote Sensing of Environment 95 (1), 115–124.

Koetz, B., Morsdorf, F., Sun, G., Ranson, K. J., Itten, K., Allgower, B., 2006. Inversion of a lidar waveform model for forest biophysical parameter estimation. IEEE Geoscience and Remote Sensing Letters 3, 49–53.

Koetz, B., Schaepman, M., Morsdorf, F., Itten, K., Allgöwer, B., 2004. Radiative transfer modeling within a heterogeneous canopy for estimation of forest fire fuel properties. Remote Sensing of Environment 92 (3), 332–344.

Kvalseth, T. O., 1985. Cautionary note about r^2. American Statistician 39, 279–285.

Lauber, K., Wagner, G., 1996. Flora helvetica. flora der schweiz. Bern, Stuttgart, Wien, Paul Haupt Verlag, 1613.

Lefsky, M. A., Cohen, W. B., Acker, S. A., Parker, G. G., Spies, T. A., Harding, D., 1999. Lidar remote sensing of the canopy structure and biophysical properties of douglas-fir western hemlock forests. Remote Sens. Environ. 70, 339–361.

Lovell, J., Jupp, D., Culvenor, D., Coops, N., 2003. Using airborne and ground-based ranging lidar to measure canopy structure in Australian forests. Canadian Journal of Remote Sensing 29 (5), 607–622.

Means, J. E., Acker, S. A., Fitt, B. J., Renslow, M., Emerson, L., Hendrix, C., 2000. Predicting forest stand characteristics with airborne scanning lidar. Photogrammetric Engineering & Remote Sensing 66 (11), 1367–1371.

Morsdorf, F., Meier, E., Kötz, B., Itten, K. I., Dobbertin, M., Allgöwer, B., 2004. Lidar-based geometric reconstruction of boreal type forest stands at single tree level for forest and wildland fire management. Remote Sensing of Environment 3 (92), 353–362.

Myneni, R., Nemani, R., Running, S., 1997. Estimation of global leaf area index and absorbed PAR using radiative transfer models. IEEE Transactions on Geoscience and Remote Sensing 35, 1380–1393.

Næsset, E., 2002. Predicting forest stand characteristics with airborne scanning laser using a practical two-stage procedure and field data. Remote Sensing of Environment 80 (1), 88–99.

Næsset, E., 2004. Effects of different flying altitudes on biophysical stand properties estimated from canopy height and density measured with a small-footprint airborne scanning laser. Remote Sensing of Environment 91 (2), 243–255.

Ni-Meister, W., Jupp, D. L. B., Dubayah, R., 2001. Modeling lidar waveforms in heterogeneous and discrete canopies. IEEE Transactions on Geoscience and Remote Sensing 39 (9), 1943–1958.

Nobis, M., Hunziker, U., 2005. Automatic thresholding for hemispherical canopy-photographs based on edge detection. Agricultural and Forest Meteorology 128 (3-4), 243–250.

Riano, D., Meier, E., Allgöwer, B., Chuvieco, E., Ustin, S. L., 2003. Modeling airborne laser scanning data for the spatial generation of critical forest parameters in fire behavior modeling. Remote Sensing of Environment 86 (2), 177–186.

Riano, D., Valladares, F., Condes, S., Chuvieco, E., 2004. Estimation of leaf area index and covered ground from airborne laser scanner (lidar) in two contrasting forests. Agricultural and Forest Meteorology 124 (3-4), 269–275.

Schlerf, M., Atzberger, C., Feb. 2006. Inversion of a forest reflectance model to estimate structural canopy variables from hyperspectral remote sensing data. Remote Sensing of Environment 100 (3), 281–294.

Smolander, S., Stenberg, P., Dec. 2003. A method to account for shoot scale clumping in coniferous canopy reflectance models. Remote Sensing of Environment 88 (4), 363–373.

Sun, G., Ranson, K., 2000. Modeling lidar returns from forest canopies. IEEE Transactions on Geoscience and Remote Sensing 38 (6), 2617–2626.

Watson, D. J., 1947. Comparative physiological studies in the growth of field crops. i. variation in net assimilation rate and leaf area between species and varieties, and within and between years. Annals of Botany 11, 41–76.

Weiss, M., Baret, F., Smith, G. J., Jonckheere, I., Coppin, P., 2004. Review of methods for in situ leaf area index (LAI) determination: Part II. Estimation of LAI, errors and sampling. Agricultural and Forest Meteorology 121 (1-2), 37–53.

White, M. A., Asner, G. P., Nemani, R. R., Privette, J. L., Running, S. W., 2000. Measuring fractional cover and leaf area index in arid ecosystems: Digital camera, radiation transmittance, and laser altimetry methods. Remote Sensing of Environment 74 (1), 45–57.

Wotruba, L., Morsdorf, F., Meier, E., Nüesch, D., 2005. Assessment of sensor characteristics of an airborne laser scanner using geometric reference targets. International Archives of Photogrammetry and Remote Sensing XXXVI (3/W19), 1–6.

Yu, X., Hyyppä, J., Kaartinen, H., Maltamo, M., 2004. Automatic detection of harvested trees and determination of forest growth using airborne laser scanning. Remote Sensing of Environment 90, 451–462.

Zoller, H., 1992. Vegetationskarte des schweizerischen nationalparks und seiner umgebung. Bern, Hallwag AG.

Zoller, H., 1995. Vegetationskarte des Schweizerischen Nationalparks. Erläuterungen. National Park Forschung, 108.

Chapter 6

Assessment of the Influence of Flying Altitude and Scan Angle on Biophysical Vegetation Products derived from Airborne Laser Scanning

This chapter has been submitted to the International Journal of Remote Sensing as: F. Morsdorf, O. Frey, E. Meier, K.I. Itten, and B. Allgöwer. *Assessment of the Influence of Flying Altitude and Scan Angle on Biophysical Vegetation Products derived from Airborne Laser Scanning* **International Journal of Remote Sensing, submitted.**,

Abstract

Airborne Laser Scanning (ALS) has been established as a valuable tool for the estimation of biophysical vegetation properties such as tree height, crown width, fractional cover and leaf area index (LAI). It is expected that the conditions of data acquisition, such as viewing geometry and sensor configuration influence the value of these parameters. In order to gain knowledge about these different conditions, we test for the sensitivity of vegetation products for viewing geometry, namely flying altitude and scanning (incidence) angle. Based on two methodologies for single tree extraction and derivation of fractional cover and LAI previously developed and published by our group, we evaluate how these variables change with either flying altitude and scanning angle. These are the two parameters which often need to be optimised towards the best compromise between point density and area covered with a single flight line, in order to reduce acquisition costs. Our testsite in the Swiss National Park was sampled with two nominal flying altitudes, 500 and 900 m above ground. Incidence angle and local incidence angle were computed based on the digital terrain model using a simple backward geocoding procedure. We divided the raw laser returns into several different incident angle classes

based on the flight path data; the TopoSys Falcon II system used in this study has a maximum scan angle of 7.15 degrees. We compared the derived biophysical properties from each of these classes with field measurements based on tachymeter measurements and hemispherical photographs, which were geolocated using differential GPS. It was found that with increasing flying height the well known underestimation of tree height increases. A similar behavior can be observed for fractional cover; its respective values decrease with higher flying height. The minimum distance between first and last echo increases from 1.2 meters for 500 m AGL to more than three meters for 900 m AGL, which does alter return statistics. The behavior for incidence angles is not so evident, probably due to the small scanning angle of the system used. fCover seems to be most affected by incidence angles, with signifcantly higher differences for locations further away from nadir. As expected, incidence angle shows to be of higher importance for vegetation density parameters than local incidence angle.

6.1 Introduction

In recent years, Airborne Laser Scanning (ALS) was established as a valuable tool for the horizontal and vertical characterization of the vegetation canopy. A number of studies prove ALS to be capable of deriving canopy height, be it for stands (Lefsky et al., 1999; Means et al., 2000; Næsset and Bjerknes, 2001) or single trees (Hyyppä et al., 2001; Persson et al., 2002; Morsdorf et al., 2004). Furthermore, ALS was used to derive measures of vegetation density such as fractional cover (fCover) and/or leaf area index (LAI) (Harding et al., 2001; Lovell et al., 2003; Morsdorf et al., 2006). Tree height and crown width are mostly directly computed from either a gridded canopy height model (CHM) or the point cloud itself, whereas approaches deriving fCover and LAI most often use regression models to link ground measurements with laser predictor variables. These products comprise site and instrument specific properties, such as different sensor types, vegetation types and viewing geometry. This makes the comparison of results from different sites and sensor configurations hard, if not impossible. Acquisition settings of modern small footprint systems do influence laser return statistics, as was shown by Chasmer et al. (2006), who studied the effect of pulse energy on canopy penetration and found that pulses with higher energy penetrate further into the canopy. Thus, a need to identify universal indicators for biophysical vegetation products was adressed by Hopkinson et al. (2006), who used a vertical standard deviation as predictor for canopy height and found it to be quite robust in respect to varying site conditions and acquisition settings. Furthermore, it is expected that scan angle and flying height have an influence on the magnitude of these parameters, and that it might be systematic for some vegetation properties. Some research has already been pointing in this direction. A study of Yu et al. (2004) showed that ALS tree height underestimation as shown by Gaveau and Hill (2003) was larger for higher flying heights, as well as that fewer trees were detected the higher the flying altitude was. Ahokas et al. (2005) showed that tree height estimations would vary to some extent with scan angle. Næsset (2004) analysed the influence of flying height on the distribution of ALS predictor metrics and found little impact for flying heights lower than 1000 m above ground level (AGL). However, it is expected that especially estimations of vegetation density

will be influenced by variations of incidence angle, since the distance the laser pulse travels through the canopy will increase with scanning angle. One has to discriminate between the local incidence angle and the incidence angle. The local incidence angle is the angle between the slope of a surface (e.g. of a gridded height model) and the laser beam, while the incidence angle is the angle between the horizontal plane going through a point of a gridded height model and the laser beam. We expect the latter to have a larger influence on vegetation density estimations by ALS, while the local incidence angle will most likely have a larger influence on the accuracy of terrain height estimation, and thus on tree height estimation. Our objective is to study this effect empirically by computing incidence and local incidence angles for each flight strip of an ALS measurement campaign in the Swiss National Park. We assign differences between ALS estimates and field measurements of the most commonly derived biophysical parameters to different angle classes of both incidence and local incidence angles and test whether these differences are signficantly impacting the magnitude of derived properties.

6.2 Laser Data

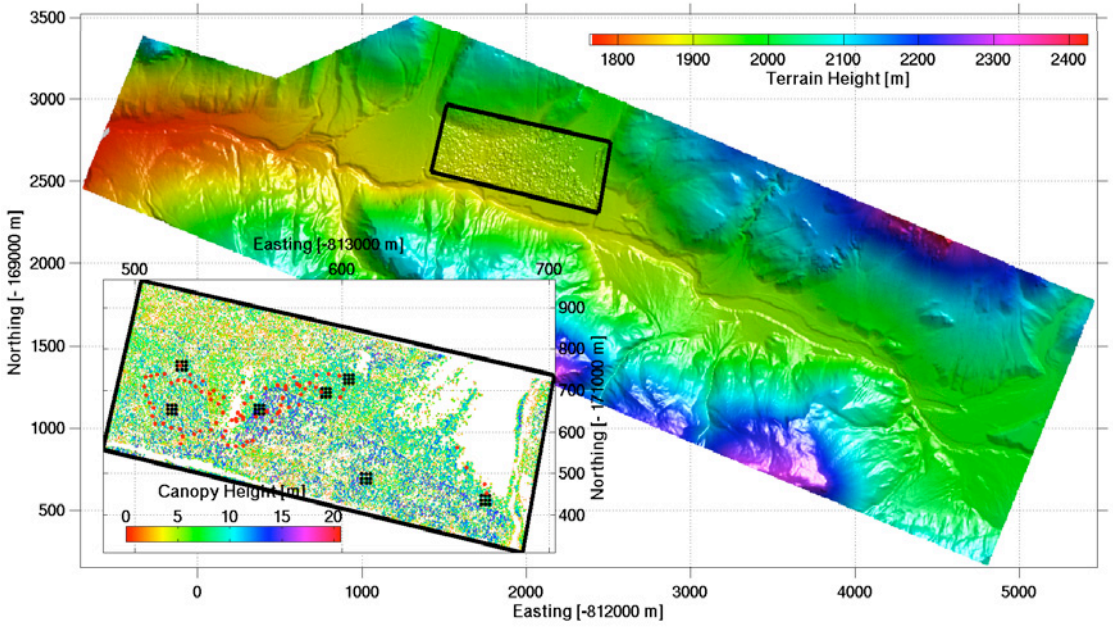

Figure 6.1: The Digital Terrain Model (DTM) of the Ofenpass area in the Swiss National Park. The smaller area marked by the black box was sampled with higher point density due to the lower flying height of 500 m above ground. A canopy height map of that area is displayed in the lower left. Black dots mark positions of hemispherical photographs that were taken in 2002 using a handheld GPS for georeferencing. Red dots indicate positions where hemispherical photographs were taken using differential GPS for georeferencing (Morsdorf et al., 2006)

In October 2002, a helicopter based ALS flight was carried out over the test area, covering a total area of about 15 km2. The ALS system used was the Falcon II Sensor developed and maintained by Toposys. The system is a fibre-array laser altimeter recording both first and last intensity peaks from the laser return signal (first/last echo FE/LE) with a fixed scan angle of ± 7.15 degrees. A flight of higher altitude was conducted with a nominal height over ground of 900 m, leading to an average point density of more than 5 points per square meter. A smaller subset of the area (0.6 km2) was overflown with a height of 500 m above ground, resulting in a point density of about 10 points per square meter in each flight strip. The footprint sizes were about 0.9 m in diameter for 900 m flight altitude and about 0.5 m in diameter for 500 m altitude. The raw data delivered by the sensor (x,y,z - triples) was processed into gridded elevation models by Toposys using the company's own processing software TopPIT. The Digital Surface Model (DSM) was processed using first echo reflections, the Digital Terrain Model (DTM) was constructed using last returns and filtering algorithms. The grid spacing of the models Toposys provided was 1 m for the large area and 0.5 m for the smaller one, with a height resolution of 0.1 m in both cases. In addition to the models provided by Toposys, we computed a DTM and DSM for each flight strip. The DSM was computed using only first echo data using gaussian weights on a set of raw data points to infer the height of each pixel. The DTM was produced using three steps. First, the minimum of all last echos contained in a pixel region was taken as a height value for that pixel. In a second step, the DTM was filtered to throw out pixel values still belonging to vegetation. This was done by using the DTM Toposys provided as a reference and all values showing a positive difference (that is our DTM was higher than the Toposys one) larger than one meter were discarded. We used one meter as threshold, since we expect systematic height errors induced through slope and scan angle effects to be smaller than one meter for a footprint size of 0.5 meter (Hodgson et al., 2005). In a third step, the resulting holes in the DTM were filled by an interpolation algorithm based on diffusion, which generally produces smoother results than algorithms which are based on Delaunay triangulation. An accuracy analysis of the raw data and the models provided by Toposys was done using six artificial reference targets being 3 by 3 meter in size and is described in detail in Morsdorf et al. (2004). The standard deviations of height estimates based on raw echos on these targets were as low as 6 cm, with the internal accuracy of the ALS data being well below the pixel size, which is 0.5 m.

6.3 Methods

6.3.1 Derivation of geophysical properties from ALS data

We derived tree height, fractional cover (fCover) and leaf area index (LAI) for each of the flight tracks separately.

6.3.1.1 Heights of single trees

For the estimation of tree heights, we used the single tree extraction algorithm presented in Morsdorf et al. (2004). This approach is based on using local maxima ex-

Falcon II Specifications	
Maximum Range	1600 m
Range Resolution	2 cm
Scanning Angle	$\pm 7.15°$
Line-scan Frequency	653 Hz
Pulse Frequency	83 kHz
Laser Wavelength	1560 nm
Number of Fibers	127
Beam Divergence	1 mrad
Pulse Length	5 ns
Pulse Energy	10 kw

Table 6.1: Specifications of Falcon II Sensor Platform. Pulse length and pulse energy were the same for the two different flying altitudes.

tracted from a Canopy Height Model (CHM) as seedpoints for a clustering algorithm being applied to the raw data. Thus, in order to obtain a CHM that will still contain effects due to incidence angle, we computed both DSM and DTM using only returns from the respective flight tracks. The algorithm for DSM generation used a weighting function to apply some smoothing in the generation process opposed to simply taking the maximum height value for each grid cell. Solely first echo data was used for generating the DSM. The DTM was computed using last echo data and was filtered subsequently to throw out spikes due to vegetetation. The quality of the DTMs was controlled by comparing them with the DTM Toposys provided for the whole test site. The raw laser echo heights were transformed into vegetation height by subtracting interpolated terrain heights from the DTM we produced by interpolation and filtering. The outcome of the single tree extraction algorithm is a structure containing n-number of trees, each with location x, y and tree height, crown diameter and crown volume. Hence, this information is derived directly from the unaltered raw laser data without using regression models. An illustration of the tree extraction method can be found in Figure 6.2.

6.3.1.2 Fractional Cover

fCover was computed directly from the terrain height reduced raw laser returns, as presented in Equations 6.1 and 6.2, which is the same way as presented in Morsdorf et al. (2006). The algorithm includes the computation of echo ratios for defined areas containing the raw data.

$$\textbf{fCover} = \frac{\sum E_{vegetation}}{\sum E_{total}} \tag{6.1}$$

with

$$E_{vegetation} = E_{total} > 1.25m \tag{6.2}$$

$E_{vegetation}$ and E_{total} denotes vegetation echos and all (ground and vegetation) echos respectively. Vegetation echos were classified using a height threshold of 1.25 meters

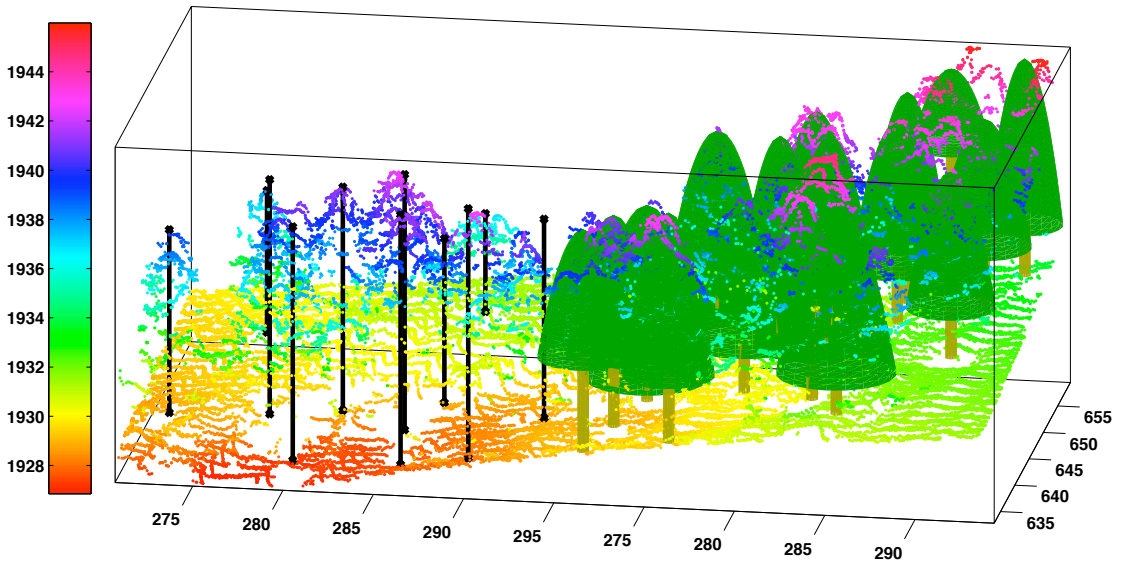

Figure 6.2: Illustration of tree segmentation algorithm. The raw data (left and right side) is segmented using cluster analysis. From the segments geometric information is derived that can be used for geometric reconstruction using primitives being parabolic cones (right side).

on the terrain height reduced point cloud. We chose a height threshold of 1.25 m, since this was the height at which the lens was placed when taking the hemispherical photographs.

We set up a grid of two meter resolution for both fCover and LAI computation. Again, for each flight track a single grid of these two parameters was computed, as shown for fCover in Figure 6.3. For both LAI and fCover, we used regression models based on all data from the lower overflight. The regression models were used as they are presented in Morsdorf et al. (2006), whith only first echo data being used for fCover estimation.

6.3.1.3 LAI

A proxy of LAI is computed from ALS data in the way it was proposed in Morsdorf et al. (2006):

$$N_{LAI} = \frac{\sum E_{FE}}{\sum E_{LE} + \sum E_{SE}} \tag{6.3}$$

E_{FE}, E_{SE} and E_{LE} denote three types of returns FE, first echo, LE, last echo and SE for single echos. The vegetation echos are classified by thresholding the height over terrain of all raw laser echos with a value of 1.25 m, according to the estimation of fCover in Eq. 6.2. This eliminates all ground echos and leaves only returns from the canopy, hence the tree crowns. This proxy is then linked through a regression model with field estimates of LAI to retrieve real LAI. As for fCover we use the regression model based on ALS data from all flight strips at 500 m AGL to compute LAI values for

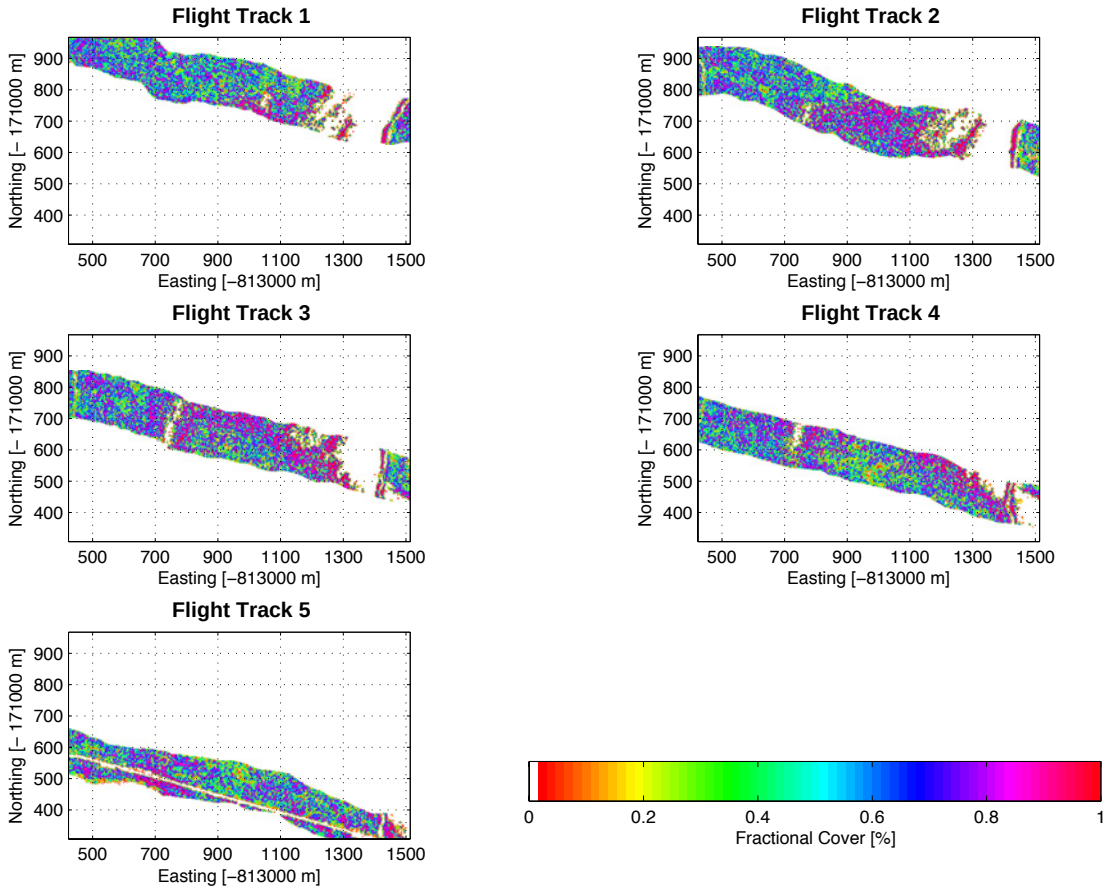

Figure 6.3: Maps of fractional cover (fCover) computed by our algorithm for each flight track. Flight strips are from the 500 m AGL overflight.

the single flight strips at 500 and 900 m AGL.

6.3.2 Field measurements

We took hemispherical photographs as field samples using a Nikon Coolpix 4500 with a fisheye lens. The small plot in Figure 7.1 shows a canopy height model (CHM) of the area over flown with the lower altitude. Black dots indicate positions where hemispherical photographs were taken in 2002. In 2005, another data collection was carried out at locations marked by red dots. In 2005, a total of 83 hemispherical photographs was taken, and the location of each image was referenced by differential GPS measurements. Since our test site is located at high altitudes with an annual mean temperature of $0°C$, the growing season is short (Dobbertin et al., 2001) and the differences in fCover and LAI introduced through growing between 2002 and 2005 can be neglected. We used three Trimble GPS receivers (one 5700 receiver and two 4700 receiver types) stations for GPS measurements. The GPS was utilized using varying occupation times according to satellite availability. GPS RMS achieved was in the range of 0.5 to 5.4 centimeters with a mean of 1.84 centimeters. For tree heights, a dataset of about 2000 dominant and subdominant tree locations was provided by the Swiss Institut for Snow and Landscape

Research (WSL, Birmensdorf). The dataset included tree height and crown diameter for each tree. We only used the dominant trees for our statistics, since tree clumping is a major issue in our study area and we were only interested in tree height understimation and not in the number of correctly identified trees or stems respectively. Dominant trees were selected from groups of trees in a radius of 1.5 meter as the tallest tree of that group. Out of originally 1984 trees, 1138 were selected as being dominant.

6.3.3 Processing of field data

The hemispherical photographs were analyzed using the Gap Light Analyzer (GLA, (Frazer et al., 1997)) software. Gap fractions were computed for zenith angles from 0 to 90 degrees with 5 degree spacing, and averaged over all azimuth angles. Areas with sun light (in about 20 images) were treated separately by a local threshold, before applying a global threshold, as was done for the rest of the images containing no illumination effects due to direct sunlight. LAI was computed for each photograph by GLA's own routines. In coniferous canopies, clumping of small scale canopy elements (e.g. needles, twigs) into shoots of some centimeters to some decimeters in size manifests an underestimation of LAI that needs to be corrected (Smolander and Stenberg, 2003). Clumping at shoot scale can be addressed by correcting the indirect LAI estimates (often called effective LAI, LAI_{eff}) with a factor depending on the projection function of canopy elements (Weiss et al., 2004). We decided to derive only LAI_{eff}, since a simple coefficient does not alter the quality of our regression. If one needs values for true LAI, one would have to multiply our values by 1.75 (Chen, 1997; Koetz et al., 2004). fCover was derived from the canopy openness measure $CO[\%]$ of GLA, which is based on the fraction of sky pixels weighted with hemispherical area by Eq. 6.4

$$fCover = 1 - CO \tag{6.4}$$

Only pixels from zenith angles smaller than 10 degrees were used for the estimation of fCover, as was proposed by Weiss et al. (2004).

6.3.4 Computation of incidence angles

Toposys provided us with the original flight path data, including sensor location and sensor attitude at a sampling rate of 200 Hz. We used this information together with the Toposys provided DTM of the lower flight to reconstruct the viewing geometry for each of the selected flight tracks. A simple backward geocoding algorithm was implemented for the computation of the incidence angle and the local incidence angle for each pixel of the DTM. An illustration of the two terms local incidence angle and incidence angle can be found in Figure 6.4.

For the sake of simplicity, we used a push broom scanner model with across track opening angle of 14.3 degrees (same as the scanning angle of the Falcon II system) and along track opening angle of 1 mrad, which resembles the beam divergence of the laser used. As the line scanning frequency is as large as 653 Hz and the largest variation of incidence angle is in accross track direction, we believe that we introduce only a small error by this simplification. The computation of incidence angles was carried out according to the following scheme:

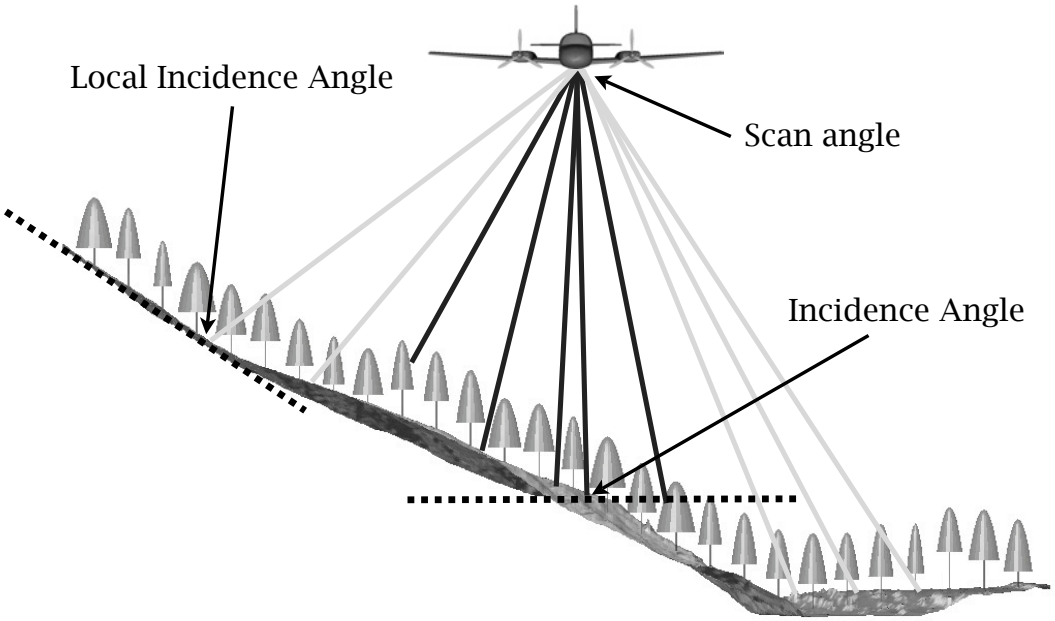

Figure 6.4: Illustration of terms local incidence angle (angle to surface normal of DTM) and incidence angle (angle to a normal of the horizontal plane). Dark gray lines symbolize first echos, light grey last echos.

1 for each element n of the flight path data

2 a section of the DTM based on the current location of the measurement platform was selected, excluding areas unlikely to be illuminated from current location

3 for each pixel i, j of the DTM

4 if the pixel with location $x(i), y(j), z(i, j)$ is inside the illuminated area based on the sensor model

5 incidence angles are computed for pixel i, j as the angle between the surface normal of the DTM (local incidence angle) and the difference vector of pixel location and sensor location or as angle between an upright vector and the difference vector (incidence angle)

6 if at location $x(i), y(j), z(i, j)$ in the angle matrix there is already a value assigned (from a previous n), then these two values are averaged and stored

7 $else$ values are stored at location i, j in angle matrix which has the same size as the DTM

For the lower overflight, a total number of five flight tracks were used to compute the incidence angle of the laser beam for every pixel of a ALS-derived DTM, while for the higher overflight only three flight strips were necessary to cover the area of the DTM. These angles were then used to classify differences between ALS estimates of fCover and tree height into different angle classes. For each of these angle bins, mean and

standard deviation of the differences were computed. Note that for vegetation hits, the ground reference point is where the laser beam intersects with the ground and not vertically below the location of the vegetation hit.

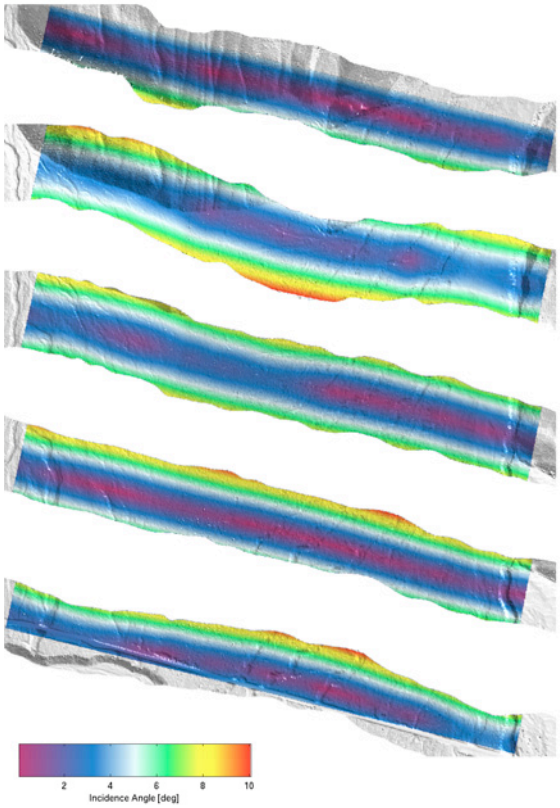

Figure 6.5: Digital terrain model computed by our algorithm for each flight track. Incidence angles that were computed for each flight track are colorcoded.

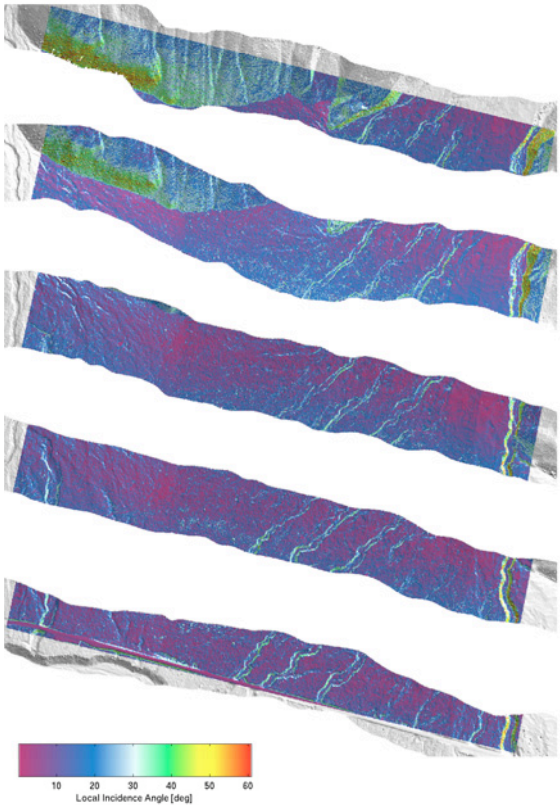

Figure 6.6: Digital terrain model computed by our algorithm for each flight track. Local incidence angles that were computed for each flight track are colorcoded.

6.3.5 Computation of differences

For both tree height and fCover, we followed two ways of computing the difference of these properties according to (local) incidence angle. First, we used field measurements to derive a difference of our ALS estimated property with the respective field measurement. These differences were then assigned to a (local) incidence angle class based on the maps presented in Figures 6.6 and 6.5. As a second method, we compared values of fCover and tree height for the same locations from overlapping flight strips. A difference of both the property and the incidence angle were computed. Since the overlap of each flight strip is about 50 % with each neighboring strip, we were able to retrieve differences of ALS based estimates based on (local) incidence angle for almost the entire study site. For both ways of computing differences we then set up angle classes to compute the mean and the standard deviation of the differences for each angle class, which can be found in the errorbar diagrams of Figures 6.7,6.9,6.11 and 6.12. We only show results from the lower overflight, since the angular variation for our system is quite small

due to it's narrow opening angle, with expected incident angles getting even smaller with higher flying altitude.

6.3.6 Significance testing

In order to jugde the statistical significance of the differences computed, we carried out two-sampled t-tests for the null hypothesis that field data and ALS based estimates are independent random samples from normal distributions with equal means and equal but unknown variances, against the alternative that the means are not equal. The same tests were carried out for the differences based solely on ALS data. For all tests, a significance level of 5% was used. For testing distributions of laser echos (see Figure 6.13) for being different or not, we used a Kolmogorov-Smirnov test. This test compares the distributions of values in two data vectors, representing random samples from some underlying distribution(s). The null hypothesis for this test is that both data vectors are drawn from the same continuous distribution. The alternative hypothesis is that they are drawn from different continuous distributions. As for the t-tests, a signifcance level of 5% was applied.

6.4 Results

6.4.1 Influence of incidence angle

6.4.1.1 Differences based on field measurements

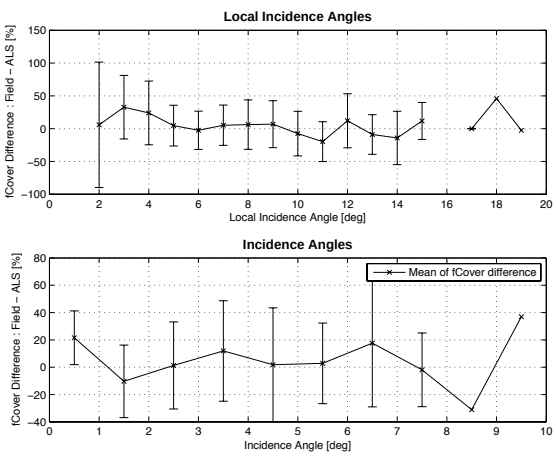

Figure 6.7: Difference of fCover for each local incidence angle class (bottom) at 500 m above ground level (AGL). Vertical bars indicate the standard deviation for each class, while the star marks the mean value. Positive values indicate underestimation by ALS.

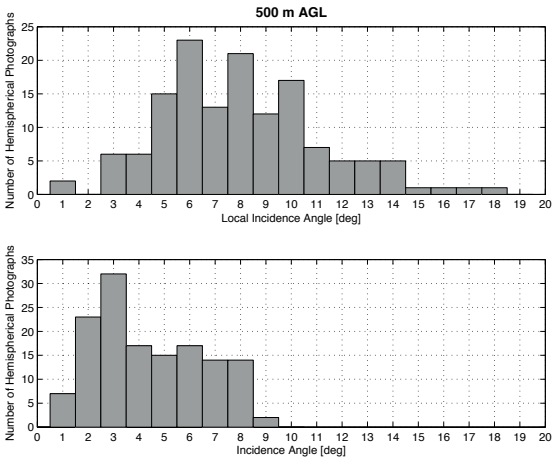

Figure 6.8: Number of hemispherical photographs per angle class for both local incidence angle (top) and incidence angle (bottom).

Figure 6.7 shows the differences of fCover estimations for different angular classes

of incidence angles from flight tracks being 500 m above ground level (AGL). The upper panel of Figure 6.7 shows the difference between ALS based estimations and field measurements for local incidence angle, while the lower panel shows results for incidence angles. One can note that there is no significant increase of differences for fCover towards larger local incidence angles. The standard deviations are larger than the differences itself, being between 30 and 50 %, while the differences are in the range of -20 to 20 %. For incidence angle, which should exhibit the strongest influence on fCover, there is no significant trend either. Standard deviations are again large, between 20 and 30 % while the difference is inbetween 0 and 20 %. Thus, the curve never detaches significantly from the line of zero difference. Values at the smallest and largest local incidence angles should be taken with caution, since only few samples contribute to the estimates, as can be seen from the distribution of samples per angle class, which is displayed in Figure 6.8. The average value of 15 to 20 field estimates for each mid range angle class drops down to only 5 for very small and very large angles. Note that the histogram contains more samples than hemispherical photographs in total, which is due to the overlapping of flight strips where one hemispherical photograph can be used as reference in two angle classes.

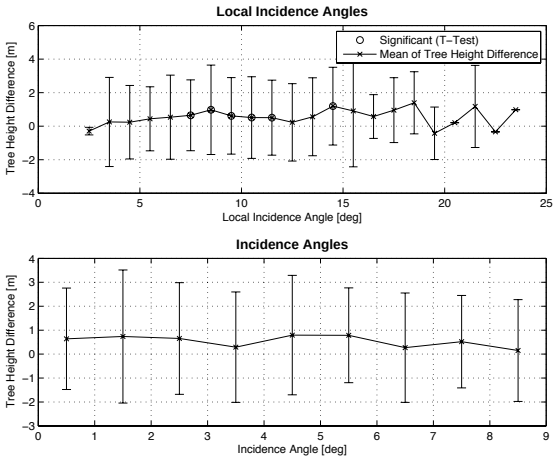

Figure 6.9: Difference of tree height for each local incidence angle (top) and incidence angle class (bottom) at 500 m above ground level (AGL). Vertical bars indicate the standard deviation for each class, while the star marks the mean value. Positive values indicate underestimation by ALS.

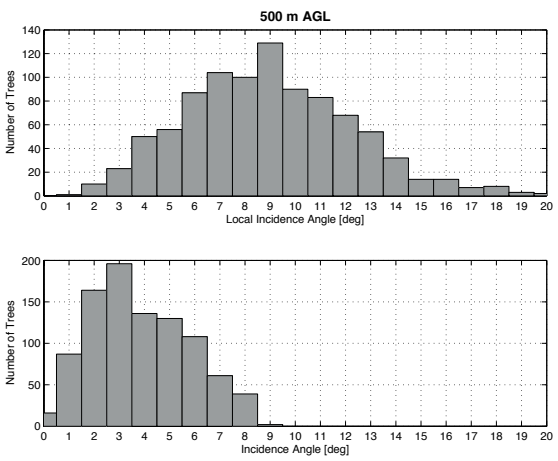

Figure 6.10: Number of matched reference tree measurements per angle class for both local incidence angle (top) and incidence angle (bottom).

Figure 6.9 displays the differences between field measured and ALS derived tree heights for different angle classes. Positive values indicate tree height underestimation by ALS. As for fCover the upper panel shows the values for local incidence angle, while the lower panel shows differences for incidence angle. Standard deviations are again much larger (two to three meters) than the mean differences (zero to one meter) for each angle class, so that there is no signifcant increase of differences neither with incidence or local incidence angle. For local incidence angle there seems to be a slight increase of

tree height underestimation from some decimeters at small angles (up to $5°$) to values of about a meter at larger angles (above $14°$). This is even more so since for larger angles than $5°$, the differences of tree height based on comparison with field measurements are significantly larger than zero, whereas for smaller angles they are not (6.9, upper panel). But as the standard deviations are again much larger, further studies are needed to figure whether this finding is robust for even larger scanning angles. Figure 6.10 displays the distribution of reference trees per angle class. As for the results of fCover, values for very small and very large angles are based on a smaller set of samples, which are about 10 to 20 opposed to more than 100 for mid range angles.

For LAI, we did not observe any significant behavior with either local incidence or incidence angle based on field data. Thus we do not present the angular results for LAI here. The height dependency of LAI estimation will be discussed though, in Section 6.4.2.

6.4.1.2 Differences based on overlapping flight strips

Since field measurements of biophysical vegetation measurements are often error prone, especially indirect methods as used for fCover and LAI, we evaluated an alternative way of comparing properties derived under different incidence angles. We compared values of fCover and tree height for the same location of overlapping flight strips and computed an absolute difference of (local) incidence angle for each pixel pair or tree location. For tree heights, we used an automated matching algorithm (see Morsdorf et al. (2004) for details) to find locations and tree heights presumably belonging to the same tree. In Figure 6.11 the difference of fCover based on overlapping flight strips is displayed, as for the results based on field measurements the upper panel shows local incidence angle, while the lower displays incidence angle. The absolute differences values for fCover are for all local incidence angles smaller as 1% , with no significant trend for either large or small angles. Standard deviation is in the order of 7-8% for all angles. The differences are much smaller compared to those observed from the statistics based on field measurements (Figure 6.7) and are mostly signifcant, supporting our hypothesis that the large mean differences and standard deviations observed in Section 6.4.1.1 are mainly introduced by field measurements. For incidence angle (lower panel in Figure 6.11), we see as well mean difference values of about 1% for small angles, but one can recognise a trend towards larger angles, where the mean difference between fCover values measured rises monotonically up to about 2.5%. Standard deviation is again small compared to field based values (7-10% opposed to 20-30%), but still large compared to the mean values, so that the observed rise towards larger angles might still not be a significant trend, even though all mean values differ signifcantly from zero as was tested with two-sampled t-tests.

The results for tree heights based on comparing overlapping flight strips are displayed in Figure 6.12. Mean tree height difference remains small (below 60 cm) for all local incidence angles, with the standard deviation being in the order of one to two meter. Thus, as with the statistics based on field measurements, no clear trend is visible from our computations, but most differences are now statistically signifcant. The differences are in the same order of magnitude for both local incidence angle and incidence

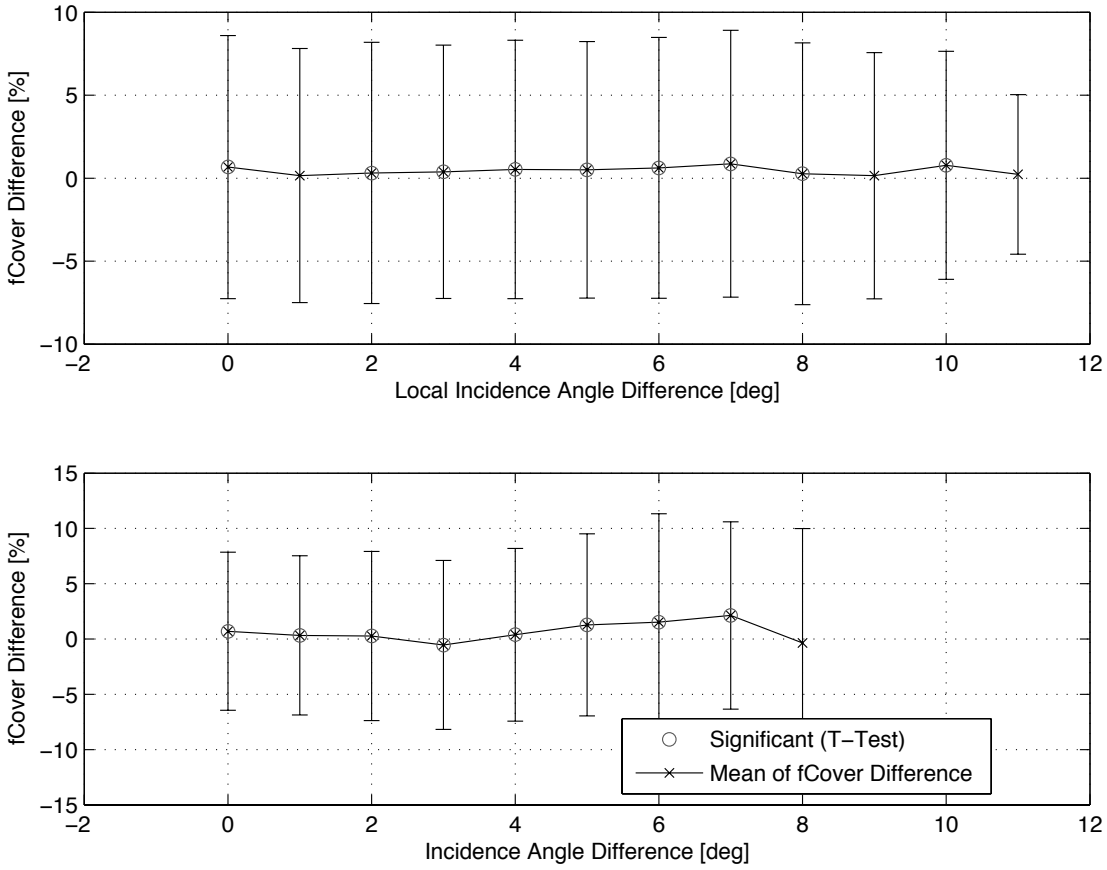

Figure 6.11: Difference of ALS based fCover estimate for each incidence angle (top) and local incidence angle class (bottom) at 500 m above ground level (AGL). Differences are computed for overlapping regions of flight strips and are assigned to (local) incidence angle classes according to the difference of the respective angles for each pixel of the overlapping area. Vertical bars indicate the standard deviation for each class, while the star marks the mean value.

angle. However, the standard deviation are still large, and thus again no significant trend towards smaller or larger angles can be observed. As for fCover, we find that the differences based on comparing overlapping flight strips are much smaller than those based on field measurements, being in the order of some decimeters for solely ALS based estimates while the differences are in the order of a meter when comparing with field measurements.

6.4.2 Influence of flying height

Table 6.2 contains the differences between fCover and tree height due to change of flight altitude. For each flight altitude, we computed the difference of field estimates and ALS based estimates using data from all angle classes. ALS based fCover is not significantly different from zero at 500 m AGL, which could be expected since our regression model is based on laser data from 500 m AGL. Values derived from data acquired with 900 m

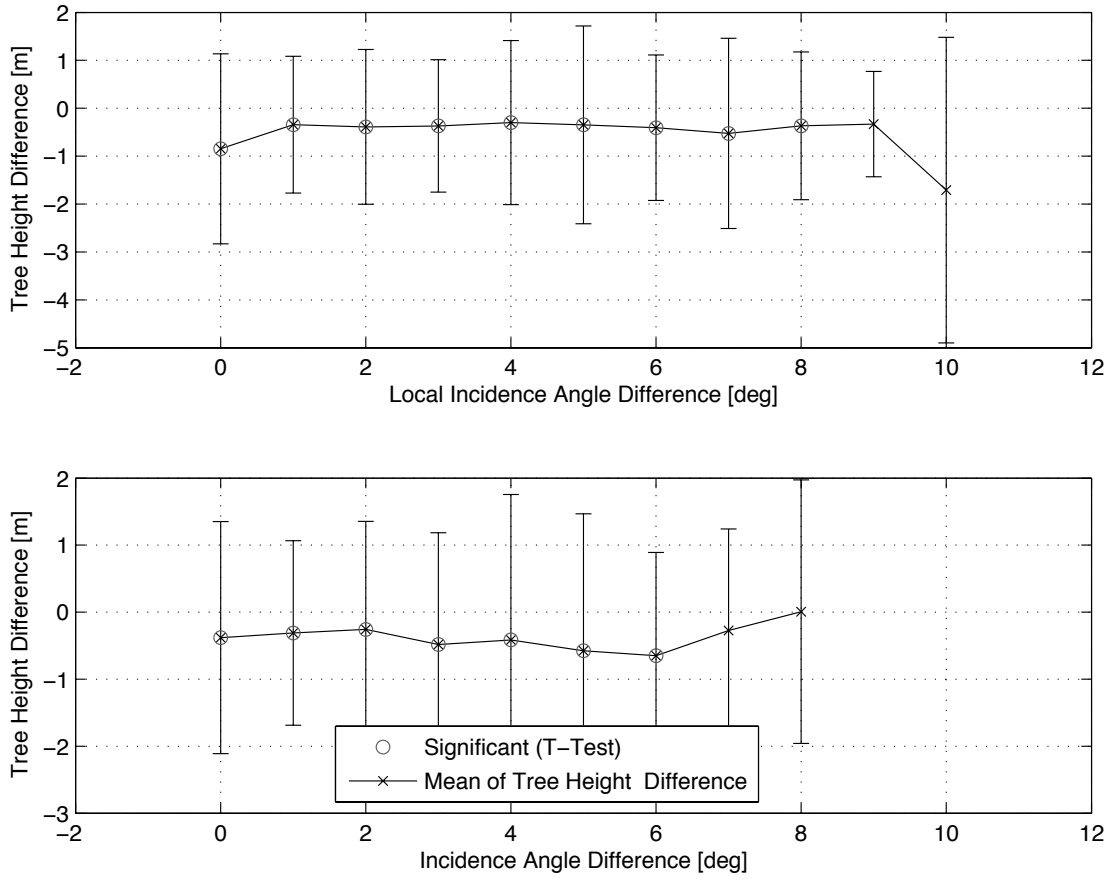

Figure 6.12: Difference of tree height for each incidence angle (top) and local incidence angle class (bottom) at 500 m above ground level (AGL).Differences are computed for overlapping regions of flight strips and are assigned to (local) incidence angle classes according to the difference of the respective angles for each pixel of the overlapping area. Vertical bars indicate the standard deviation for each class, while the star marks the mean value.

AGL underestimate absolute fCover values by about 10 %. Thus, one can state that ALS based estimates of fCover will decrease with flying height, if not for each flying altitude a different regression model is calibrated and applied. LAI shows a different behavior, with a small underestimation by ALS at 500 m AGL (-0.06), which is as for fCover not significant due to using the regression model based on the 500 m AGL data. A larger overestimation can be observed for 900 m AGL with a mean of 0.29 and a median of 0.18. The standard deviation is large for both fCover (33.7 / 30.7) and LAI (0.56 / 0.63) and is not much influenced by flying altitude.

For tree height, we find a small underestimation of field values by ALS for 500 m AGL (-0.38 m mean), which is getting larger for 900 m AGL with a mean underestimation of 0.69 m. Since tree height is estimated directly from the laser data without using regression models, this underestimation is significant and inherent to our method. The standard deviation is only a little larger for 900 m AGL, being 1.49 m, while the standard deviation at 500 m is 1.39 m. Another interesting effect related to flying altitude

ALS - FIELD	Mean	Std. Deviation	Samples
fCover 500 m AGL [%]	1.21	33.7	139
fCover 900 m AGL [%]	**-10.2**	30.7	166
LAI 500 m AGL	-0.06	0.56	156
LAI 900 m AGL	**0.29**	0.63	177
Tree Height 500 m AGL [m]	**-0.38**	1.39	658
Tree Height 900 m AGL [m]	**-0.69**	1.49	485

Table 6.2: Absolute differences between ALS estimates and field measurements for fCover, LAI and tree height. The mean, median, standard deviation and number of samples are given for each property and flying altitude. Negative values denote underestimation by ALS. Bold numbers indicate values being significantly different from zero at the 5% confidence level.

can be observed in Figure 6.13, where distribution of the difference between first and last echo for each laser pulse is displayed for both 500 AGL (upper panel) and 900 m AGL (lower panel). As can be seen by the enlarged gap in the distributions when comparing 900 m AGL with 500 m AGL, the minimum distance that two objects need to be apart to be detected separately by first and last echos, is dependent on flying altitude. For 500 m AGL, this value is about 1.2 meters, while for 900 m AGL it is almost three times as large, being about 3.6 meters. A Kolmogorov-Smirnov test was carried out to ensure that the two distributions are different at the 5% confidence level.

6.5 Discussion and conclusions

Using flight path and sensor attitude data together with field measurements of biophysical properties, we studied the influence of incidence angle and flying height on ALS based estimation of fCover, LAI and tree height. Compared to field measurements, for tree height there was a weak significant trend visible for local incidence angle which was expected to have an effect on tree height estimation. Standard deviations were very large, which could be partly explained through errors introduced through field measurements. This possible explanation is backed up by the fact that differences and standard deviations for tree height are much smaller when comparing segmented trees from overlapping flight strips. This difference in the magnitude of differences and standard deviations is as well visible for the fCover results. Again, no trend for fCover differences could be found based on the comparison with field measurements, but by comparing overlapping flight strips, we found a slight increase of fCover difference with increasing incidence angle. This behavior could be expected from theory, since the higher the incidence angle is, the higher the ALS based estimate of fCover should be due to the longer distance the laser pulse travels through the canopy and occlusion effects. For local incidence angle, the comparison of fCover values from overlapping flight strips showed no angular dependence, proving the hypothesis that ALS based fCover values should be independent from local slope. Probably due to the small scan angle (7.15 degrees) of the system used, we could not find a significant trend comparing

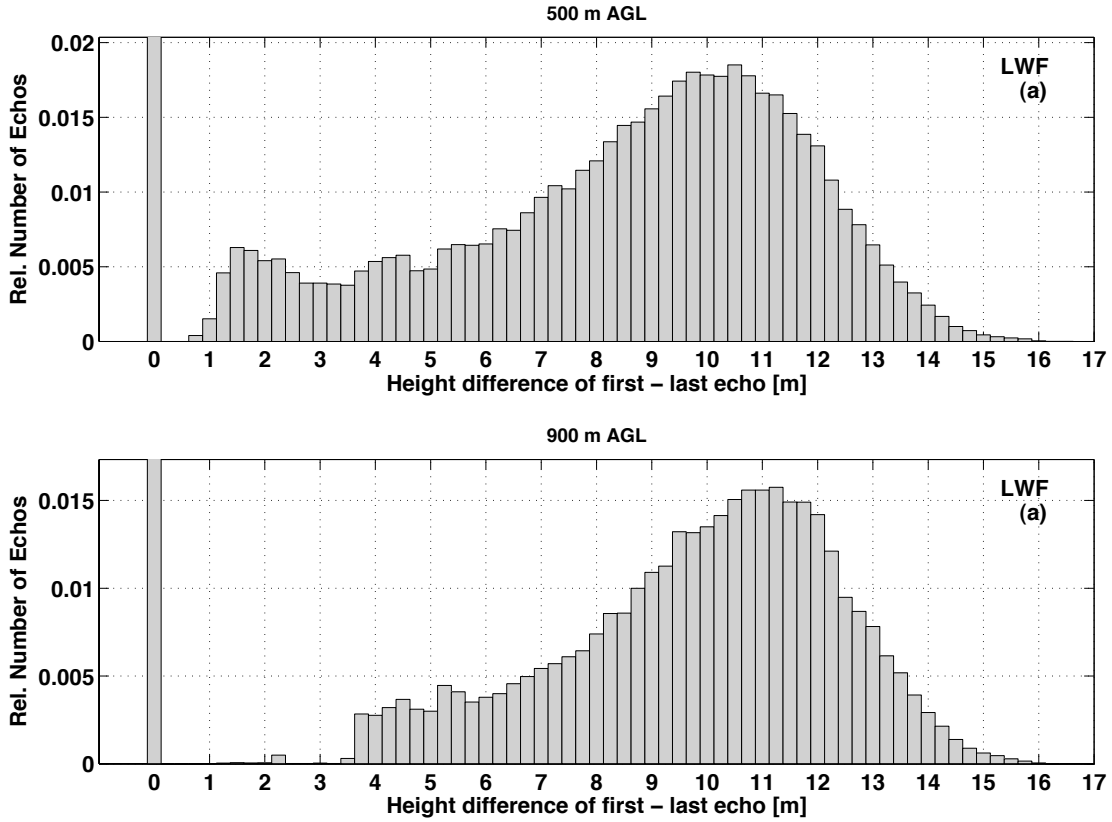

Figure 6.13: Histograms for difference of first and last echo for 500 m AGL (top) and 900 m AGL (bottom), both computed from the exactly same area. The vertical distance of object separation is about three times larger for 900 m AGL than for 500 m AGL.

solely ALS based estimates of LAI and tree height for different incidence angle classes. This is backed by the results from Ahokas et al. (2005), who found significant differences only for scan angles larger than 15 degrees. fCover estimates showed a small increase of values for larger incidence angles, but further studies, including systems utilzing larger scan angles, are needed to test whether this finding is robust. Flight altitude dependencies were much more evident in our data. Tree height underestimation by ALS increased from 500 to 900 m flying altitude by about 30 cm, which is in good agreement with previous findings (Yu et al., 2004). This tree height underestimation is caused by either hitting less tree tops due to lower point density at higher flying altitude or by less energy being reflected from the tree crowns due to the widened footprint diameter (Gaveau and Hill, 2003), which is almost double as large for 900 m AGL opposed to 500 m AGL. ALS based LAI estimates were overestimating true LAI for the higher overflight by about 0.2, opposed to a small underestimation at 500 m AGL. This is in opposition to the observed decrease of ALS based fCover values with flying height. This manifests a difference in which the two echo ratios used for computing fCover and LAI are altered by changing the flight altitude. Since LAI was computed by a ratio of first and last echos inside the canopy, one can state that there are more last echos recorded inside the canopy for higher flying heights. This must be related to

illumination issues due to the larger footprint. Finding the exact relation causing this effect will be subject of further studies, maybe using an approach similar to the one presented by Wagner et al. (2003). Opposed to theory, where the vertical separability of objects should only depend on pulse length and thus be independent of flying altitude, we found the minimum distance that needs to be inbetween two objects to be detected separately by first and last echo data to be dependent on flying height. The source of this dependency remains unclear, however, we suppose that it is related to the lower energy per unit area due to the larger footprint size for 900 m AGL, which is almost as double as large as for 500 m AGL (0.9 m opposed to 0.5 m). Another important factor influencing this effect will very probably be the kind of echo detection methods applied by the system manufacturer, as e.g. stated by Wagner et al. (2006). This effect manifests a potential source of errors for methods that use the distribution of echos inside the canopy as a predictor variable for the derivation of vegetation properties. It should be noted that the errors of the biophysical parameters are still in a tolerable range at 900 m AGL, and that flying at 500 m does not improve that much on the differences. Yu et al. (2004) made similar observations in a study using three flight altitudes (500,900 and 1500 m AGL), the quality of the ALS based data dropped only significantly when changing from 900 m AGL to 1500 m AGL. In order to study further the effect of scan angle on vegetation density products, we propose using ALS data acquired using larger scan angles. This is especially necessary, as for smaller scanning angles errors induced by field measurements are still in the same order of magnitude as the variations induced by scan angle changes. However, for the methods presented in Morsdorf et al. (2004, 2006) the effect of scan angle variation can be neglected, if a system with a small maximum scanning angle such as the TopoSys Falacon II is used. Conducting a similar study using a system bearing larger scan angles might identify the scan angles, up to which the influence of incidence angle variation might be negligible. Furthermore, it might be helpful to utilize radiative transfer models such as the ones which are commonly used in the passive optical remote sensing community (Koetz et al., 2004). A first step towards this aim has been taken by Holmgren et al. (2003), who used a simple geometric forest model to simulate the effects of scanning angle on ALS derived tree height and canopy closure (fCover). Advances in modeling of plant canopies by using L-systems and raytracing should enable one to simulate individually the effects of acquisition properties such as incidence angle, point density, terrain slope, laser footprint size, laser wavelength and canopy reflectance on the accuracy of biophysical vegetation data products. This is an advantage over realworld scenarios, where all these effects contribute indifferently to differences between ground truth and ALS based estimations of biophysical parameters.

6.6 Acknowledgments

This project is funded by the EC project "Forest Fire Spread and Migitation" (SPREAD), EC-Contract Nr. EVG1-CT-2001-00027 and the Federal Office for Education and Science of Switzerland (BBW), BBW-Contract Nr. 01.0138.

Bibliography

Ahokas, E., Yu, X., Oksanen, J., Hyyppä, J., Kaartinen, H. and Hyyppä, H., 2005. Optimization of the scanning angle for countrywide laser scanning. In: G. Vosselman and C. Brenner (eds), International Archives of Photogrammetry, Remote Sensing and Spatial Information Sciences, 115-119, Vol. XXXVI, PART 3/W19number ISSN 1682-1777, ISPRS.

Chasmer, L., Hopkinson, C. and Treitz, P., 2006. Investigating laser pulse penetration through a conifer canopy by integrating airborne and terrestrial lidar. Canadian Journal of Remote Sensing 32(2), pp. 116–125.

Chen, J. M., P. M. R. e. a., 1997. Leaf area index of boreal forests: Theory, techniques, and measurements. Journal of Geophysical Research-Atmospheres 102 (D24), pp. 29429–29443.

Dobbertin, M., Baltensweiler, A. and Rigling, D., 2001. Tree mortality in an unmanaged mountain pine (pinus mugo var. uncinata) stand in the swiss national park impacted by root rot fungi. Forest Ecology and Management 145, pp. 79–89.

Frazer, G., Trofymow, J. and Lertzman, K., 1997. A method for estimating canopy openess, effective leaf area index and photosynthetically active photon flux density using hemispherical photography and computerized image analysis techniques. Technical report, Information Report BC-X-373, Natural Resources Canada, Canadian Forest Service, Pacific Forestry Centre, Victoria, BC.

Gaveau, D. and Hill, R., 2003. Quantifying canopy height underestimation by laser pulse penetration in small-footprint airborne laser scanning data. Canadian Journal of Remote Sensing 29, pp. 650–657.

Harding, D., Lefsky, M., Parker, G. and Blair, J., 2001. Laser altimeter canopy height profiles: Methods and validation for closed-canopy, broadleaf forests. Remote Sensing of Environment 76, pp. 283–297.

Hodgson, M. E., Jensen, J., Raber, G., Tullis, J., Davis, B. A., Thompson, G. and Schuckmann, K., 2005. An evaluation of lidar-derived elevation and terrain slope in leaf-off conditions. Photogrammetric Engineering & Remote Sensing 71(7), pp. 817–823.

Holmgren, J., Nilsson, M. and Olsson, H., 2003. Simulating the effects of lidar scanning angle for estimation of mean tree height and canopy closure. Canadian Journal of Remote Sensing 29, pp. 623–632.

Hopkinson, C., Chasmer, L., Lim, K., Treitz, P. and Creed, I., 2006. Towards a universal lidar canopy height indicator. Canadian Journal of Remote Sensing 32(2), pp. 139–152.

Hyyppä, J., Kelle, O., Lehikoinen, M. and Inkinen, M., 2001. A segmentation-based method to retrieve stem volume estimates from 3-d tree height models produced by laser scanners. IEEE Transactions on Geoscience and Remote Sensing 39, pp. 969–975.

Koetz, B., Schaepman, M., Morsdorf, F., Itten, K. and Allgöwer, B., 2004. Radiative transfer modeling within a heterogeneous canopy for estimation of forest fire fuel properties. Remote Sensing of Environment 92(3), pp. 332–344.

Lefsky, M. A., Cohen, W. B., Acker, S. A., Parker, G. G., Spies, T. A. and Harding, D., 1999. Lidar remote sensing of the canopy structure and biophysical properties of douglas-fir western hemlock forests. Remote Sens. Environ. 70, pp. 339–361.

Lovell, J., Jupp, D., Culvenor, D. and Coops, N., 2003. Using airborne and ground-based ranging lidar to measure canopy structure in Australian forests. Canadian Journal of Remote Sensing 29(5), pp. 607–622.

Means, J. E., Acker, S. A., Fitt, B. J., Renslow, M., Emerson, L. and Hendrix, C., 2000. Predicting forest stand characteristics with airborne scanning lidar. Photogrammetric Engineering & Remote Sensing 66(11), pp. 1367–1371.

Morsdorf, F., Kotz, B., Meier, E., Itten, K. and Allgower, B., 2006. Estimation of LAI and fractional cover from small footprint airborne laser scanning data based on gap fraction. Remote Sensing of Environment 104(1), pp. 50–61.

Morsdorf, F., Meier, E., Kötz, B., Itten, K. I., Dobbertin, M. and Allgöwer, B., 2004. Lidar-based geometric reconstruction of boreal type forest stands at single tree level for forest and wildland fire management. Remote Sensing of Environment 3(92), pp. 353–362.

Næsset, E., 2004. Effects of different flying altitudes on biophysical stand properties estimated from canopy height and density measured with a small-footprint airborne scanning laser. Remote Sensing of Environment 91(2), pp. 243–255.

Næsset, E. and Bjerknes, K.-O., 2001. Estimating tree heights and number of stems in young forest stands using airborne laser scanner data. Remote Sensing of Environment 78(3), pp. 328–340.

Persson, A., Holmgren, J. and Söderman, U., 2002. Detecting and measuring individual trees using an airborne laser scanner. Photogrammetric Engineering & Remote Sensing 68(9), pp. 925–932.

Smolander, S. and Stenberg, P., 2003. A method to account for shoot scale clumping in coniferous canopy reflectance models. Remote Sensing of Environment 88(4), pp. 363–373.

Wagner, W., Ullrich, A. and Briese, C., 2003. Der Laserstrahl und seine Interaktion mit der Erdoberfläche. Österreichische Zeitschrift für Vermessung & Geoinformation 4, pp. 223–235.

Wagner, W., Ullrich, A., Ducic, V., Melzer, T. and Studnicka, N., 2006. Gaussian decomposition and calibration of a novel small-footprint full-waveform digitising airborne laser scanner. ISPRS Journal of Photogrammetry and Remote Sensing 60(2), pp. 100–112.

Weiss, M., Baret, F., Smith, G. J., Jonckheere, I. and Coppin, P., 2004. Review of methods for in situ leaf area index (LAI) determination: Part II. Estimation of LAI, errors and sampling. Agricultural and Forest Meteorology 121(1-2), pp. 37–53.

Yu, X., Hyyppä, J., Kaartinen, H. and Maltamo, M., 2004. Automatic detection of harvested trees and determination of forest growth using airborne laser scanning. Remote Sensing of Environment 90, pp. 451–462.

Chapter 7

Assessment of sensor characteristics of an airborne laser scanner using geometric reference targets

This chapter has been published as: L. Wotruba, F. Morsdorf[1], E. Meier, and D. Nüesch *Assessment of sensor characteristics of an airborne laser scanner using geometric reference targets* **International Archives of Photogrammetry and Remote Sensing, 2005 , XXXVI , 1-6**,
Reprinted with Permission.

7.1 Abstract

In order to get an experimental insight on the characteristics of a modern airborne laser scanning system, we carry out a set of experiments using geometrical targets on an air strip and use different flying heights. Sensor noise and relative accuracy is evaluated through 4 cardboard tables, being plain and homogeneously reflecting. The standard deviation of all laser returns from such a target decreases with lower flying altitude, as well as positional offsets computed tend to increase with flying altitude. The positional error along track is smaller than across track, probably due to different point spacing in these two directions. Target size and reflectance effects are assessed using wooden slats of different widths and colors. The effect of reflectance on target visibility is much larger than the effect of target size, which is in agreement to theoretical findings. Effective footprint size is attempted to be determined by slats with high reflectance forming a star. The difference between geometric (computed only by beam divergence) and effective footprint size increases with measurement distance, with the effective diameter being smaller than the geometric one.

7.2 Introduction

[1]Corresponding author

LIght **D**etection **A**nd **R**anging (LIDAR) is able to deliver coordinates on a reflecting surface based on an accurate measurement of position and orientation of a sensor platform and a time of flight measurement of a laser pulse. An introduction to airborne laser scanning was given by Wehr and Lohr (1999), while a comprehensive summary of it's underlying theory is given by Baltsavias (1999). Airborne laser scanning first was only a tool for generating digital terrain models (Kraus and Pfeifer, 1998; Petzold et al., 1999), but soon its use was extended to more complex applications such as vegetation analyses (Hyyppä et al., 2001; Næsset, 2002; Lefsky et al., 2002) and building reconstruction (Haala and Brenner, 1999; Brenner, 2005). Despite this broad field of applications, relatively little is known about the interaction of the laser pulse with its reflecting objects. This information will become increasingly important for applications that use the raw laser data instead of raster models (e.g. (Morsdorf et al., 2004; Roggero, 2001)). For generating raster models, in most cases several echos are combined for one raster pixel, thus reducing random errors in height and position. Systematic errors, e.g. introduced through reflectance effects, however will affect as well raster models. Most small footprint scanners rely on some sort of thresholding the return signal to trigger their first and last or even multiple returns. Many effects influence the triggering of an echo from the return signal, e.g. the object's geometrical properties and reflectance, the sensor characteristics (beam divergence, thresholding algorithm) and viewing geometry (incident angle and distance to object). For simple geometric objects such as houses and roads, these effects are quite easy to handle. The added noise (e.g. through reflectance changes) to single measurements will add some uncertainty to the position and orientation of the objects; but they remain 'visible' in the raw laser data due to their inherent geometry, provided this geometry is large enough to capture a significant amount of laser echos. For complex surfaces such as e.g. vegetation, the nature of the triggered returns is much less evident. For instance, it is known that tree height is systematically underestimated by laser scanners not only due to sampling effects, but also by penetrating the canopy until a critical vegetation density is reached to trigger e.g. a first return (Gaveau and Hill, 2003; Morsdorf et al., 2004). If a vegetation density can be considered critical in this context depends on quite a few factors: distribution, size and reflectance of canopy elements, foot print size and laser beam energy distribution. Attempts have been made to use geometrical and statistical models of vegetation to model the return waveform of large footprint sensors (Sun and Ranson, 2000; Ni-Meister et al., 2001), but this has not been carried out for small footprint data. However, the same principles can be applied, just at much smaller scales. If, for large footprint sensors (diameter $\sim 10m$) tree size and distribution are important parameters, with small footprint scanners (diameter $\sim 1m$) we need to address canopy characteristics at the branch and leaf level. But for these modeling approaches, a detailed knowledge about the sensor characteristics is needed. Our objective is to use self constructed geometric reference targets to infer estimates of sensor characteristics in respect to effective footprint size, echo separation, reflectance effects as well the dependence of these effects on flying height.

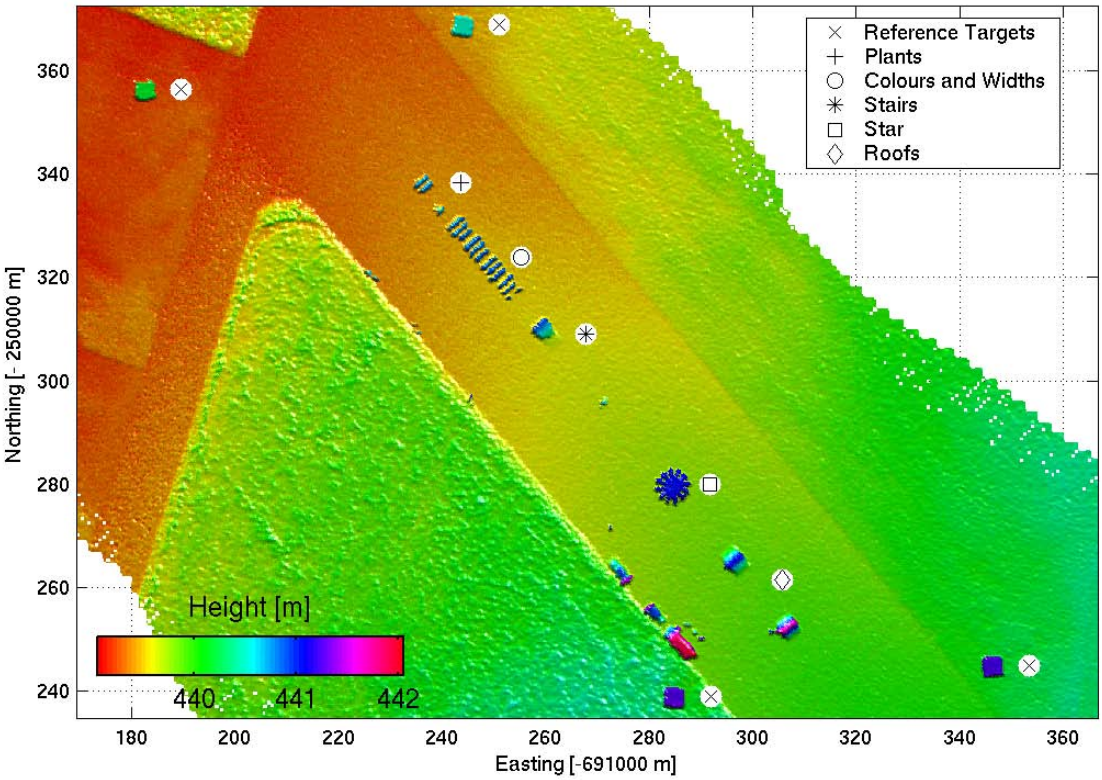

Figure 7.1: The Digital Surface Model (DSM) of our study site, an air strip. The positions of our reference targets are marked by white circles with the respective marker being explained in the legend. The DSM is from one of the 500 m above ground flights. The stair and the roof targets are not discussed in this paper due to the constraints in paper length.

7.3 Laser-scan Data

The LIDAR system used was the Falcon II Sensor developed and maintained by the German company TopoSys. The specifications of the TopoSys Falcon II system can be taken from Table 7.1. The system is a fiber array laser altimeter recording both first and last reflection from the laser signal (first/last echo). For some return signals, only one echo is triggered, meaning that both first and last echo have the same values in x,y,z, which we will call *single echo*. This is a special case for very dense or opaque targets.

The raw data delivered by the sensor (x,y,z - triples) was processed into gridded elevation models by TopoSys using the company's processing software, TopPIT. The Digital Surface Model (DSM) was processed using the first echo reflections, the Digital Terrain Model (DTM) was constructed using the last returns and filtering algorithms.

Falcon II Specifications	
Maximum Range	1600 m
Range Resolution	2 cm
Scanning Angle	$\pm 7.15^{\circ}$
Line-scan Frequency	653 Hz
Pulse Frequency	83 kHz
Laser Wavelength	1560 nm
Number of Fibers	127
Beam Divergence	1 mrad

Table 7.1: Specifications of Falcon II Sensor Platform

7.4 Experiment Setup

We set up a collection of geometric reference targets on an air-strip about 10 kilometers north-east of Zurich, Switzerland. For georeferencing, 4 cardboard covered tables were put up at the four corners of our experiment area being roughly 120 by 180 meters in size. These tables have first been used in Morsdorf et al. (2004), a more detailed description is given there. They were used to compute the planimetric offsets, height offset and height variations of the raw laser data. A detailed discussion of these values can be found in Section 7.4.1. Furthermore, a set of geometric reference target was constructed to gain insights in different sensor aspects. The test site was over flown in different heights, with four flights being 500 m AGL and one each for 700, 900 and 1100 m AGL. The flight direction was parallel to the air strip, and all geometric targets were setup along a line in the middle of the air strip, as can be seen in Fig. 7.1. We will only focus on three types of targets due to constraints in paper length, which will be presented in detail in the following sections.

7.4.1 Reference Targets

The quality of the LIDAR data was assessed using 4 geometric reference targets being 3 by 3 meter in size. The targets were leveled to less than 0.5 degrees, using a digital angle meter. The positions of the 4 corners of each target were determined using a GPS and theodolite measurements, resulting in an internal accuracy of less than 2 cm. Regarding the models (**DSM/DTM**), the absolute positional accuracy was determined by Toposys (using the target positions) to be similar to or less than the resolution of the models, with horizontal positional accuracy being better than 0.5 m and vertical accuracy better than 0.15 m.

7.4.2 Colors and Widths

Wooden slats with three different widths and four different colors, each three meter long were set up about 1 meter apart. Their orientation was perpendicular to the flying direction, and the height over ground was 1.5 meters (see Fig. 7.2). The slat positions (as well as all other target positions) were measured using a theodolite. This target was

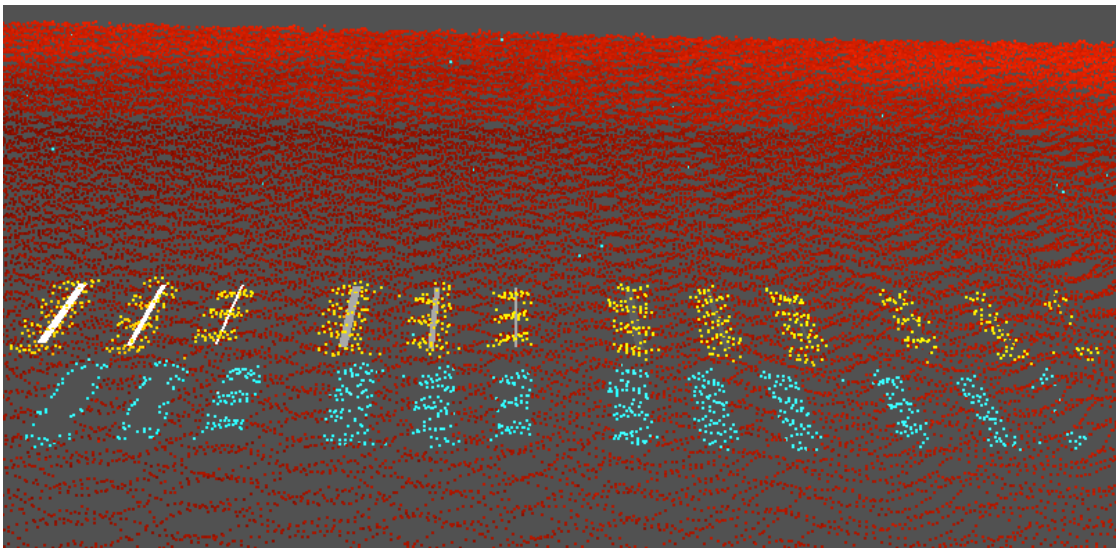

Figure 7.2: Slats with four different colors, white, light grey, dark grey and black (from left to right) and three different widths, 15, 10 and 5 cm (from left to right for each color). The length of the slats was three meter each. The lidar raw data from all 500 m AGL flights is superimposed. First echo data is colored orange to red, last echo data is colored cyan to magenta.

intended to deliver some insights on the reflectance and width needed to trigger echos at different flying heights. The reflectance values of the different colored slats have been measured using an Advanced Spectral Devices (ASD) field spec and are listed in Table 7.2. All spectra were converted to absolute reflectance by reference measurements over a Spectralon panel with known spectral properties. Since the TopoSys system has a small scanning angle of $\pm 7.15°$, the values for the nadir view should be representative.

Color	Reflectance at 1560 nm		
	Forward	Orthogonal	Nadir
Black	0.06	0.02	0.02
Dark Grey	0.14	0.09	0.1
Light Grey	0.42	0.12	0.16
White	0.66	0.48	0.52

Table 7.2: Reflectance values at laser beam wavelength for the different colored wooden slats. Three different views have been measured using an ASD field spec.

7.4.3 Siemens star

The star target (Fig. 7.3) was constructed to get an estimate of the effective footprint size. The fraction of area covered by the target versus the area covered by ground increases from outside to inside, thus simulating different densities.

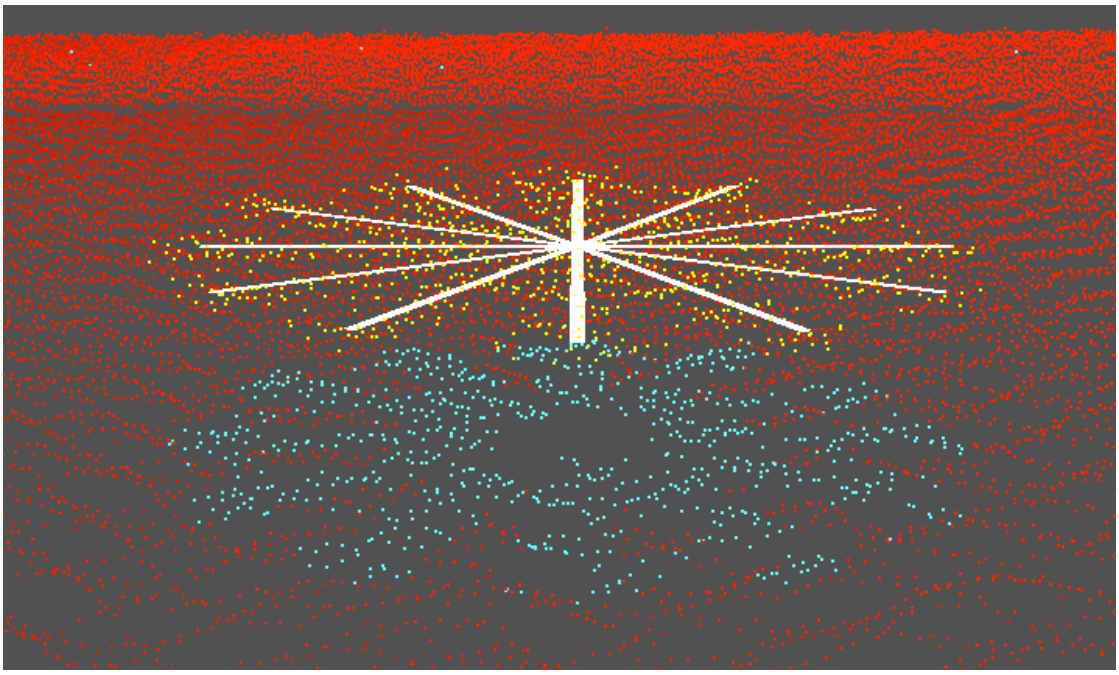

Figure 7.3: The *star* target. 12 white painted slats with a width of 5 cm were setup forming a star with a diameter of 6 meters and a height above ground of 1.5 m. The lidar raw data from all 500 m AGL flights is superimposed. First echo data is colored orange to red, last echo data is colored cyan to magenta.

7.5 Results

7.5.1 Reference Targets

We used the reference targets to infer the noise of the sensor on a plain, homogeneously reflecting surface, which can be seen as a best case scenario. In order to get an estimate on the sensors noise, we calculated the standard deviation of all points reflected from the target. A slight flying height dependency of the noise can be derived from Table 7.3. The mean values for $\sigma height$ for 500 m AGL is 4.02 cm, while being 5.18 and 5.2 for 700 and 900 m AGL respectively. For 1100 m AGL, this value is again lower, being 4.63 cm. This could be explained through the lower amount of echos from the targets at 1100 m AGL. A positional offset was calculated by minimizing the distances from the raw laser data off the target to a simple square model in an iterative manner. The model of the square was shifted in it's x and y coordinates until a global minimum of distances was found. The values for offsets and noise are listed in Table 7.3. The offset have been calculated for along track and across track direction, with the presumption that errors might be systematically larger across track. This would be due to the different point spacing of the Falcon II system, with higher point spacing along track. The values in Table 7.3 for mean differences ($\overline{\Delta x}$ and $\overline{\Delta y}$) are a little larger for along track; for the standard deviations $(\Delta x)'$ and $(\Delta y)'$ the difference is larger, suggesting lower positional differences across track. Since we took a global flight angle for the separation of along track and across track, some imprecise values may have been introduced in Table 7.3

AGL	$\overline{\Delta x}$ along track	$\overline{\Delta y}$ accr. track	$\Delta x'$ along track	$\Delta y'$ accr. track	$\overline{\sigma h}$	Pts.
$[m]$	$[m]$	$[m]$	$[m]$	$[m]$	$[cm]$	
1100	0.27	0.18	0.11	0.11	4.65	75
900	0.18	0.09	0.11	0.05	5.19	88
700	0.12	0.06	0.07	0.08	5.18	88
500	0.17	0.06	0.11	0.04	4.02	122

Table 7.3: Using the reference target data, we computed the mean positional offsets $\overline{\Delta x}$ and $\overline{\Delta y}$ for all four targets and their respective standard deviations $(\Delta x)'$ and $(\Delta y)'$, as well as the mean standard deviation of all laser points on a target $\overline{\sigma h}$ and its respective standard deviation $(\sigma h)'$ when combining the data from the four different targets. For 500 m AGL, all four flights have been used, making up for 16 single estimates of the respective values, as we have four reference targets. The last column gives the mean number of points on each target for each flying height.

due to rolling of the airplane, which can change the ratio of sampling densities locally. There should be as well a height dependency of positional accuracy, since the footprint size is increasing with flying height, and one has no means of determining *where* inside the illuminated spot the reflector was. For the positional offsets, this seem to be evident, with both mean and standard deviation being larger for 1100 and 900 m AGL than for 700 and 500 m AGL.

7.5.2 Colors and Widths

The target using different colors and widths was intended to yield an estimate at which width and reflectance first and/or last echo are triggered, under consideration of flying height. In Fig. 7.4 the results of these targets concerning first echos are depicted. Plotted is the relative visibility, that is the fraction of **first** echos on the target over ground returns, each for different widths (marked by symbols), different color (marked by color) and different flying heights (x-axis). For each of the slats, a section of the raw data with the slat width added to the expected diameter of the footprint (based on beam divergence) was cut out to do the statistics. One has to use caution with interpreting the data from 1100 m AGL, since only a few echos were contained in the raw data sections. As can be seen, at 500 and 700 m AGL and for the colors white, light grey and dark grey, a large amount of first echos (70-93 $\%$) are on the target, there are only few first echos from the ground. It can be noted that the decrease of visibility with flying height is larger for the reflectivity than for slat size. Furthermore, the visibility seems to decrease in a more linear fashion for slat width (dashed lines) than for slat reflectivity, which exhibits some nonlinear behavior for the gray slats. The white and the black slats seem to lie above respective below a threshold of detection for all flying heights, except for 500 m AGL, where the black slats trigger almost 50 $\%$ first returns. The absolute numbers, however, have to be interpreted with caution, since for the higher flying height only

few echos are available for the statistics. At 1100 m AGL, only the white slats remain clearly visible, with more than 80 percent first echos on the target. The dark grey and black slats are only able to trigger less than 20 % first echos. However, as their nadir reflectance is very low (Table 7.2), it is surprising that there are *any* echos triggered by these slats. In Fig. 7.5 the first and last echo on the target are discriminated. The dark grey fill denotes the case of both first and last echo being the same *and* on the target. Light grey stands for first echo being different from last echo, with the first echo being on the target, while white stands for both single and first echo from the ground. Since the surface of the air strip was tarmac we only get single echos off the ground. The visibility of the targets decreases both with color and width, as well as with higher flying height. The wider slats (15 and 10 cm) and brighter slats (white and light grey) are able to trigger as well single echos at lower flying heights (500 and 700 m) as there is echo separation. This manifests a "shadowing" effect, which is also visible in Fig. 7.2 on the left. At 500 meter AGL, the wider ones of the white targets are able restrain echos (even last echos) from an area that is larger than slat width. This is a well known effect from for instance power lines, their LIDAR cross-section is often almost as large as almost double the footprint size. For higher flying heights (900 and 1100 m) there is no separation of footprints, a behavior that is visible as well for all other 'transparent' targets. One exception is the five centimeter wide black slat at 900 m AGL, which triggers one separated echo. This hints towards a possible explanation of the observed height dependence of echo separation. The reflectance difference seems to play a role if the vertical distance of two objects is close to the theoretical distance for echo separation, which is half the pulse length of the laser system. That is, two objects in that range may only be separable if their reflectance is similar, as is for the black slats and the tarmac.

7.5.3 Siemens star

According to Baltsavias (1999), one has to distinguish laser footprint diameter (geometric footprint diameter) and laser beam diameter, which is often defined by distance of two opposing point in a beam cross section at a certain energy value, e.g. $1/e^2$ of the intensity at the beam center. We define another footprint size, the effective footprint, which will depend as well on the reflectivity of the target. Thus, it will give us an estimate on how large the footprint can be in order to fit in-between two slats without triggering a first echo. From Fig. 7.6 one can draw that there is no first and last echo separation for 1100 and 900 meter AGL. There are either single echos on the target or single echos on the ground, with a transition zone between the two cases, which starts at 2.5 m from the star center (1100 m AGL) or at about 2 m distance from the star's center point (900 m AGL). From the position of this transition zone, one can infer the size of the effective footprint, since at that distance the laser pulses fit in between the wooden slats. Effective means that not only the simple geometric footprint size based on beam divergence is used, but that the energy distribution across the laser beam is accounted for as well. This effective footprint will depend on the targets reflectivity, for instance, if we would have build the star using aluminum foil, we would have measured larger effective footprint diameters. It should be noted that the values for effective footprint size are less reliable for the higher flying heights, since the sampling density was not high

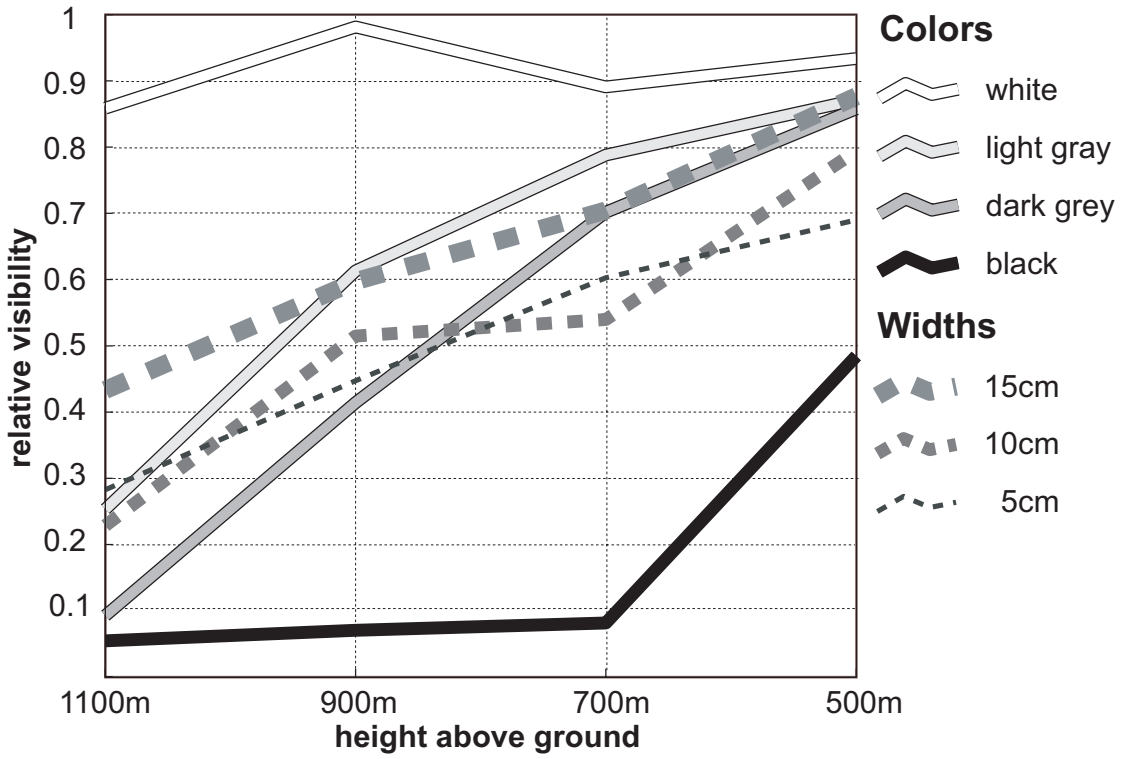

Figure 7.4: Height dependency of first returns statistics regarding the percentage of target hits in an area of slat width $\pm$ *geometric* footprint size. The legend gives information about the different colors and widths. For the widths, all 4 colors have been put together.

enough to ensure that every density (radius) of the star target was effectively hit by a laser pulse. From Fig 7.6 one can draw as well that the size of the effective footprint is height dependent. The black lines denote simulated percentages for hit target/hit ground based on the geometric laser footprint. The simulation was carried out adding a virtual buffer as large as the geometric footprint to the target. This new object is now being sampled with a large amount of infinitesimally small impulses, thus constructing a virtual data-set of laser echos containing only either target or ground hits. This data-set is treated in the same way as the real laser data to yield the percentages depicted as dashed line in Fig. 7.6. For the geometric footprint size, Baltsavias (1999) introduced following equation:

$$A = D + 2\,h\,tan(\frac{\gamma}{2}) \tag{7.1}$$

A is the footprint diameter, D the diameter of the aperture of the laser scanner (which is 6 cm for the Falcon II system), h the flying height above ground and γ the beam divergence. For the geometric footprint size, Equation 7.1 can be used, but often the sensor aperture D is neglected. At 500 m AGL the effective footprint size seems to be larger than the geometric one calculated using Eq. 7.1. This can be concluded by the simulated curve being above the ground echo distribution, opposed to the other three flying altitudes. This suggests that D can not be neglected from Eq. 7.1 for low flying

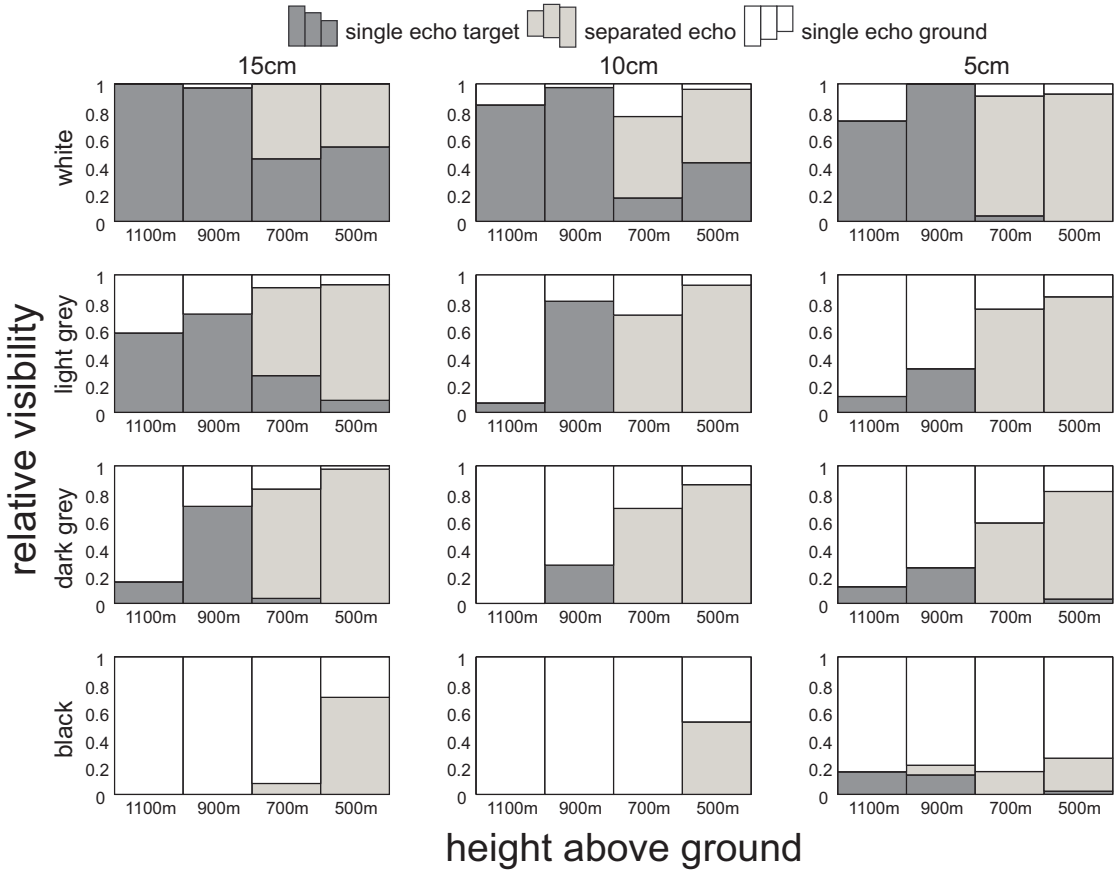

Figure 7.5: The percentage of target hits for the different colors (top to bottom) and different widths (left to right).The different colors denote different echo cases. White are ground echos (only single echos), light grey are separated echos (first always on target) and dark grey are single echos off the target. The different flying heights are labeled at the bottom of each plot.

heights. Due to signal strength issues one will not notice this effect for higher flying heights or low reflecting targets, since there the effective footprint is always smaller than the geometric footprint.

7.6 Discussion and Conclusions

We have successfully conducted a set of experiments regarding sensor characteristics of an airborne laser scanning system. Most of our findings are in good agreement with theoretical concepts, but our work furthermore allows some insights on absolute numbers of sensor properties in a practical context. The noise contained in return echos from a plane, homogeneously reflecting surface seems to be height dependent, with lower noise at low flying altitudes. This could probably be caused by edge effects, as with larger flying heights a higher number of echos have their beam diameter not fully contained on the target. As expected from theory, point density and footprint size have an effect on positional accuracy, even though our data does not show a clear linear re-

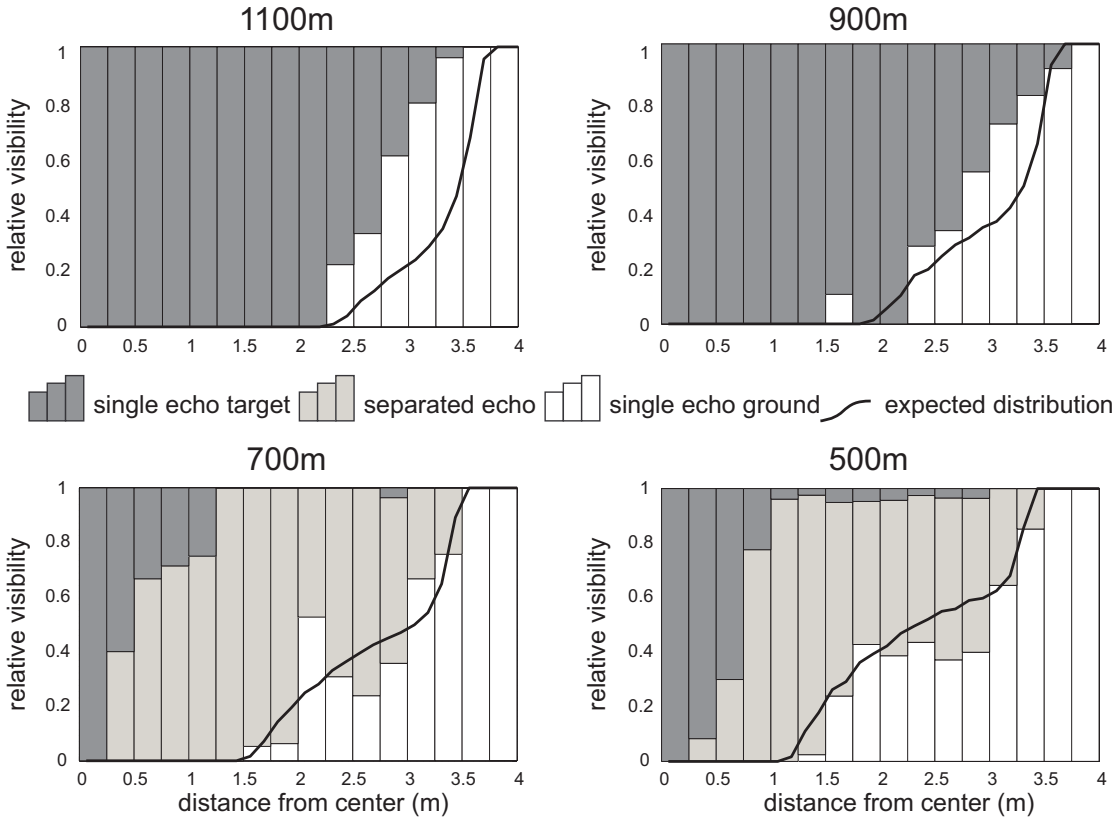

Figure 7.6: The ratio of echos from target to all echos from the center of the star to the outside. Color denotes the type of echo. The four panels are four different flying heights. For 500 m, all four flights have been put together.

lationship. This could be due to sampling issues, since for higher flying heights, our targets are sampled by fewer echos. Based on the findings from Section 7.5.2 we can set up the following rule of thumbs:

- target size is less important than target reflectivity in respect to a targets visibility.
- the flying height dependence of target visibility due to reflectivity is stronger than for target size
- footprint separation depends on flying height, probably caused through illumination and reflectance differences

In our case, with the artificial targets we build and the reflection properties we have, the effect of reflectance seems to be larger than the effect of target size. This as well can be founded by theory. But even for targets with a quite high reflectance of 0.52, as the white slats have, not every illumination of the slat might result in an echo for higher flying heights such as 1100 m AGL.

We used a target formed as a star to simulate different target to ground area ratios and to get an insight on the effective footprint size. That is, at which distance of two high reflecting slats will the laser beam fit in-between without triggering a first echo.

The effective footprint seemed to be larger than the geometric laser footprint at 500 m AGL. This is probably due to the sidelobes of the gaussian energy distribution across beam below $1/e^2$ of the energy maximum containing sufficient energy for triggering returns for high-reflecting targets at low flying heights. In order to get a better estimate on the energy distribution across the laser beam, one could construct star targets using differently colored slats, e.g. for a star target made out of aluminum foil, the effective footprint size should be close to the geometric one. The effect of diffraction could not be studied with our targets, but as stated by Baltsavias (1999), it would only add some few centimeters to the laser footprint size. As the applications using airborne laser scanner data are getting more and more sophisticated, an sufficient knowledge of potential error sources and their approximate sizes becomes vital. For instance, two objects having the same size, but with different reflectivity, could be measured different in size, with the object having the higher reflectivity being larger. Intensity data, that nowadays most laser scanners provide, could help identifying problematic spots in the laser data set. Using geometric reference targets such as we constructed can help getting a practical insight on the characteristics of a laser scanner and the reliability of its delivered data. Even an inter-comparison or calibration of different sensors over the same reference site would be possible.

7.7 Acknowledgments

We thank Stephan Heiner for carrying out the theodolite measurements as well as Othmar Frey and Maurice Rüegg for their support setting up the targets. Special thanks go to TopoSys for their ongoing support and the technical information they provided.

Bibliography

Baltsavias, E. P., 1999. Airborne laser scanning: basic relations and formulas. ISPRS Journal of Photogrammetry & Remote Sensing 54(2-3), pp. 199–214.

Brenner, C., 2005. Building reconstruction from images and laser scanning. International Journal of Applied Earth Observation and Geoinformation 6(3-4), pp. 187–198.

Gaveau, D. and Hill, R., 2003. Quantifying canopy height underestimation by laser pulse penetration in small-footprint airborne laser scanning data. Canadian Journal of Remote Sensing 29, pp. 650–657.

Haala, N. and Brenner, C., 1999. Extraction of buildings and trees in urban environments. ISPRS Journal of Photogrammetry & Remote Sensing 54(2-3), pp. 130–137.

Hyyppä, J., Kelle, O., Lehikoinen, M. and Inkinen, M., 2001. A segmentation-based method to retrieve stem volume estimates from 3-d tree height models produced by laser scanners. IEEE Transactions on Geoscience and Remote Sensing 39, pp. 969–975.

Kraus, K. and Pfeifer, N., 1998. Determination of terrain models in wooded areas with airborne laser scanner data. ISPRS Journal of Photogrammetry & Remote Sensing 53, pp. 193–203.

Lefsky, M. A., Cohen, W. B., Parker, G. G. and Harding, D. J., 2002. Lidar remote sensing for ecosystem studies. BioScience 52(1), pp. 19–30.

Morsdorf, F., Meier, E., Kötz, B., Itten, K. I., Dobbertin, M. and Allgöwer, B., 2004. Lidar-based geometric reconstruction of boreal type forest stands at single tree level for forest and wildland fire management. Remote Sensing of Environment 3(92), pp. 353–362.

Næsset, E., 2002. Predicting forest stand characteristics with airborne scanning laser using a practical two-stage procedure and field data. Remote Sensing of Environment 80(1), pp. 88–99.

Ni-Meister, W., Jupp, D. L. B. and Dubayah, R., 2001. Modeling lidar waveforms in heterogeneous and discrete canopies. IEEE Transactions on Geoscience and Remote Sensing 39(9), pp. 1943–1958.

Petzold, B., Reiss, P. and Stüssel, W., 1999. Laser scanning - surveying and mapping agencies are using a new technique for the derivation of digital terrain models. ISPRS Journal of Photogrammetry & Remote Sensing 54(2-3), pp. 95–104.

Roggero, M., 2001. Airborne laser scanning: Clustering in raw data. International Archives of Photogrammetry and Remote Sensing XXXIV-3/W4, pp. 227–232.

Sun, G. and Ranson, K., 2000. Modeling lidar returns from forest canopies. IEEE Transactions on Geoscience and Remote Sensing 38(6), pp. 2617–2626.

Wehr, A. and Lohr, U., 1999. Airborne laser scanning - an introduction and overview. ISPRS Journal of Photogrammetry & Remote Sensing 54(2-3), pp. 68–82.

Chapter 8

Synopsis

8.1 Main findings

Airborne laser scanning allows for a direct measurement of the locations of single scatterers on the earth's surface with unprecedented quality. Its primary application is the generation of high resolution terrain models by interpolating the raw laser echos into gridded elevation models. Since the raw laser data provides as well a direct measurement of the three-dimensional vegetation structure, foresters, ecologists and fire researchers have a keen interest in this technology.

Our research questions were what kind of vegetation properties could be derived from the laser point cloud (either direct or indirect), what are the accuracies that can be obtained, and how do the acquisition conditions influence the parameters to be derived. Furthermore, the interaction of the laser pulse with the scatterers was suspected to influence the outcome of the laser range measurement. The vegetation properties that were expected to be contained in the raw laser point cloud include canopy geometry (e.g. tree locations and heights) and properties related to canopy density, such as fractional cover and leaf area index. In order to discuss the main findings, the research questions formulated in Section 3.9 are presented again and are confronted with the findings from each publication.

How can the three-dimensional structure of the vegetation at the single tree level automatically be extracted from ALS raw data, and what are the accuracies obtained? *(Chapter 4, first publication)*

We have shown (Morsdorf et al., 2004) that it is possible to segment ALS raw data with high point densities into single trees. Using cluster analysis, the point cloud was divided into groups of raw laser returns that presumably belonged to the same tree. Cluster analysis offers the advantage that it is quite straightforward to apply to the raw data, by using an euclidean feature space, even though it is computationally expensive. Clustering in an euclidean feature space with all three coordinate dimensions being equally scaled will favor the segmentation of ball shaped objects. The way we used cluster analysis can be looked at as simple way of template matching, since we compressed the vertical axes of our feature space to convert ellipsoidal tree crowns into

ball shaped objects. We derived tree location, tree height and crown diameter from the segmented point cloud. Since the developed algorithm is fully automatic, it can be applied to larger areas without much effort. The accuracies obtained are well within the range of standard errors of traditional field work, with the ALS data offering the advantage of being able to measure thousands of trees in a few minutes of acquisition time. A problem arose from trees that were clumped very close together, with distances between stems being below one meter. These tree clusters could in most cases not be resolved as single trees by our algorithm. Thus, only the dominant height and a group diameter could be derived for these clusters. However, for most applications, this information should be sufficient. Tree height is systematically underestimated by ALS, which was some decimeters in our case. This underestimation is influenced by canopy density and point density, and should be larger the lower the point density and the lower the canopy density is.

Does discrete return raw ALS data contain information about vegetation density at scales as small as the laser footprint and if so, can that information be extracted in a direct fashion? *(Chapter 5, second publication)*

Since the raw laser point cloud is made up from both first and last echos, one could expect that it might implicitly contain information on scales smaller than that of the laser footprint. This information should be related to the density and reflectivity of scattering material inside the laser beam (see Section 2.3.2). Thus, it might be that the number of last echos inside the vegetation canopy could serve as a proxy for vegetation density. The more last echos are contained in the vegetation, the higher its density should be, if variations in canopy reflectance can be neglected. We showed (Morsdorf et al., 2006b) that it is possible to estimate the LAI of the canopy by using the fraction of first to last echos in the canopy as a proxy variable. Validation was carried out using hemispherical photographs, which are the traditional way of assessing canopy density in the field. Special emphasis was given to the scales on which the field measurements and ALS based estimates correlate best. For LAI, larger radii provided best results, while for fCover very small radii resulted in the best fit. This is due to the way of derivation of these values from hemispherical photographs, where small zenith angles are used for fCover, while LAI is computed from a larger part of the hemisphere. We were able to establish the ratio of first and last echos inside the canopy as a direct predictor variable for LAI. Furthermore, our approach allowed for the LAI estimation of the trees alone, since we could discriminate between canopy and ground returns based on a height threshold. The intrinsic semantic information added by filtering algorithms to convert elevation models into terrain models allows for using a simple height threshold for this discrimination. This ability of deriving an LAI only for the trees is an advantage that small footprint ALS systems provide over traditional field methods and passive optical imaging sensors, where the signatures of either tree distribution and/or ground reflectance are mixed with the information relevant for LAI retrieval recorded by those systems.

How robust are the derivation methods with respect to acquisition conditions

such as flight altitude and scan angle? *(Chapter 6, third publication)*

In Section 2.3.1 we presented an equation to compute the return energy of a simple scatterer. Parameters contributing to this equation were distance of emitter and scatterer as well as the incidence angle of the laser beam. These parameters are intrinsic properties of ALS acquisition conditions such as scan angle and flying height. Thus, it can be expected that the properties that we derive from the laser point cloud are altered by these conditions. Our third study (Morsdorf et al., 2006a) is an attempt to empirically study the influence of both flying altitude and scan angle on the methodologies developed in the first and second publication (Morsdorf et al., 2004, 2006b). We used flight path information provided by Toposys to reconstruct the incidence and local incidence angles for eight different flight tracks at either 500 and 900 m AGL. Comparing differences between field estimates and ALS estimates for different incidence angle classes, we found no significant change in neither tree height, fCover or LAI. Thus, the effects of scanning angle can be neglected for our acquisition settings. This is very probably due to the small scan angle $\pm 7.15^{\circ}$ of the system used, for systems using larger scan angles the influence of scanning angle might not be neglected. Flying altitude alters the derived parameters in more direct fashion, with different behavior for tree height, fCover and LAI. We observed an increase of tree height underestimation of about 30 centimeters, which could be due to the lesser point density of the higher flying altitude or to the widened footprint, which should give higher canopy penetration. Due to the nature of the computation of the LAI proxy, it is supposed that it is more susceptible to changes in flying altitude. LAI values were increasing by about 0.3 with higher flying altitude, which is about 20 percent for our canopy type. Thus, the effect of flying altitude on LAI retrieval can not be neglected and needs to be accounted for by calibrating the regression model for each flying altitude. fCover showed a similar behavior, but with fCover values being smaller for higher flying altitudes. As well as for LAI, the regression models for fCover will need to be re-calibrated if the flying altitudes differ as much as in our study.

How might different spatial or spectral properties of the targets affect object detectability and measured object dimensions?*(Chapter 7, fourth publication)*

Since it was not a priori known how the interaction of the laser pulse with the target objects will influence the range measurement, we conducted an empirical field test using artificial geometric reference targets (Wotruba et al., 2005). The targets were designed in order to give an insight into echo separation, effects of target size and reflectance as well the effective footprint size. To further incorporate different acquisition conditions, the targets were overflown with different flying altitudes. One main finding was that target reflectivity influences target visibility more than target size, a fact that is sustained by theory and practical experiences, if one considers the power-line example from Section 2.7. Furthermore, the minimum distance that can be resolved vertically between two objects was found to be dependent on the distance of emitter and scatterer, as it was increasing with flying altitude. The effective footprint size was found to comply well with computations based on beam divergence and flying altitude.

However, these findings manifest a caveat, that needs to be considered when planning ALS data acquisitions; especially for vegetation applications, since many ALS based statistics might be affected by these effects.

8.2 Conclusions

This thesis was motivated by an ecological process (wildland fire) being controlled, among other things, by the three-dimensional arrangement of fuel on the one hand and the availability of a remote sensing method (ALS) providing direct three-dimensional measurements of the earth's surface on the other hand. The challenge was to develop methods and algorithms that derive the relevant ecological parameters from this, in its raw form unusable ALS data and to assess the robustness of these methods in respect to typical ALS surveying parameters. The methods we derived prove the potential of ALS data for generating valuable structural information in assessing ecological problems, be it wildland fire or other ecosystem related processes.

We were able to demonstrate that ALS data does contain information on the three-dimensional canopy structure with an unprecedented quality, but that in some cases the acquisition conditions might influence the quality of the derived properties. Furthermore, it was shown that ALS data implicitly contains information about vegetation density even on smaller scales than that of the laser footprint and that one is able to exploit that information for the derivation of ecological parameters such as LAI and fCover. Even though physically meaningful variables were chosen for predicting these parameters from ALS data, the need of calibration using regression models and field estimates remains since the nature of laser pulse interaction with the canopy is yet not well enough understood.

A step towards a more thorough understanding of laser pulse interaction with scatterers was undertaken by empirically assessing this interaction trough geometrically well defined reference targets, proving the importance of target reflectance for object detectability. Summarizing, airborne laser scanning has been established as reliable source of information when assessing vegetation properties and can be considered as a the remote sensing reference for the three-dimensional characterization of the canopy.

8.3 Outlook

Future research should be focused in two directions; fusing alternate data sources with ALS data or ALS derived information and gaining a more thorough understanding of physical processes that are involved when laser light is scattered inside the vegetation.

The method developed for geometric reconstruction of single trees could benefit by complementing the ALS based information with spatially high resolution multispectral data of instruments such as a line scanner. Many ALS systems are operated together with such systems bearing four or more spectral channels. This additional information could either be helpful in the segmentation of single trees or in a classification of segmented tree clusters into different species. There are first studies, which show the potential of such approaches (Gougeon et al., 2001; Leckie et al., 2003; Hyde et al., 2006).

Furthermore, interfacing the parameters we were able to derive from ALS data with end-users such as modelers of wildland fire is not a trivial task and needs to be undertaken seriously. Of special importance are issues as on which scales are these parameters relevant for these models. A first study that did not find it's way into this thesis was concerned with how the resolution of input layers alters the output of the fire behavior model (Morsdorf et al., 2005). A sensitivity analysis using four different resolutions (5, 10, 20, and 30 m) of FARSITE inputs such as slope, aspect and fuel layers was conducted and the results were analysed in a qualitative way with the final aim of knowing the scales that are inherent to this fire behavior model.

In order to take the derivation of biophysical properties from ALS data a step ahead, one needs to understand better the nature of scatterers. That can for instance be achieved by ALS systems that allow for recording the full-waveform while maintaining the small size of the footprint. These systems will allow for the derivation of the so-called cross-section of the scatterer, which is a more physical meaningful property than a first and last echo distribution.

However, to fully exploit the potential of these systems for vegetation applications, one will need to understand which properties control the cross-section of vegetation at such small scales. For this, the combined use of ecologically calibrated fractal plant models such as AMAP (Castel et al., 2001a,b), which resolve the tree structure down to the leaf level and special radiative transfer models will become important. These models offer the advantage of being based on physically accurate ray-tracing and would be similar to the ones used by (Koetz et al., 2004, 2006). This combination should allow for a characterization of return waveforms depending on plant parameters such as leaf density and leaf reflectance, but as well for assessing the influence of ALS system properties such as laser wavelength and footprint size.

Bibliography

Castel, T., Beaudoin, A., Floury, N., Toan, T. L., Caraglio, Y., Barczi, J., 2001a. Deriving forest canopy parameters for backscatter models using the amap architectural plant model. IEEE Transactions on Geoscience and Remote Sensing 39 (3), 571–583.

Castel, T., Caraglio, Y., Beaudoin, A., Borne, F., 2001b. Using SIR-C SAR Data and the AMAP Model for Forest Attributes Retrieval and 3-D Stand Simulation. Remote Sensing of Environment 75 (2), 279–290.

Gougeon, F. A., St-Onge, B. A., Wulder, M., Leckie, D. G., 2001. Synergy of Airborne Laser Altimetry and Digital Videography for Individual Tree Crown Delineation. Proc. 23rd Canadian Symposium on Remote Sensing / 10e Congrés de l'Association québécoise de télédétection Sainte-Foy, Qubec, Canada, (CD–ROM).

Hyde, P., Dubayah, R., Walker, W., Blair, J. B., Hofton, M., Hunsaker, C., May 2006. Mapping forest structure for wildlife habitat analysis using multi-sensor (lidar, sar/insar, etm+, quickbird) synergy. Remote Sensing of Environment 102 (1-2), 63–73.

Koetz, B., Morsdorf, F., Sun, G., Ranson, K. J., Itten, K., Allgower, B., 2006. Inversion of a lidar waveform model for forest biophysical parameter estimation. IEEE Geoscience and Remote Sensing Letters 3, 49–53.

Koetz, B., Schaepman, M., Morsdorf, F., Itten, K., Allgöwer, B., 2004. Radiative transfer modeling within a heterogeneous canopy for estimation of forest fire fuel properties. Remote Sensing of Environment 92 (3), 332–344.

Leckie, D., Gougeon, F., Hill, D., Quinn, R., Armstrong, L., , Shreenan, R., 2003. Combined high-density lidar and multispectral imagery for individual tree crown analysis. Canadian Journal of Remote Sensing 29, 633–649.

Morsdorf, F., Frey, O., Meier, E., Itten, K., Allgöwer., B., 2006a. Assessment on the influence of flying height and scan angle on biophysical vegetation products derived from airborne laser scanning. ISPRS Journal of Photogrammetry & Remote Sensing, subm.

Morsdorf, F., Kötz, B., Itten, K., Isenegger, D., Allgöwer, B., 2005. Sensitivity of a Forest Fire Behavior Model to High Resolution Remote Sensing Data. In: EARSeL 5th International workshop on Remote Sensing and GIS Applications to Forest Fire Management: Fire Effects Assessment. Zaragoza, Spain.

Morsdorf, F., Kotz, B., Meier, E., Itten, K., Allgower, B., Sep. 2006b. Estimation of LAI and fractional cover from small footprint airborne laser scanning data based on gap fraction. Remote Sensing of Environment 104 (1), 50–61.

Morsdorf, F., Meier, E., Kötz, B., Itten, K. I., Dobbertin, M., Allgöwer, B., 2004. Lidar-based geometric reconstruction of boreal type forest stands at single tree level for forest and wildland fire management. Remote Sensing of Environment 3 (92), 353–362.

Wotruba, L., Morsdorf, F., Meier, E., Nüesch, D., 2005. Assessment of sensor characteristics of an airborne laser scanner using geometric reference targets. International Archives of Photogrammetry and Remote Sensing XXXVI (3/W19), 1–6.

Acknowledgments

This dissertation was in major parts financed by the EC project "Forest Fire Spread and Migitation" (SPREAD), EC-Contract Nr. EVG1-CT-2001-00027 and the Federal Office for Education and Science of Switzerland (BBW), BBW-Contract Nr. 01.0138. Toposys provided not only the data, but as well help on technical issues and offered a detailed insight into their ALS system, of which this thesis really benefits. I am greatly indepted to the Remote Sensing Laboratories, namely Klaus Itten, for supplying such a great infrastructure for conducting research and for all the possibilities of fruitful coorparations that his team and the network of RSL offer. A special thank goes to Erich Meier, for keeping me on track and pointing out the right directions at the right time. Furthermore, I would like to thank Britta Allgöwer for initiating and supporting this Ph.D. and always being burning for action when it came to applying the methods established in this thesis. I greatly appreciate the willingness of Benjamin Koetz to support this work in all of its aspects, and still being focused even after a long exchange of arguments. Of high importance for this thesis being finished succesfully was the familiar background established by my colleagues in the SARLab, namely Othmar Frey, Michael Jehle and Maurice Rüegg, who really became my friends during these years. I would like to thank the following persons at GIUZ for their support with either collecting data in the field, proof-reading manuscripts, supplying technical and/or research related help or just being there for discussions at social events: Jason Brazil, Stephan Bojinski, Stephan Dangel, Stephan Gruber, Felix Hebeler, Stephan Heiner, Daniel Nüesch, Daniel Schläpfer, Ronald Schmidt, Adrian Schubert, Lukas Wotruba. Finally, I would like to mention the supportive colleagues outside GIUZ for inspiring discussuions at conferences and collaborative work on hot research topics, Chris Hopkinson (COGS Geomatics, Canada) and Mark Danson (University of Salford, England).

Curriculum Vitae

Felix Morsdorf
Remote Sensing Laboratories
Geographisches Institut
Winterthurerstr. 190
University of Zürich
Zürich, CH-8057

Phone: +41446355164
Fax: +41446356842
morsdorf@geo.unizh.ch
http://www.geo.unizh.ch/~morsdorf

Education

1986-1993	High school at Ratsgymnasium Osnabrück, Abitur in May 1993
in 1990	two months visit at a high school in Evansville, IN, U.S.A.
1993-1994	Alternative national service at the city hospital of Osnabrück
October 1994	Start of studies of physical oceanography at the Christian-Albrechts Universität zu Kiel
29. October 1996	Vordiplom (pre-diploma)
March 1999	Diploma in theorethical and physical oceanography (major), applied physics und geophysics (minor) Masters thesis under supervision of Prof. Dr. Schott, "Boundary current variability in the Labrador Sea"
21. March 2001	Graduation as Dipl.-Oz., Mark 1.0
5. February 2007	PhD, University of Zürich, Institute of Geography

Workexperience

March 2002 – Present	UNIVERSITY OF ZÜRICH, DEPT. OF GEOGRAPHY (Zürich, Switzerland) *Research Assistant* Worked with Prof. K.I. Itten, Remote Sensing Laboratories. Extraction of biophysical vegetation parameters from airborne laser scanner data. Assessment of sensor properties using geometric reference targets. Evaluation of influence of incidence angle on accuracy of biophysical vegetation data products.
March 2001– March 2002	FRAUNHOFER INSTITUTE FOR COMPUTER GRAPHICS (Darmstadt, Germany) *Research Assistant* Worked with Prof. Georgios Sakas, Cognitive Computing and Medical Imaging. Using content based image retrieval systems for interactive web-based television.

Teaching Experience

- Fernerkundung IVc, Laser Signal and Detection, University of Zürich, 2006
- Introduction to laser scanning, University of Zürich, 2005
- Introduction to MATLAB, University of Zürich, 2005
- Image Processing: Segmentation, TU Darmstadt, 2001

Skills

Languages	German, English, French
Computing	MATLAB, C++, FORTRAN, LaTeX, OpenSceneGraph, ArcGIS, Unix, Mac OS X, Visual Studio, Xcode, MS Office
Other	Total of 6 months on research cruises during studies.

Chairs

- Chair of LIDAR session at EARSEL - 4th International Workshop: Remote Sensing and GIS applications for Forest Fire Management, Ghent, Belgium, 2003.
- Chair of Forestry session at ISPRS Workshop Laser Scanning 2005, ITC, Enschede, Netherlands, September 12-14 2005.

Reviewer for following journals:

- Remote Sensing of Environment
- ISPRS Journal of Photogrammetry and Remote Sensing
- Photogrammetric Engineering and Remote Sensing
- IEEE Geoscience and Remote Sensing Letters

Personal Bibliography

Chuvieco, E. (2003). Wildland Fire Danger Estimation and Mapping - The Role of Remote Sensing Data. World Scientific.

Danson, F. M., Hetherington, D., Morsdorf, F., Koetz, B., and Allgöwer, B. (2006). Three-dimensional forest canopy structure from terrestrial laser scanning. In 3d Remote Sensing in Forestry, 14-15. Feb. 2006, Vienna, Austria.

Danson, F. M., Hetherington, D., Morsdorf, F., Koetz, B., and Allgöwer, B. (2007). Forest canopy gap fraction from terrestrial laser scanning. IEEE GEOSCIENCE AND REMOTE SENSING LETTERS, 4(1):157–160.

Koetz, B., Morsdorf, F., Kneubühler, M., Schaepman, M., Meier, E., Itten, K., and Allgöwer, B. (2004a). Combination of imaging spectrometer data and high resolution lidar data by 3-d radiative transfer modeling. In R.O. Green (Ed.), AVIRIS workshop, Pasadena, CA, USA, 2004.

Koetz, B., Morsdorf, F., Schaepman, M., Meier, E., Itten, K., and Allgöwer, B. (2003). Specific parameterization of a boeral forest for a 3-d radiative transfer modelling approach based on imaging spectrometer data and high resolution lidar data. In M. Rast (Ed.), Second SPECTRA Workshop. ESA/ESTEC, Noordwijk.

Koetz, B., Morsdorf, F., Sun, G., Ranson, K. J., Itten, K., and Allgower, B. (2006). Inversion of a lidar waveform model for forest biophysical parameter estimation. IEEE Geoscience and Remote Sensing Letters, 3:49–53.

Koetz, B., Schaepman, M., Morsdorf, F., Itten, K., and Allgöwer, B. (2004b). Radiative transfer modeling within a heterogeneous canopy for estimation of forest fire fuel properties. Remote Sensing of Environment, 92(3):332–344.

Koetz, B., Sun, G., Morsdorf, F., Ranson, K., Kneubuhler, M., Itten, K., and Allgower, B. (2007). Fusion of imaging spectrometer and lidar data over combined radiative transfer models for forest canopy characterization. Remote Sensing of Environment, 106(4):449–459.

Kötz, B., Schaepman, M., Morsdorf, F., Bowyer, P., Itten, K., and Allgöwer, B. (2003a). Multiresolution imaging spectroscopy resolving the structure of heterogeneous-canopies for forest fire fuel properties mapping. In IGARSS 2003, Toulouse.

Kötz, B., Schaepman, M., Morsdorf, F., Bowyer, P., Itten, K., and Allgöwer, B. (2003b). Scaling-up based on radiative transfer modeling in a pine (pinus montana ssp. arborea) dominated canopy for forest fire fuel properties mapping using imagingspectrometer data. In EARSEL - 4th International Workshop: Remote Sensing and GIS applications for Forest Fire Management, Ghent.

Morsdorf, F., Frey, O., Meier, E., Itten, K., and Allgöwer, B. (2006a). Assessment on the influence of flying height and scan angle on biophysical vegetation products derived from airborne laser scanning. In 3d Remote Sensing in Forestry, 14-15. Feb. 2006, Vienna, Austria.

Morsdorf, F., Frey, O., Meier, E., Itten, K., and Allgöwer., B. (2006b). Assessment on the influence of flying height and scan angle on biophysical vegetation products derived from airborne laser scanning. ISPRS Journal of Photogrammetry & Remote Sensing, page subm.

Morsdorf, F., Koetz, B., Meier, E., Itten, K., and Allgwer, B. (2005a). The potential of discrete return, small footprint airborne laser scanning data for vegetation density estimation. In Vosselman, G. and Brenner, C., editors, International Archives of Photogrammetry, Remote Sensing and Spatial Information Sciences, volume VOLUME XXXVI, PART 3/W19 of 198-203. ISPRS.

Morsdorf, F., Kötz, B., Itten, K., Isenegger, D., and Allgöwer, B. (2005b). Sensitivity of a Forest Fire Behavior Model to High Resolution Remote Sensing Data. In EARSeL 5th International workshop on Remote Sensing and GIS Applications to Forest Fire Management: Fire Effects Assessment. Zaragoza, Spain.

Morsdorf, F., Kotz, B., Meier, E., Itten, K., and Allgower, B. (2006c). Estimation of LAI and fractional cover from small footprint airborne laser scanning data based on gap fraction. Remote Sensing of Environment, 104(1):50–61.

Morsdorf, F., Meier, E., Allgöwer, B., and Nüesch, D. (2003a). Clustering in airborne laser scanning raw data for segmentation of single trees. In Proceedings of the ISPRS working group III/3 workshop "3-D reconstruction from airborne laserscanner and InSAR data" Dresden, Germany 8-10 October 2003, ISSN 1682-1750 VOLUME XXXIV, PART 3/W13.

Morsdorf, F., Meier, E., Allgöwer, B., and Nüesch, D. (2004a). Cluster-Analyse von LIDAR-Vektordaten zur Erfassung geomatrischer Eigenschaften von einzelnen Bäumen. Photogrammetrie Fernerkundung Geoinformation, (4):259–268.

Morsdorf, F., Meier, E., Koetz, B., Itten, K., and Allgöwer, B. (2003b). High resolution airborne laser scanning for forest fuel type mapping. In EARSEL - 4th International Workshop: Remote Sensing and GIS applications for Forest Fire Management.

Morsdorf, F., Meier, E., Koetz, B., Nüesch, D., Itten, K., and Allgöwer, B. (2003c). The potential of high resolution airborne laser scanning for deriving geometric properties of single trees. In EGS - AGU - EUG Joint Assembly, Nice, France.

Morsdorf, F., Meier, E., Kötz, B., Itten, K. I., Dobbertin, M., and Allgöwer, B. (2004b). Lidar-based geometric reconstruction of boreal type forest stands at single tree level for forest and wildland fire management. Remote Sensing of Environment, 3(92):353–362.

Schaepman, M., Kneubühler, M., Koetz, B., Schlaepfer, D., Morsdorf, F., Meier, E., Allgöwer, B., and Itten, K. (2003). Validation and calibration of envisat/meris level 1 and 2 products over land. In EARSEL - 23rd annual Symposium, Ghent.

Wotruba, L., Morsdorf, F., Meier, E., and Nüesch, D. (2005). Assessment of sensor characteristics of an airborne laser scanner using geometric reference targets. International Archives of Photogrammetry and Remote Sensing, XXXVI(3/W19):1–6.